ACRYLIC POLYMERS AT LIQUID INTERFACES

by

MARIA SEVASTAKI

A thesis submitted to the department of Materials Science and Technology of University of Crete for the degree of

Master of Science

DEPARTMENT OF MATERIALS SCIENCE AND TECHNOLOGY
UNIVERSITY OF CRETE

JUNE 2016

THESIS CERTIFICATE

This is to certify that the thesis titled ACRYLIC POLYMERS AT LIQUID INTERFACES, submitted by Maria Sevastaki, to the department of Material Science and Technology of University of Crete, for the award of the degree of Master of Science, is a bona fide record of the research work done by her under our supervision. The contents of this thesis, in full or in parts, have not been submitted to any other Institute or University for the award of any degree or diploma.

Committee:

Dr. Benoit Loppinet

Prof. George Petekidis

Prof. Dimitris Vlassopoulos (supervisor)

Place: Heraklion

Date: 11/7/2016

ACKNOWLEDGEMENTS

I would like to express my gratitude to my supervisor Dimitris Vlassopoulos for his guidance and support during my Master studies and for giving me the opportunity to travel and attend schools and conferences in interesting places. I feel sincerely grateful to him especially for having expressed his full confidence in me and for having allowed me to work with independence. Also, I would like to acknowledge appreciation to Benoit Loppinet for his brilliant ideas while I was facing problems with the experiments. I would like to thank all the members of the committee for the helpful comments that surely contributed to the development and the improvement of my thesis. Furthermore, I would like to thank prof. A. Hirao and prof. M. Pitsikalis for the preparation of the samples. Their contribution was significant. It would be an important omission not to thank prof. J. Vermant and dr. J. Samaniuk. I thank them for their collaboration at the project. I would also like to thank my laboratory colleagues of the polymer group at FORTH with who I shared most of the time and for their support and friendship. Especially, I need to express my deep and thankful appreciation to Antigoni Theodoratou for teaching me how to use the Langmuir trough and for her great help, support and friendship at the beginning of my master. Also, I would like to express my special acknowledgment to Prof. Moshe Gottlieb and Maria Merola for the collaboration concerning the PEO-PDMS project at the air-water interface. Last, but certainly not least, huge thanks and gratitude to my family, George, Kathrin, Christina and Hercules for their support and love over the years.

ABSTRACT

In the present thesis the structural and rheological properties of viscoelastic films of acrylic polymers were studied. The experiments were performed at the air-water interface using a Langmuir trough.

Our aim was to understand the relation between the macromolecular conformation and interfacial properties, and compare against respective behavior in the bulk. To this end, well-characterized samples of acrylic polymers of varying molecular weights and molecular structure were used. Langmuir monolayers were built with two different types of molecular systems, two series of homopolymers, poly (methyl methacrylate) (PMMA) and poly n(butyl acrylate) (PBA), with different molecular architectures. These two types of polymers were chosen because they have an affinity for air -water interface, yet they have different glass transition temperatures. The protocol involved compression-expansion cycles and rheology by means of the magnetic rod interfacial stress rheometer and step-compression measurements.

We observe that upon compression, the materials (linear and more complex architectures), exhibit phase transitions due to packing, which are distinct for each polymer. All acrylics exhibit reversible layers at the air-water interface, with a reproducible phase transition for all different structures and molecular weights. Flory radius analysis suggests a behavior akin to ideal conditions. Finally, the layer relaxation at different conditions (different initial concentration) is primarily independent, hence the well-known scaling in the bulk does not apply at the interface.

Keywords: air-water interface, interfacial rheology, surface pressure, PMMA, linear, dendritic, PBA, star, compression- expansion, relaxation time.

Table of Contents

Table of Symbols

Symbol	Definition	Units
A	Surface area	Å/monomer
A_s	Constant area	Å/monomer
B_q	Boussinesq number	-
C	Concentration	mg/ml
C*	Overlap concentration	mg/ml
E	Energy	
G_s*	Dynamic Shear modulus	mN/m
G_s’	Interfacial storage modulus	mN/m
G_s’’	Interfacial loss modulus	mN/m
L	Characteristic length	m
L_I	Length scale of velocity at interface	m
L_S	Length scale of velocity at subfase	m
Mw	Molecular weight	g/mol
N	Number of polymerization	-
P_I	Perimeter	m
R	Rod-wall distance	m
R_F	Flory radius	Å
T	Temperature	^oC
V	Volume	ml
v	Velocity	m/s
α	Radius	m
γ_S	Surface strain	-
Γ	Surface tension of monolayer	mN/m
Γ_0	Surface tension of water	mN/m
δ	Relative phase	^{o}
η	Viscosity for bulk	Pa s

η_S	Surface viscosity	Pa s m
Π	Surface pressure	mN/m
σ_S	Surface stress	N/m
τ	time	s
Ω	Frequency	rad/s

List of Figures

List of Tables

1. INTRODUCTION

In the last 40 years, a great deal of progress has been made in the analysis of structural and viscoelastic properties of 3D (bulk) polymer systems. A main outcome is the current state of the art understanding of the viscoelasticity of entangled polymers.

It is known that for linear polymer chains in the bulk the zero-shear viscosity scales with the molecular weight to the power of 1 or 3.4 depending on whether the polymers are unentangled or entangledm respectively (Figure 1) In the latter case, the characteristic relaxation time follows the same (3.4) scaling. For entangled star polymers the relaxation time scales with the exponential of the number of entanglements per arm (DE GENNES (1971), RUBINSTEIN AND COLBY (2003)). Figure 1 depicts experimental results of different linear polymers in terms of zero-shear viscosity versus molecular weight.

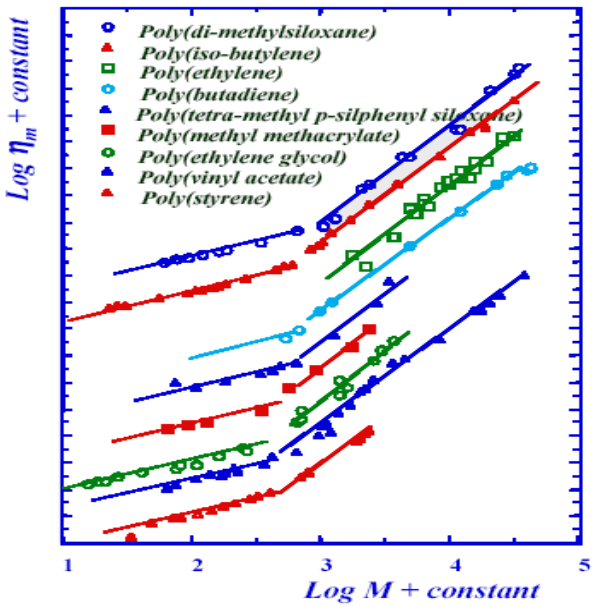

Figure 1: Zero-shear viscosity as a function of molecular weight (BERRY ET AL. (1968)).

Figure 2 depicts linear viscoelastic spectrum of an entangled polymer in the bulk. The graph with modulus G' and G'' versus frequency can be seperated in to five regions.

1. The viscous/ terminal region, where G'' dominates and viscous behavior prevails (G''~ ω) (G' ~ ω^2). Often the frequency range where this takes place is too low to be detected.

2. The transition-to-flow region occurs at higher frequencies marked by the moduli crossover. The latter signifies the inverse of the relaxation time τ;

3. The rubbery or plateau region where elastic behavior dominates and G'~ω^0. In reality, there is always a slight increase of G' with frequency. The value of G'' is of course always lower than that of G';

4. The leathery/ transition region is also seen, where, due to high-frequency relaxation and dissipation mechanisms, the value of G'' again rises, this time faster than G'. Once more at G' = G'', a crossover frequency can be defined, from which another characteristic time can be obtained;

5. At the highest frequencies usually encountered in this form of testing, a glassy region detected, where G' again dominates (RUBINSTEIN AND COLBY (2003)).

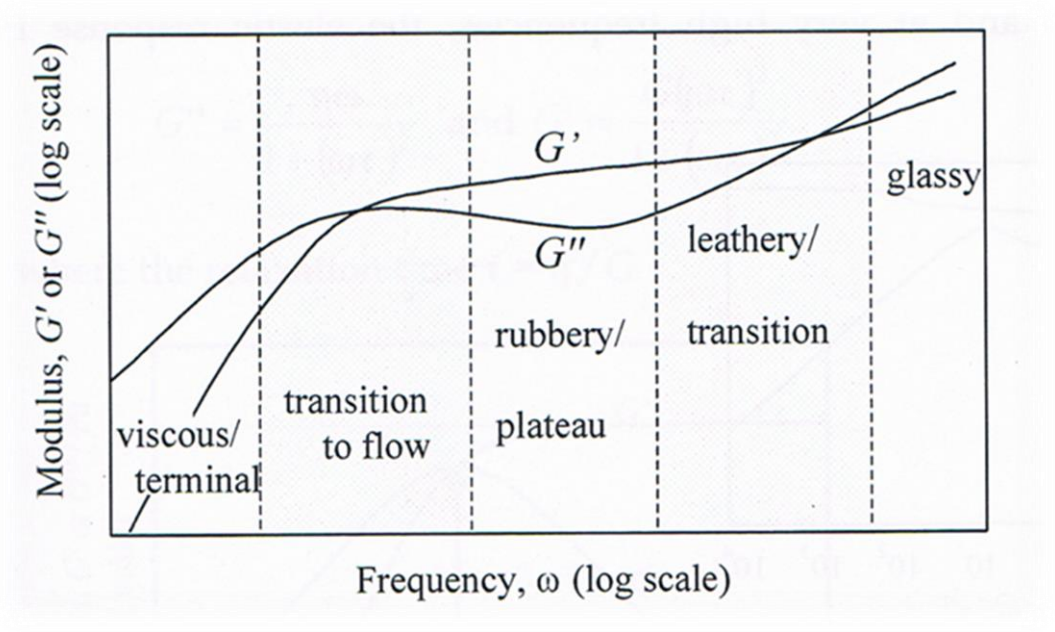

*Figure 2: Linear viscoelastic spectrum of an entangled polymer. Taken from (*BARNES *(2000)).*

On the other hand, the structural and rheological properties of 2D systems (for example, fluid interfaces) have not been explored in detail. Also, the role of molecular characteristics of materials, such as molecular weight, and more specific parameters, such as tacticity, architecture, monomer type and concentration at the interface is only recently starting to be studied (HSU ET AL. (2005)).

Recently, linear polymers have been studied at fluid interfaces. For example MAESTRO ET AL. (2010) found a similar dynamic response of PtBA in surface and in the bulk. The characteristic time of PtBA scaled with the degree of polymerization to the power of 3 as can be seen in figure 3. This is a remarkable result, yet at the same time surprising. Whereas the scaling of figure 1 seems clear, one wonders how times ranging from 1 to 10^7s were measured! Moreover, one wonders why the conferment in 2D

has apparently no effect on polymer dynamics! These issues constitute the main motivation for this work.

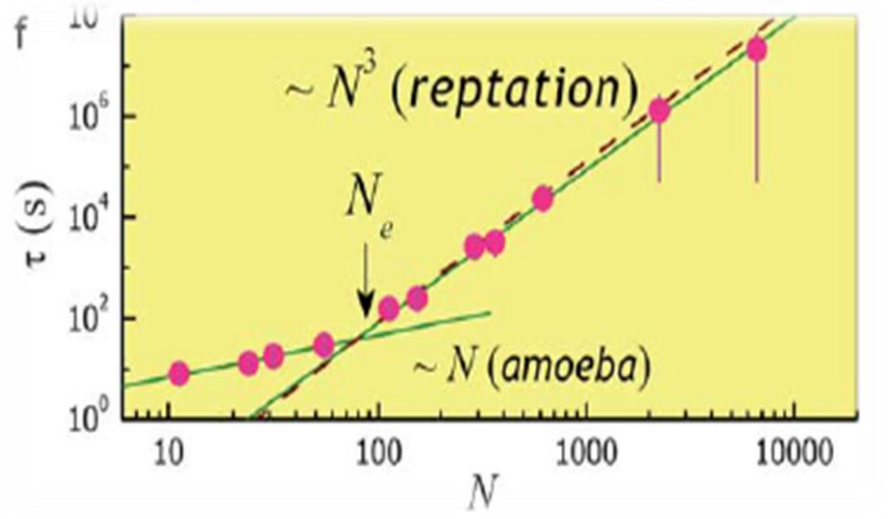

Figure 3: Characteristic time vs degree of polymerization for PtBA at air-water interface. Taken from MAESTRO ET AL. (2010).

Since we deal with interfaces, we point out that interface is the boundary between two phases. Materials at an interface are typically amphiphilic. Concerning air-water interfaces acrylic polymers represent ideal model systems. In 1994 SRIVASTAVA ET AL. (2011) studied PMMA as a function of surface concentration and temperature. Thereafter, many groups performed experiments with PMMA trying to understand the characteristics of that film and the glassy behavior (CAPANA ET AL. (2005), HSU ET AL. (2005), MAESTRO ET AL. (2009) AND MAESTRO ET AL. (2011)). An interesting example is the work of HSU ET AL. (2005). They studied PMMA linear samples with different molecular configurations. They used isotactic, syndiotactic and atactic PMMA with molecular weight 100000g/mol. In figure 4 we can see the pressure isotherm from compression expansion experiments. The onset of pressure increase marks the coil overlap at the interface and is analogous to 3D overlap

concentration. Beyond this point the molecules interact. This means that they create a different configuration at the interface. Another important point is the pressure plateau (phase transition). Note that for syndiotactic PMMA a change of slope rather than plateau is observed during compression. This led the authors to conclude that the layers have different configuration which is reflected primarily during compression. They observe a reversibility behavior for all the configurations until pressure 15mN/m.

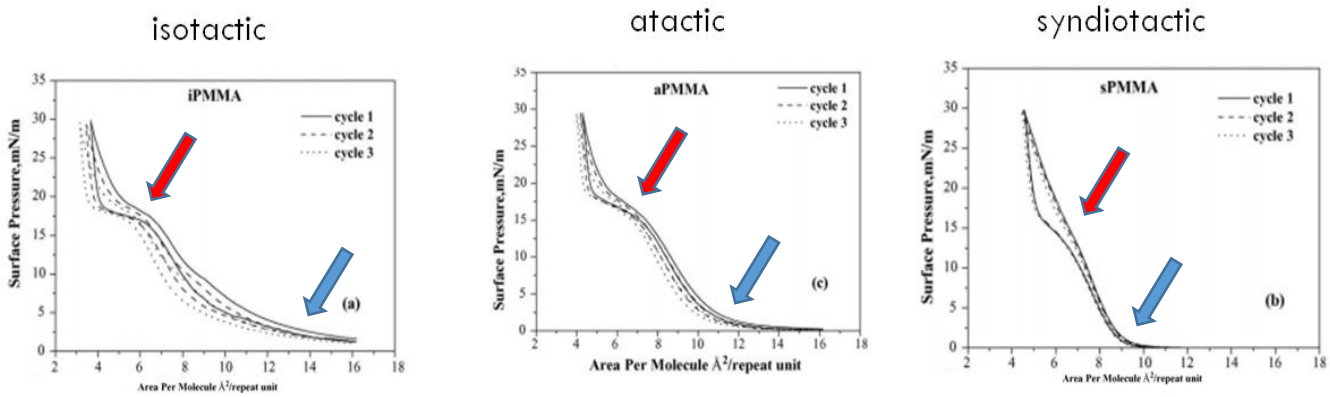

Figure 4: Compression- expansion data (pressure isotherms) for PMMA with molecular weight 100000g/mol with three different molecular configurations (isotactic, atactic, syndiotactic) HSU ET AL. *(2005). Blue arrows show the coil overlap at the interface. Red arrows show the "plateau".*

PMMA and PtBA layers have been employed by SAMANIUK AND VERMANT (2014) in order to perform 2D micro-rheology. In additions computer simulations were performed in order to understand the conformation of polymers in 2D as seen in figure 5. They suggest that upon compression the layer buckles and a 2D to 3D transition is possible. These results supported experimental findings with the interfacial stress rheometer

which was used in order to measure rheological properties of Langmuir monolayers of poly (tert-butyl methacrylate) (GAVRANOVIC ET AL. (2005)).

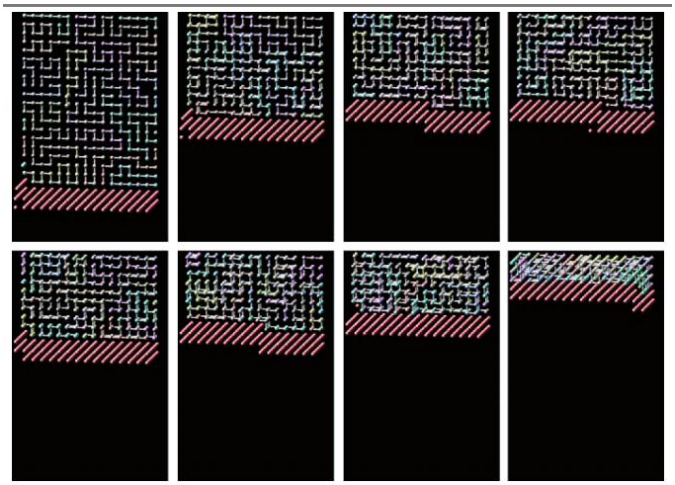

Figure 5: Snapshots of configurations (molecular arrangement) for a representative computer-simulated system as a function of increasing surface pressure. The simulated moving barrier is shown compressing the polymer system. The density-1 values corresponding to these (left-right, top-bottom) are 0.99, 0.68, 0.55, 0.51, 0.50, 0.44, 0.35, and 0.16. (GAVRANOVIC et al. (2005)).

Langmuir monolayers find applications in the biomedical field, for example the study of cells, lipid membranes (GRIMARD ET AL. (1993), ESPINOSAA ET AL. (2010)), lung surfactants (CLEMENTS AND AVERY (1998)) and tear films (RIESS (2009)), but also in thin film technology e.g. sensors (SWALEN ET AL. (1987)). Over the last years, rheology at gas/liquid and liquid/liquid interfaces has become a very important research tool for exploring a variety of problems in food industry (DICKINSON ET AL. (1991)), in biomedicine (ZASADZINSKI ET AL. (2001)) in stability of emulsions and foams (GEORGIEVA ET AL. (2009)) and in personal care products.

In this thesis the interfacial properties of insoluble monolayers using shear rheology with a magnetic rod interfacial stress rheometer were studied. The

goal is to address the behavior in quasi-two dimensional polymer films. We focused on the film properties of PMMA and PBA series because the characteristic carboxyl group of the acrylics is hydrophilic hence, these molecules are effectively surfactants that can sit at the air-water interface.

We have studied the interplay between structure and rheology of these acrylic systems at the air-water interfaces. The basic points we want to focus in this study were the role of molecular weight (Mw), tacticity, architecture and the high Tg at acrylics. To accomplish our goal, at this we have structured the study as follows. Initially we collected data concerning the effects of molecular weight on structure and rheology of the polymer samples. More specifically, two categories of linear PMMA were studied, namely atactic, syndiotactic and one dendritic PMMA category as well. Also, two PBA configurations were studied, linear and star. Afterwards, atactic and syndiotactic PMMA samples were compared, and data regarding their behavior were analyzed. Then, we addressed the role of molecular architecture on the polymer behavior by comparing linear atactic versus dendritic PMMA samples. Lastly, we explore the consequences of the glassy behavior of atactic linear PMMA by investigating the effect of concentration of the polymer on the relaxation time of the layer. The results will guide us to understand if the acrylic polymers behave differently at interfaces compared to the bulk.

2. MATERIALS AND METHODS

2.1. Materials

We study acrylic polymers with different architectures. First we build poly (methyl methacrylate) (PMMA) monolayers and then we study PBA monolayers. Both of them are acrylic homopolymers but with different characteristics as we will analyze below.

2.1.1. Atactic linear poly(methyl methacrylate) (PMMA)

Poly(methyl methacrylate) (PMMA) polymer was synthesized anionically and obtained by PSS (Mainz, Germany). Figure 6 depicts the chemical formula of PMMA. We studied eight samples with the weight-average molar mass between 24k-2000k g/mol and the polydispersity index PDI=Mw/Mn between 1.02 -1.25 (Table 1). For the higher molar matter (above about 100k) the glass transition temperature (Tg) is about 110^{o}C.

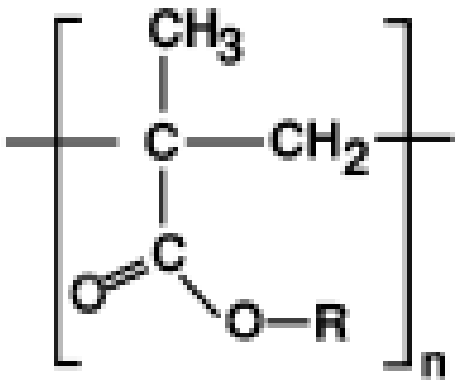

Figure 6 :Poly(methyl methacrylate) (PMMA).

Table 1: Molecular weight and polydispersity of atactic linear PMMAs

LINEAR PMMA	Mw (g/mol)	PDI
24k	24300	1.03
65k	64700	1.02
125k	125000	
134k	134000	
600k	603000	1.03
850k	790000	1.1
1000k	936000	1.1
2000k	2250000	1.25

2.1.2. Syndiotactic linear poly(methyl methacrylate) (PMMA)

Poly (methyl methacrylate) (PMMA) syndiotactic linear polymers were obtained by the group of Prof. Pitsikalis in University of Athens that was synthesized anionically. Figure 7 depicts the chemical formula of syndiotactic PMMA. We studied seven samples, with the weight-average molar mass between 64.7k-205.3k g/mol and the polydispersity index PDI=Mw/Mn between 1.26 -2.72 (Table 2). Slightly higher Tg values compared to atactic (140^{o}C) have been repeated here.

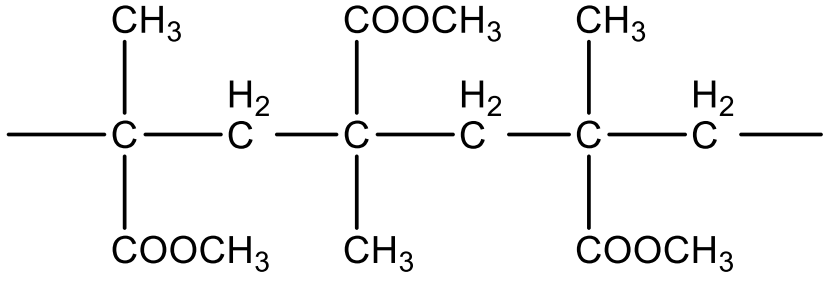

Figure 7: Syndiotactic Poly(methyl methacrylate) (PMMA).

Table 2: Molecular weight and polydispersity of syndiotactic linear PMMAs

LINEAR PMMA	Mw (g/mol)	PDI
PMMA 5	64700	1.26
PMMA 9	69300	1.30
PMMA 3	78400	1.26
PMMA 4	81100	1.69
PMMA 13	111800	1.78
PMMA 11	120100	1.26
PMMA 10	205300	2.72

As we can see in the figure 7 the side groups of syndiotactic PMMA oriented alternatively to the main carbon chain, which affects their persistence length (1.3nm (Catherine A. Tweedie (2007)) with respect to atactic PMMA. This, in turn, may affect their interfacial properties.

2.1.3. Dendritic poly(methyl methacrylate) (PMMA)

Dendritic poly(methyl methacrylate) (PMMA) polymers were obtained from Prof. A. Hirao (Tokyo Institute of Technology, Japan). Figure 8 depicts the first and fourth generation of dendrimers. These are symmetric macromolecules with the average molar mass of segments between branches being 11000 g/mol. Table 3 lists the total molar mases. Same Tg values hold here as well.

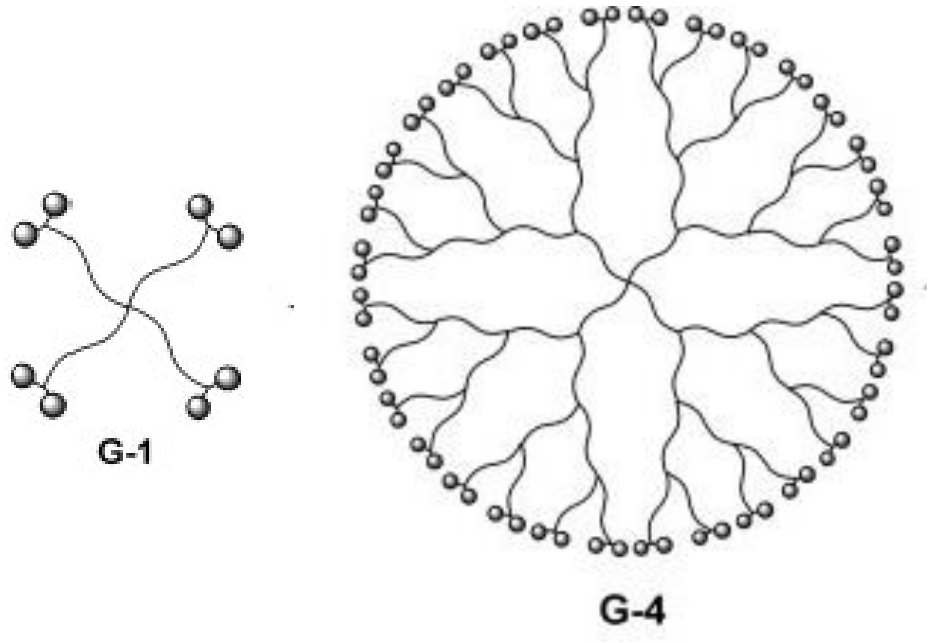

Figure 8: 1st and 4th generation dendritic PMMA.

Table 3: Molecular weight of dendritic PMMAs

DENDRITIC PMMA	Mw (g/mol)
G1	44000
G4	660000

2.1.4. Linear poly (n-butyl acrylate) (PBA)

Poly(n-butyl acrylate) (PBA) polymer was obtained by the group of Prof. M. Pitsikalis of University of Athens was synthesized anionically. Figure 9 depicts the chemical formula of PBA. The weight-average molar mass was 84180 g/mol and the polydispersity index PDI=Mw/Mn was 1.15. Here, Tg is about -55ºC.

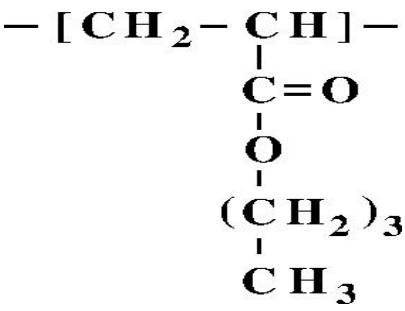

Figure 9: Poly(n-butyl acrylate) (PBA).

2.1.5. Star Poly (n-butyl acrylate) (PBA)

Star poly(n-butyl acrylate) (PBA) polymer was obtained from Prof. K. Matyjazewski (Carnegie – Mellon University, USA). Figure 10 depicts a typical example of star structure. Table 4 lists be presented the characteristics of the samples which we used.

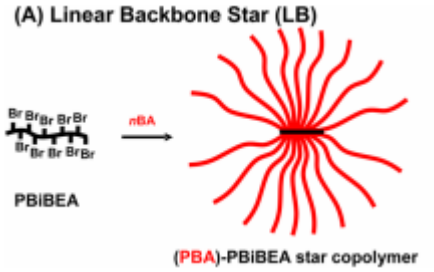

Figure 10: Typical example of star structures. (SNIJKERS ET AL. (2014))

Table 4: Molecular weight of star PBAs

	Mw (total) (g/mol)	PDI
PBA 31	466100*	1.19
PBA 72	180000*	1.17
PBA 10/240	208600**	1.14
PBA 20/210	288600**	1.15

* (VAN RUYMBEKE ET AL. (2011))

**(SNIJKERS ET AL. (2014))

2.1.6. Layer deposition method

The spreading solution was prepared by using chloroform (Sigma Aldrich, 99% purity) with at a concentration of 1- 60 mg/ml. Double distilled and deionized water from a Milli-Q-RG system was used to prepare the sub phase. The surface depositions of the PMMA at the water-air interface were performed drop-wise by spreading the solution using a 50 μL syringe. The polymer layer was left at rest for about 15 minutes for the evaporation of the solvent. Finally, fast compression and expansion cycles were performed to ensure a homogeneous layer.

2.2. The Pockels - Langmuir - Blodgett trough

Molecular systems between two fluids can be studied with many different ways. First Agnes Pockels described a device she had designed to measure the surface tension of monolayers of hydrophobic and amphiphillic substances. This device was a trough made from a tin pan with tin inserts for determining the size of the surface and a balance with a 6 mm disk on one end to measure the force required to pull the disk from the surface (POCKELS (1891)). Pockels continued her experiments and calculated the amount of several materials (mostly household oils) required to form a monolayer. She reported values of the thickness of films of various amphiphillic substances on the surface of water (POCKELS (1892)) and studied the effects of different ratios of hydrophobic to amphiphilic molecules on surface tension and monolayer formation (POCKELS (1893)). After some years Pockels's trough was improved by Irving Langmuir to study insoluble monolayers at the water-air interface and for this reason the new setup take his name as Langmuir trough (LANGMUIR (1917), LANGMUIR (1920)).

Concerning the layers, three types can be described. First, the Langmuir monolayers that are insoluble, secondly, the Langmuir-Blodgett (LB) films and finally the Gibbs monolayers. In LB films one or more monolayers of an organic material are deposited from the surface of a liquid onto a solid substrate by emerging the solid substrate into (or from) the liquid (BLODGETT (1939)). Last but not

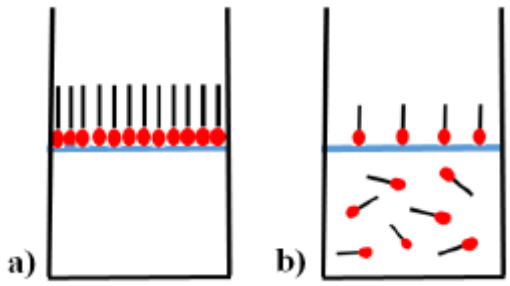

Figure 11: a) Langmuir films and b) Gibbs films.

least there are the Gibbs monolayers that are soluble in one of the phases separated by the interface on which the monolayer is formed (Figure 11).

In Figure 12 we can see the Langmuir trough which we use and is attached to a metal block in contact with a bath in order to allow temperature control. The trough is made of a material that is easy to keep clean, Teflon. Two barriers are made of a hydrophilic material and they move towards/away from each other in order to change the surface concentration of the molecules at the interface.

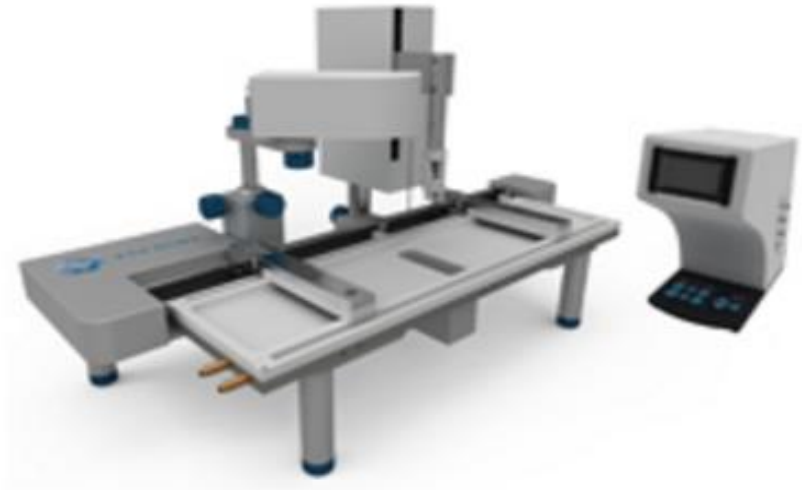

Figure 12: KSV NIMA Langmuir-Blodgett Trough. This image is taken from the official webpage of KSV Instruments (www.biolinscientific.com/ksvnima/products/).

The Wilhelmy plate is usually made by platinum and it is an important part of the setup. The Wilhelmy balance is responsible for monitoring the surface tension according to eq. 1 The surface pressure, Π , is the surface tension of the monolayer, Γ, subtracted from the surface tension of the water, Γ_0 , that is 72.8 mN/m at 20 °C (eq. 1) (GAINES (1966)).

$$\Pi = \Gamma_0 - \Gamma \qquad (1)$$

For the preparation of the monolayer, the homopolymers have to be dissolved in a mutual volatile solvent. Using a microsyringe the solution is deposited drop-wise at the interface. A time of around 15 min is needed for the solvent to evaporate. After that the barriers start to move changing the concentration of the monolayer. The surface pressure-area isotherm indicates several phase transitions of the monolayer. In Figure 13 a typical compression surface pressure isotherm of a Langmuir monolayer is presented.

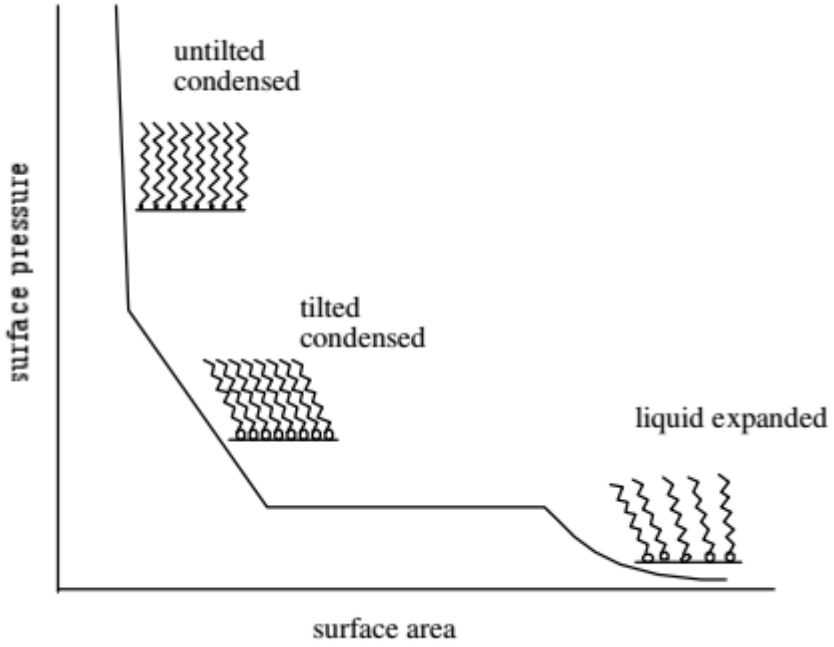

Figure 13: A generalized isotherm curve of Langmuir monolayer. The image is taken from (FULLER (2003)).

The surface pressure zero corresponds to the gas-like state of the monolayer and the liquid-like and solid-like states of the monolayer occur upon compression. These diagrams are analogous to the three dimensional pressure-volume isotherms at a constant temperature.

2.3. Magnetic Rod Interfacial Stress Rheometer (ISR)

The magnetic rod interfacial stress rheometer (ISR) was developed by BROOKS ET AL. (1999). Figure 14 depicts the basic components of an ISR. According to the design of BROOKS ET AL. (1999), a commercial Langmuir trough is equipped by a pair of Helmholtz coils to generate a magnetic field gradient. This gradient applies a force on a magnetized rod that is supported by surface tension at the water-air interface.

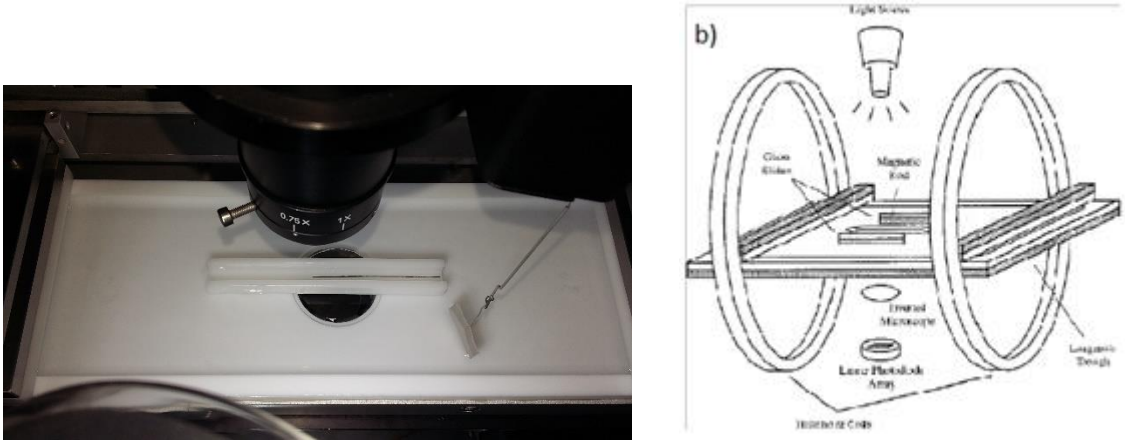

Figure 14 : a) The ISR can be combined with a KSV NIMA Langmuir trough. This figure depicts our set up. b) Schematic representation of the magnetic rod interfacial stress rheometer. This image has been taken from BROOKS ET AL. (1999)

In the set up where this thesis was performed, the magnetized rod is positioned in the middle of a channel with a variable width R. The position of the needle is detected by a camera which is focused at the edge of the needle. In a typical set up the one of the magnetic coils generates a magnetic field gradient and the other produces a constant magnetic field by fixing the orientation of the magnetic needle. There are two dc power supplies (Hewlett-Packard Model 6644A) that are used to drive the pair of Helmholtz coils. The current set point of one of these power supplies is

controlled by an analog signal from a function generator (Hewlett-Packard Model 3325B) to create a time dependent magnetic field gradient. A third dc dual-power supply (Hewlett-Packard Model 6205C) is used to power the constant field coils. The forces that can be applied with the present design range from 0.001 to 30 μN.

The channel was made of hydrophilic material (Teflon) so the magnetic rod had a good alignment at the centerline of the channel. The meniscus created by the hydrophilic material contributes to the self-centering of the needle. In Figure 15 the geometry produces a linear velocity profile neglecting the influence of the subphase.

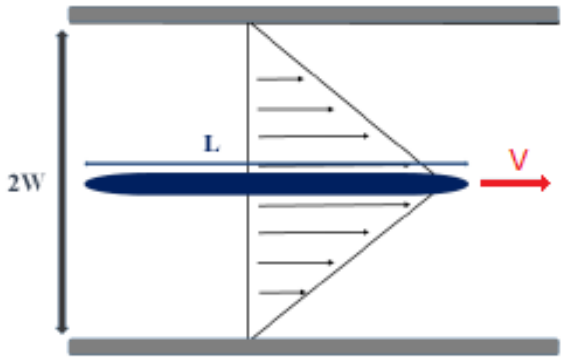

Figure 15: The channel with the magnetic needle.

This problem is solved both numerically and analytically starting from the Navier-Stokes equations and using the generalized Boussinesq-Scriven equation as a suitable boundary condition (VERWIJLEN ET AL. (2011)). In the last work good agreement was found between numerical simulations, analytical solutions and experiments describing the flow field and the resulting local interfacial shear rate at the rod. Based on this research, an algorithm to correct the experimental data of different types of interfacial shear rheometers and geometries was proposed and evaluated.

The Boussinesq number (eq. 2) is important to estimate the relative surface and subphase contributions. When Bq << 1, the subphase stresses dominate, while when Bq >> 1 the surface stresses dominate. It is defined as:

$$B_q = \frac{\eta_S \frac{V}{L_I} P_I}{\eta \frac{V}{L_S} A_S} = \frac{\eta_S L_S P_I}{\eta L_I A_S} = \frac{\eta_S}{\eta \alpha} \quad (2)$$

where,

η_S : the surface viscosity (Pa s m),

η : the bulk viscosity of the subphase,

V : the characteristic velocity,

L_I : the characteristic length scale at which the velocity decays at the interface,

L_S : the characteristic length scale at which the velocity decays at, the subphase,

P_I : the contact perimeter between the rheological probe and the interface and

A_S : the contact area between the probe and the subphase.

The parameter α is related to the radius of the entire geometry. For example, for the magnetic needle it is determined by the radius of the needle. According to the previous equation a small value of α, would be preferable to achieve a sensitive interfacial rheometry device.

Data analysis

For data analysis, two basic assumptions have been made. First, the velocity developed between the stationary walls and the rod is a linear shear profile. Therefore, the displacement of the rod is a direct measure of the interfacial strain. Secondly, the contribution of the surface to the total drag is larger than that of the subphase drag (BROOKS ET AL. (1999)). The analogy between the surface stress, σ_S, and the surface strain, γ_S, is the surface dynamic shear modulus (G_S^*).

$$G_S^*(\omega) = G_S'(\omega) + iG_S''(\omega) \tag{3}$$

The surface stress can be seen at eq 4 where F_o is the drag on the rod and L is the length of the rod. The surface strain can be calculated as shown, given that the velocity profile between rod and walls is linear. In eq 5 z_o is the displacement of the rod, the distance between the rod and the walls is R, and α is the radius of the rod.

$$\sigma_S = \frac{F_o}{2L} \tag{4}$$

$$\gamma_S = \frac{z_o}{R - a} \tag{5}$$

In accordance to the previous, the surface dynamic shear modulus can be calculated knowing the geometrical parameters α, R and L as well as the amplitude ratio (AR) and the relative phase (δ) (eq. 6). The units of G* in two-dimensional rheology is in Pa m = N m^{-1}.

$$G_S^*(\omega) = \frac{\sigma_S}{\gamma_S} e^{i\delta(\omega)} = \frac{(R-a)}{2L}\frac{F_o}{z_o} e^{i\delta(\omega)} = \frac{(R-a)}{2L}\frac{1}{AR} e^{i\delta(\omega)} \tag{6}$$

3. RESULTS

The glass transition temperature (Tg) is an important property concerning the behavior and structure of the polymer layer on the air water interface. Thus, when the layer is being studied at temperatures close or above Tg, due to the glassification process, the layer is not homogenous. As is visible on Table 5, atactic linear and syndiotactic linear PMMA exhibit Tg much higher than room temperature. On the other hand, linear PBA was studied at a temperature higher than its Tg.

Table 5: Polymer systems and glass transition temperature.

Polymer System	Tg (ºC)
Atactic Linear PMMA	110*
Syndiotactic Linear PMMA	140**
Dendritic PMMA	110***
Linear PBA	-55****
Star PBA	-55

*(ROTH AND DUTCHER)

**(HSU ET AL.)

***(VAN RUYMBEKE ET AL. (2010))

****(GERARD (2001))

3.1. ATACTIC LINEAR PMMA: EFFECT OF MOLECULAR WEIGHT ON STRUCTURE AND RHEOLOGY

3.1.1. Surface Pressure Area Isotherms

Figure 16 depicts the surface pressure/area compression -expansion of different molecular weight of atactic linear PMMA (24k, 65k, 125k, 134k, 1000k and 2000k). The experiment was performed in stable conditions. The temperature (T) was 25°C, the volume (V) of the solution PMMA was 25μl, the plate was vertical to the trough and the spreading was symmetric. We can observe that the pressure begins its increase faster as we increase the molecular weight. This observation shows that the molecules interact faster with each other and that is related to the amount of material on the interface. Another important point is at a surface pressure equal to 15mNm^{-1}. At that point there is a phase transition and the plateau is more visible at samples with lower molecular weight instead with a change at slope for the others.

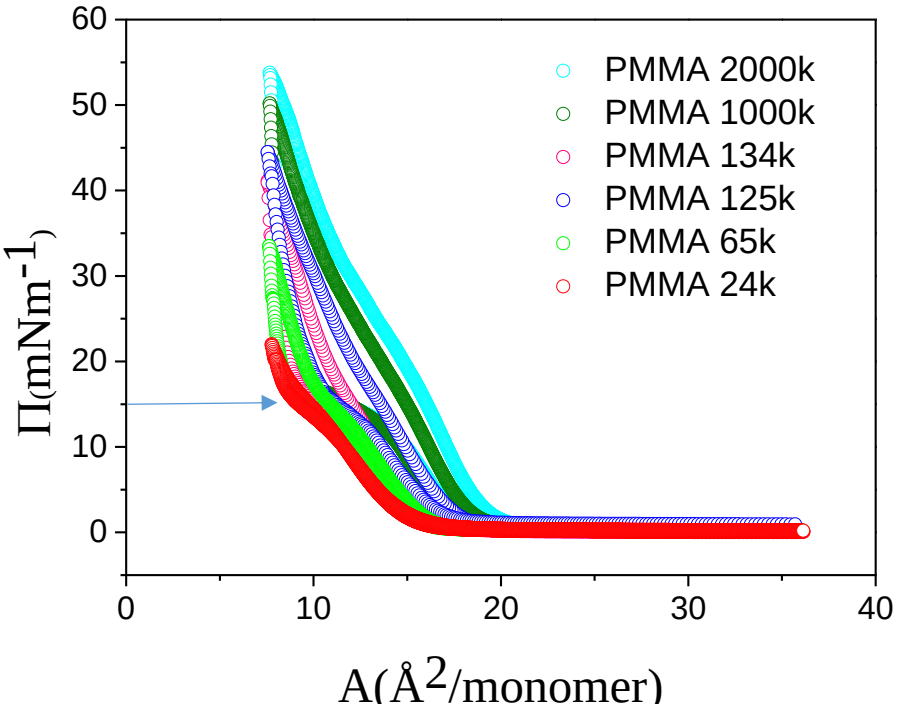

Figure 16: Compression - expansion data (pressure isotherm) for atactic linear PMMAs (c=1mg/ml, V=25μl, T=25°C, barrier speed 10mm/min) Mw= 24k, 65k, 125k, 134k, 1000k, 2000k. Arrow shows "plateau".

Initially, experiments of reproducibility (Figures 17, 18) and speed test (Figure 19) were performed to verify the correctness of the results. The small differences at the graph has to do with the experimental error. Also the area in Figure 19 shows the energy (E~Π*A) which is needed for each circle. A good way to understand this is to think an isotherm graph for 3D systems. The way to think is exactly the same with one less dimension. With the increase of the speed, increase of the energy is observed, which can be explained by the lack of time to find the polymer in equilibrium situation.

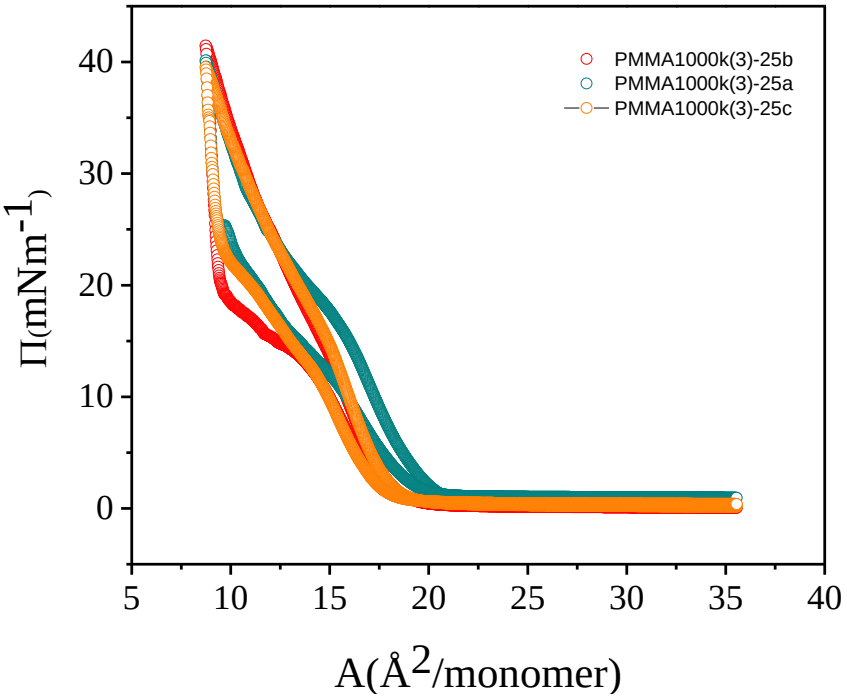

Figure 17 : Reproducibility test for PMMA 1000k (c=1mg/ml, V=25µl, T=25°C, barrier speed 10mm/min).

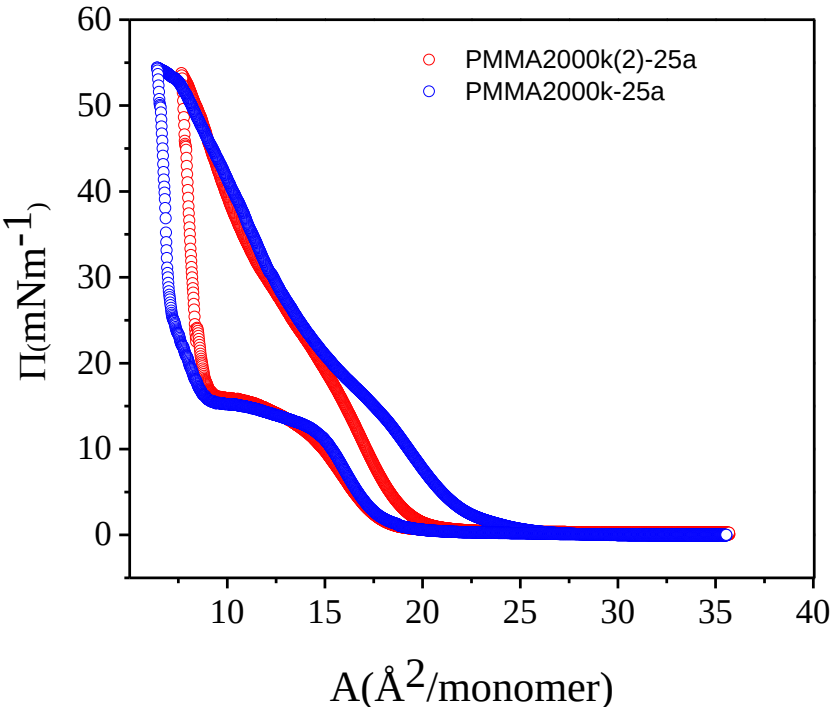

Figure 18 : Reproducibility test for PMMA 2000k (c=1mg/ml, V=25µl, T=25°C, barrier speed 10mm/min).

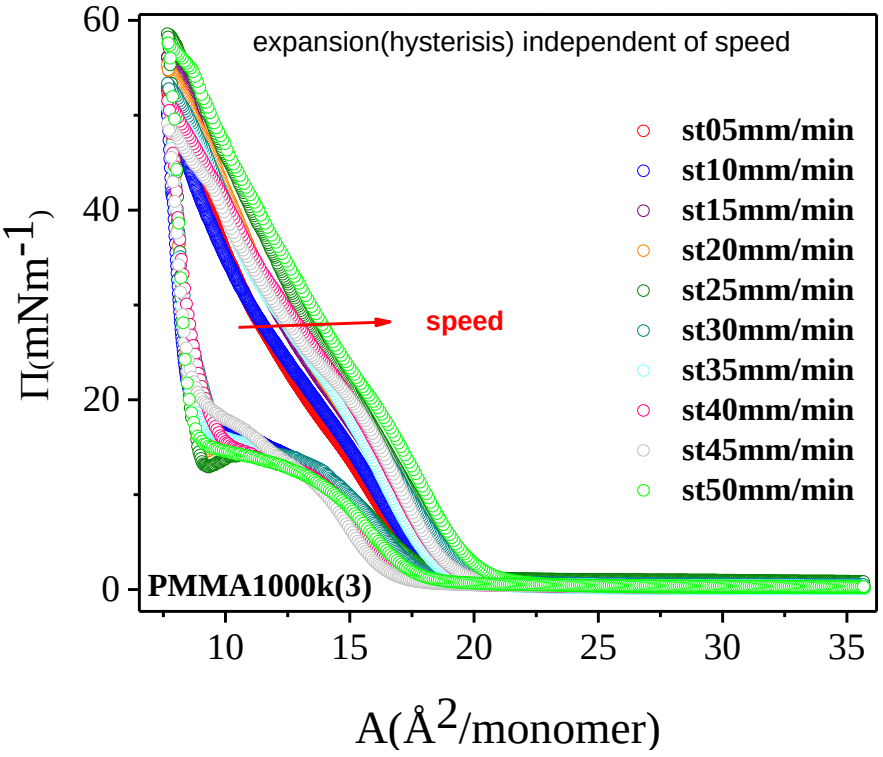

Figure 19: Compression- expansion speed test for PMMA 1000k (c=1mg/ml, V=25µl, T=25°C, barrier speed 5-50mm/min) Arrow shows the change with the increase of the speed.

Figure 20 shows the differences from the 1st to 3rd circle with different final target pressure. Also, Flory radius analysis of PMMA is demonstrated in figures 21 and 22. From the compression experiments we find the overlap surface concentration by fitting to tangent lines from the high and low surface concentrations as shown graphically in figure 22. The intersection point marks the specific area where coils overlap. From the 'line crossing' area we find the radius of the molecules (R_F) ($R_F = \sqrt{\frac{Area}{pi}}$), which is plotted as function of the degree of polymerization $N = \frac{Mw_{polymer}}{Mw_{monomer}}$ in figure 21. The error bars computed from the points where the line cut across the plot are shown in figure 22. Likewise, calculation of R_F for all

molecular weights have been made. The error bars are much smaller than the point size (Figure 21).

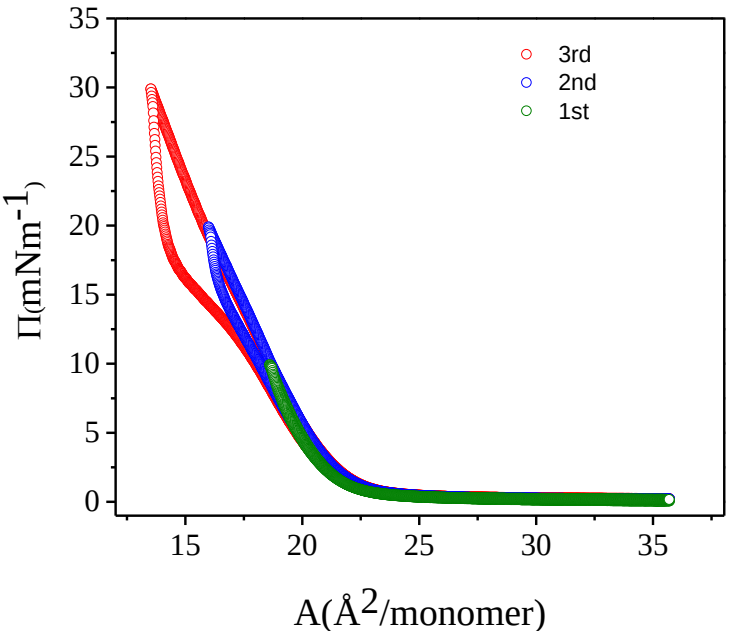

Figure 20: Compression - expansion data (pressure isotherm) for PMMA1000k (3), 1st circle (green) has target pressure 10mNm-1, 2nd circle (blue) has target pressure 20mNm-1, 3rd circle (red) has target pressure 30mNm-1(c=1mg/ml, V=25µl, T=25°C, barrier speed 10mm/min).

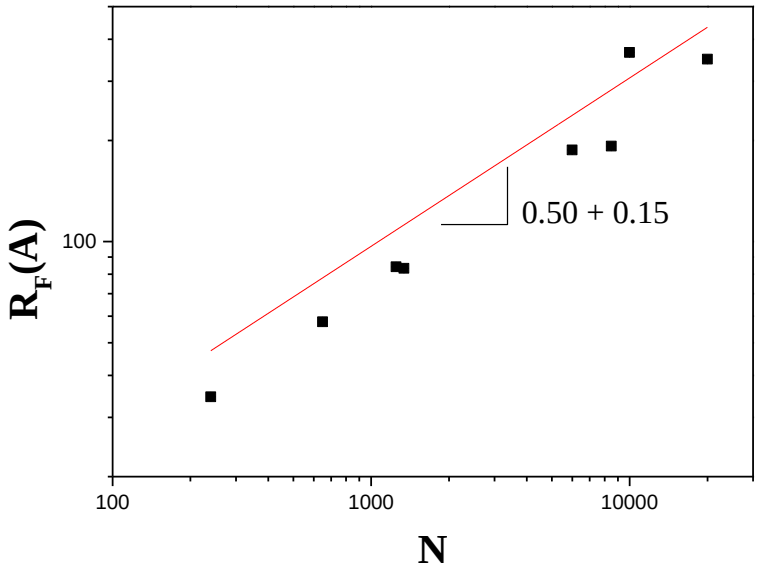

Figure 21: Flory radius analysis. The error bar is much smaller than the point size.

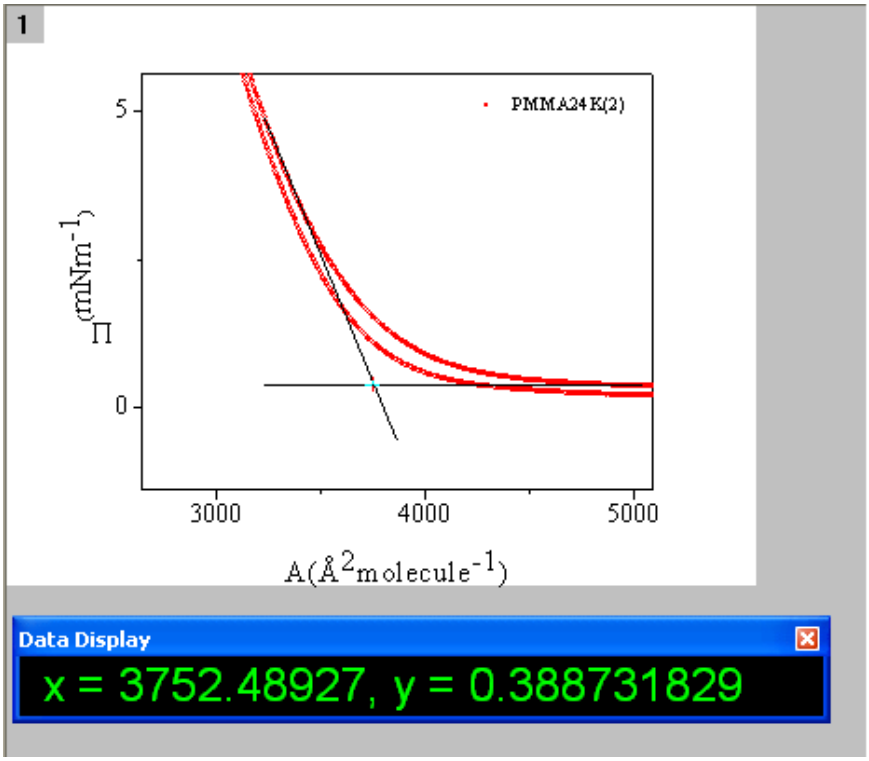

Figure 22 : Graphic determination of the Flory radius. The area at the intersection is used to find RF.

From the above results we observe that the expansion (hysteresis) is independent of speed as seen in figure 19. Also, the energy which is needed for a circle increases with the increase of the speed. Furthermore, there is reversibility to the PMMA linear samples before a specific pressure as we can see in Figure 20, because when we stop the compression before that pressure and then we expand the layer the curves overlapped. Finally, the Flory radius analysis shows that the film behaves similarly to materials in theta solvent (ideal) conditions.

3.1.2. Interfacial Rheology

Figure 23 shows the dynamic frequency sweeps of the same linear polymer PMMA 1000k at different surface pressures. The polymer solution was spread close to the channel and the layer (compressed and expanded) was mixed twice.

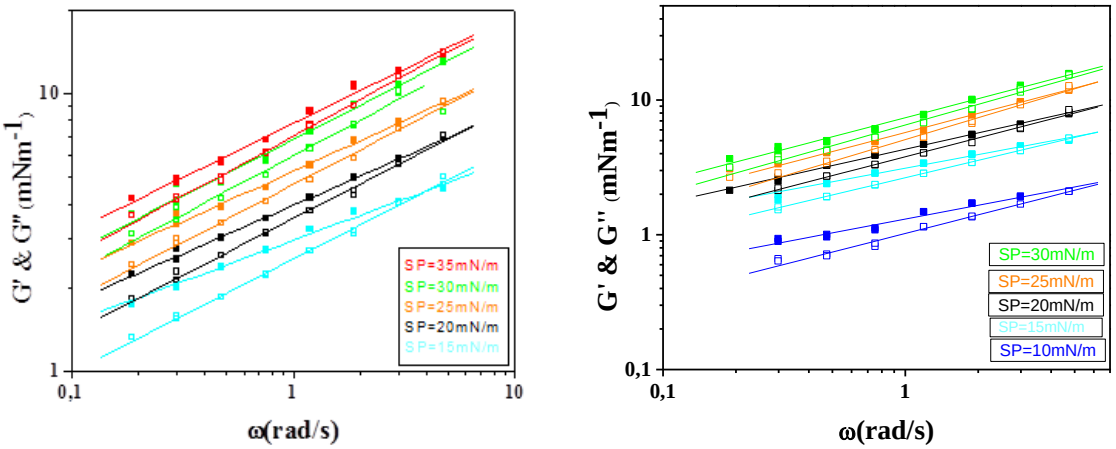

Figure 23: Reproducibility rheology test for PMMA 1000k, G' is symbol full, G'' is symbol empty (c=1mg/ml, V=25μl, T=25oC). Lines are drawn to guide the eye.

After that we did the analysis of the data. The equations

$$\eta = G^*/\omega \quad (7)$$

$$G^* = (G'^2+G''^2)^{1/2} \quad (8)$$

were used to present the data of Figure 24.

We observe that (i) no zero shear viscosity was reached and (ii) increasing the surface pressure yields an increase of viscosity (see also Fig. 24).

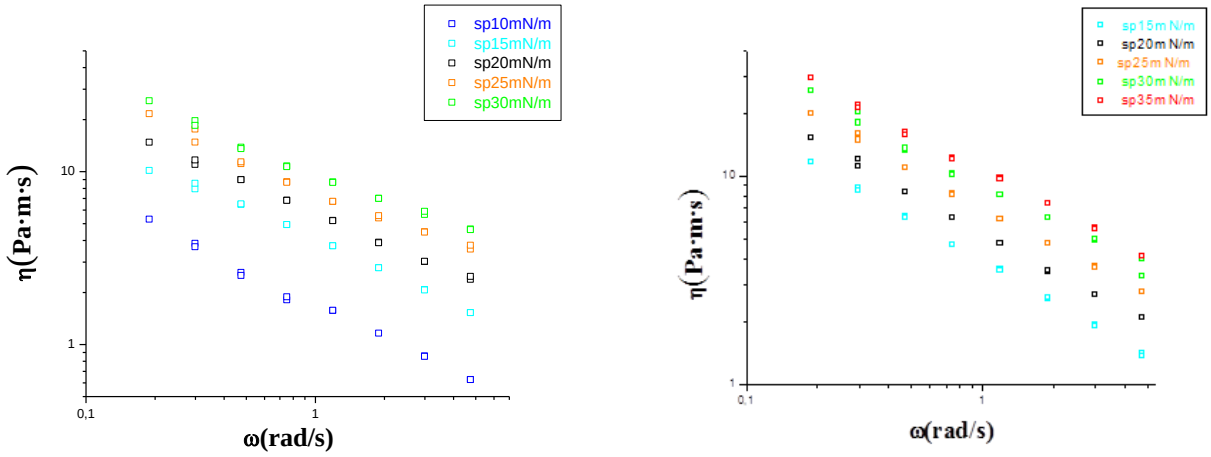

Figure 24: Zero- shear viscosity vs frequency for PMMA 1000k.

Subsequently, rheological experiments were performed for atactic linear PMMA with different molecular weights (24k, 65k, 125k, 134k, 600k, 850k, 1000k and 2000k). The temperature (T) was 25° C, the volume (V) of the solution PMMA was 25μl, the plate was vertical to the trough, the spreading was symmetric and close to channel and the layer was mixed. Appendix I shows the results of that experiments.

Finally, Figure 25 shows G' versus pressure (Π) for frequency (ω) equal to 1.19 rad/s for different molecular weight of linear PMMAs and Figure 26 shows G' versus molecular weight (Mw) for surface pressure 2 to 35mN/m for a specific ω equal to 1.19 rad/s.

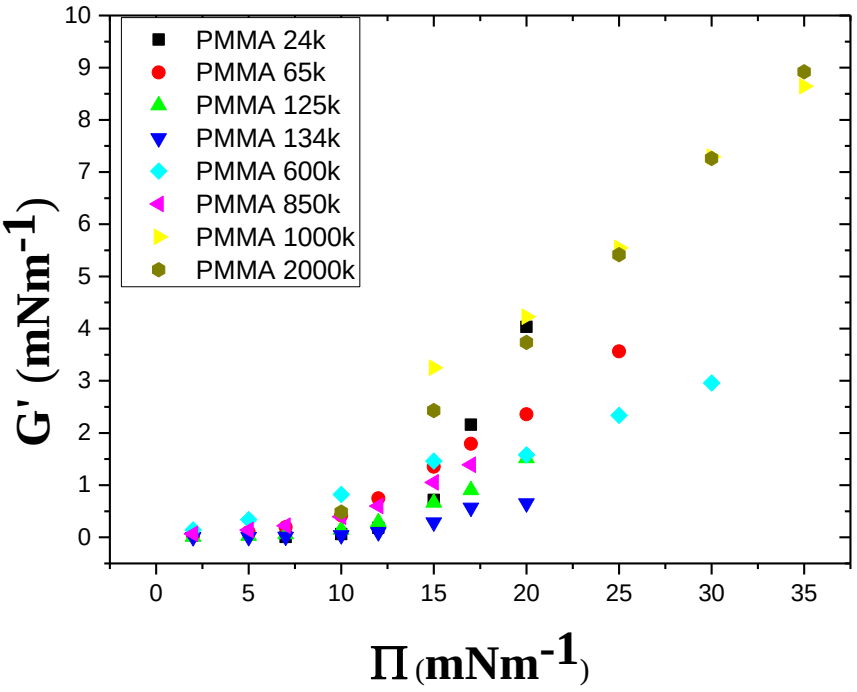

Figure 25: G' vs Π (pressure) for PMMA with different molecular weight (600k, 1000k, 2000k), ω=1.19 rad/s.

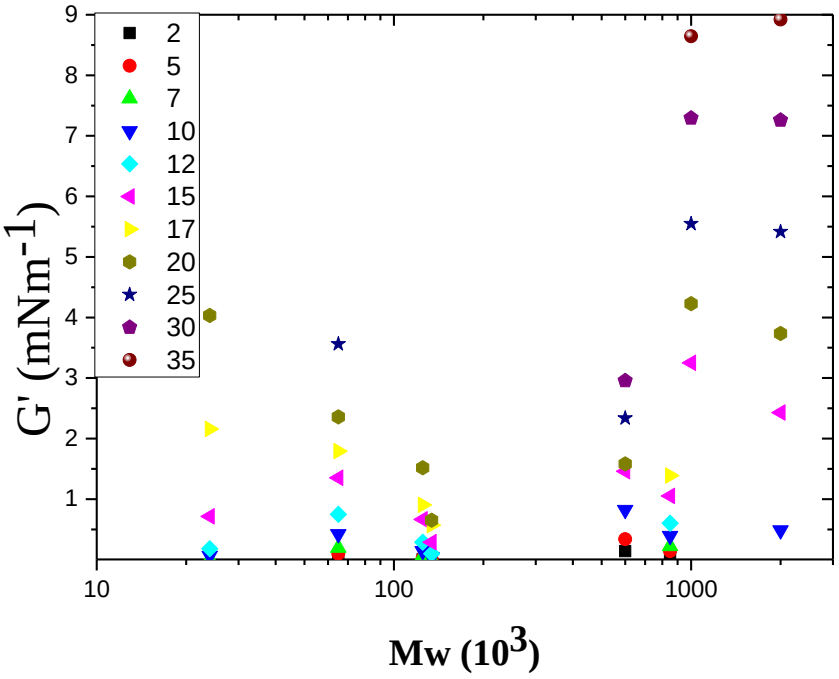

Figure 26: G' vs Mw (molecular weight) for PMMA with different surface pressure (2 – 35mN/m), ω=1.19 rad/s.

We observe that G’ and G’’ became higher with the increase of the surface pressure. There is a characteristic time where there was a crossover between G’ and G’’ which is independent from the molecular weight (figure 23). Also there is a difference between PMMA24k and the others. At this polymer G’’ is higher than G’. A possible explanation is because of its lower molecular weight and the reactions between the chains. Finally graphs of viscosity versus frequency have no terminal.

3.2. SYNDIOTACTIC LINEAR PMMA: EFFECT OF MOLECULAR WEIGHT ON STRUCTURE AND RHEOLOGY

3.2.1. Surface Pressure Area Isotherms

Figure 27 depicts the surface pressure/area compression –expansion of different molecular weight of syndiotactic linear PMMA (69.3k, 78.4k, 81.1k, 120.1k, 205.3k). The temperature (T) was 25^{o}C, the volume (V) of the solution PMMA was 25μl, the plate was vertical to the trough (i.e., parallel to the barriers) and the spreading was symmetric. Here, there is a phase transition and the apparent plateau is more visible with samples having lower molar mass. This observation shows that the molecules interact faster with each other and it has to do with the amount of material at the interface. Another important point is at a surface pressure equal to 15mNm^{-1}. At this point there is a phase transition and the plateau is more visible at samples with lower molecular weight instead with a change at slope for the others.

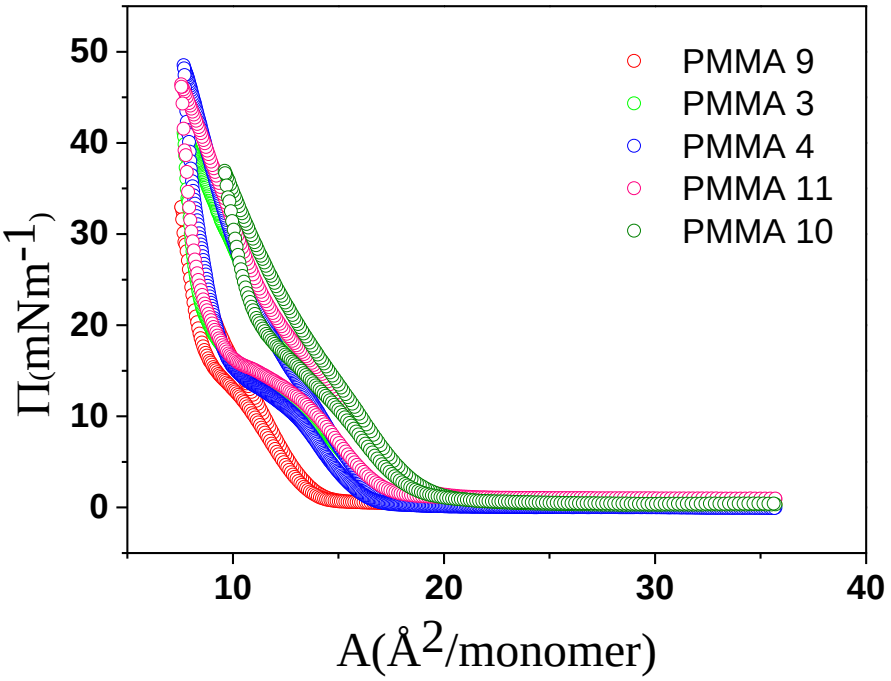

Figure 27: Compression - expansion data (pressure isotherm) for syndiotactic linear PMMAs (c=1mg/ml, V=25μl, T=25°C, barrier speed 10mm/min) Mw= 69.3k, 78.4k, 81.1k, 120.1k, 205.3k.

Initially, experiments for testing reproducibility (Figures 28,29) were performed in order to test the measurements. Results for all syndiotactic samples are reported in Appendix II..

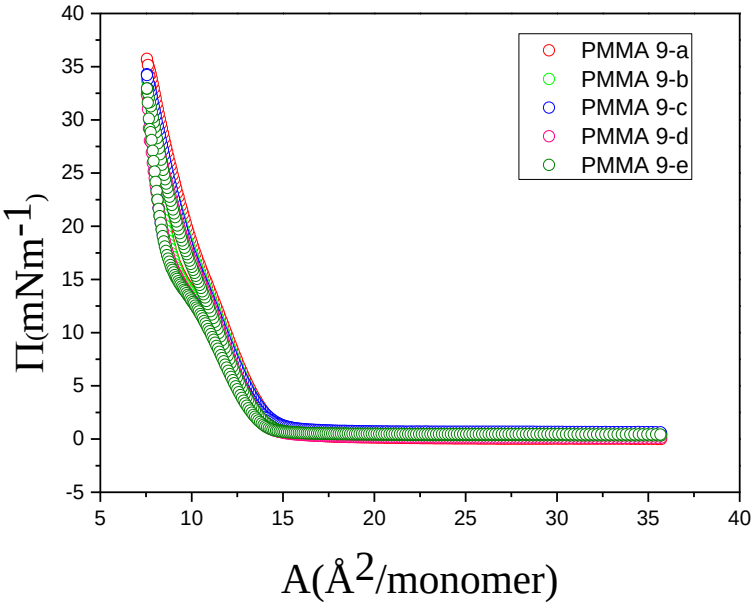

Figure 28: Reproducibility test for PMMA 9 (c=1mg/ml, V=25µl, T=25°C, barrier speed 10mm/min).

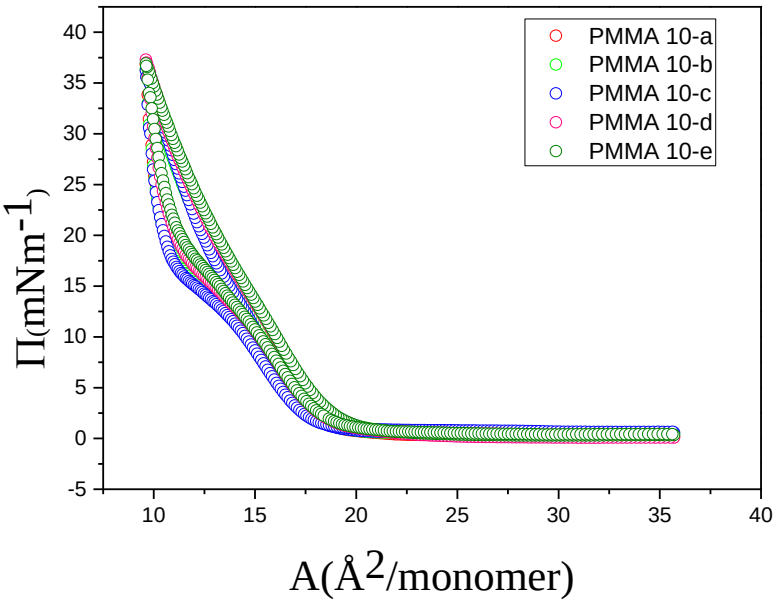

Figure 29: Reproducibility test for PMMA 10 (c=1mg/ml, V=25µl, T=25°C, barrier speed 10mm/min.

Figures 30 and 31 show the differences from the 1st to 5th circle with different final target pressure. Flory radius analysis of PMMA is shown at figures 32 and 33. The procedure for that analysis was the same as the one for atactic linear PMMAs. The results suggest that progressive cycling experiments are superposable at lowe surface pressures, confirming the reversibility of the layers below the plateau region. Above, there is a hysteresis on expansion following the compression test and an associated lack of superposition (albeit weak). This is more apparent for the highler molar mass (Fig. 31). More importantly, the layer appears to have a memory as the pressure profile follows the same path with continuous cycling of further increase of final target pressure.

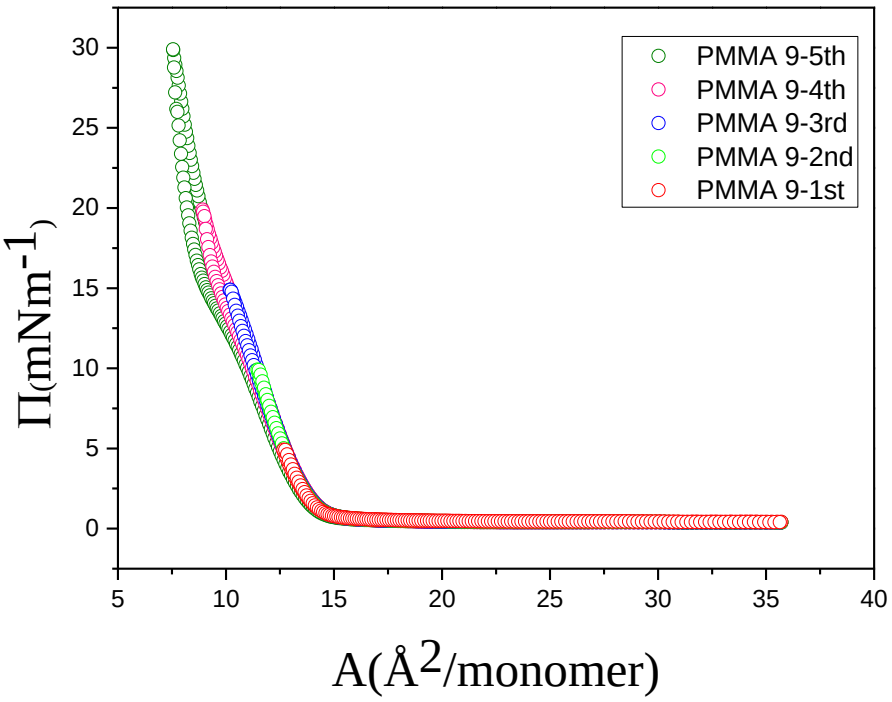

Figure 30: Compression - expansion data (pressure isotherm) for PMMA 9, 1st circle (red) has target pressure 5mNm-1, 2nd circle (green) has target pressure 10mNm-1, 3rd circle (blue) has target pressure 15mNm-1, 4th circle (pink) has target pressure 20mNm-1 5th circle (olive) has target pressure 30mNm-1 (c=1mg/ml, V=25μl, T=25°C, barrier speed 10mm/min).

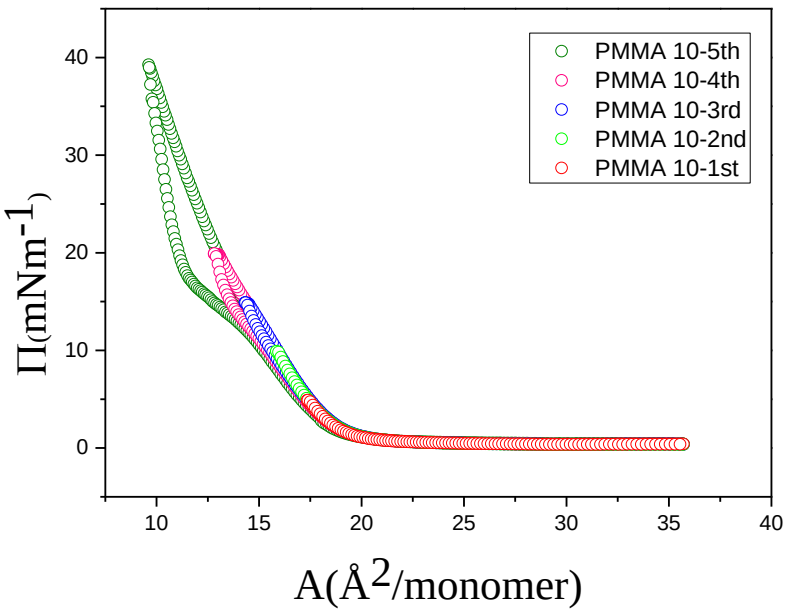

Figure 31: Compression - expansion data (pressure isotherm) for PMMA 10, 1st circle (red) has target pressure 5mNm-1, 2nd circle (green) has target pressure 10mNm-1, 3rd circle (blue) has target pressure 15mNm-1, 4th circle (pink) has target pressure 20mNm-1, 5th circle (olive) has target pressure 40mNm-1 (c=1mg/ml, V=25µl, T=25°C, barrier speed 10mm/min).

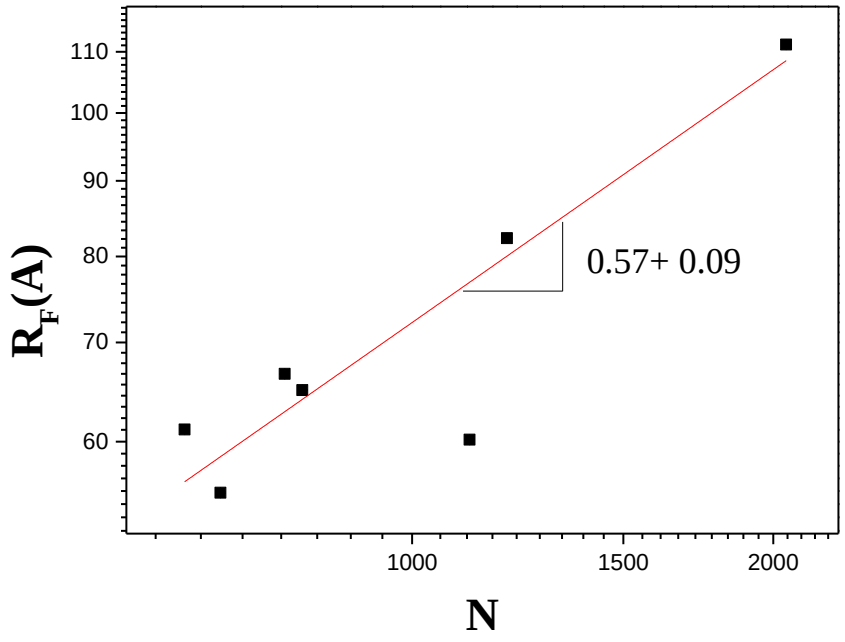

Figure 32: Flory radius analysis. The error bar is much smaller than the point size.

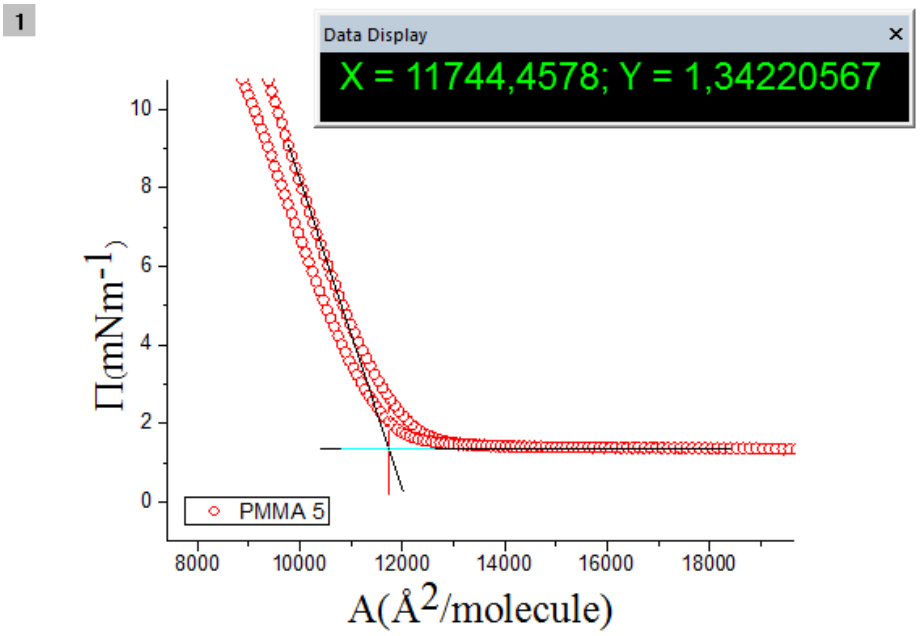

Figure 33: Graphic determination of the Flory radius. The area at the intersection is used to find RF.

There is reversibility to the PMMA linear syndiotactic samples before a specific pressure as we have demonstrated before (Figures 32 and 33). Flory radius analysis shows that the film departs from that like materials in theta solvent conditions. Hence, the material does not follow any known scaling law. On the other hand, significant scattering of the data may be the reason for deviation from known scaling predictions. Nevertheless, the difference between syndiotactic and atactic is unambiguous.

3.2.2. Interfacial Rheology

Rheological experiments were performed for linear syndiotactic PMMAs with different molecular weights. The temperature (T) was 25ºC, the volume (V) of the solution PMMA was 25µl, the plate was vertical to the trough, the spreading was symmetric and close to channel and we mix the layer twice. The following Figure 34 shows the result of these experiments. In Appendix II the results for all samples can be found. We observe that a terminal regime with $G'\sim\omega^2$ and $G''\sim\omega$ and G''>G' is not reached. Moreover the moduli appear to increase with surface pressure and follow essentially the same scaling with frequency.

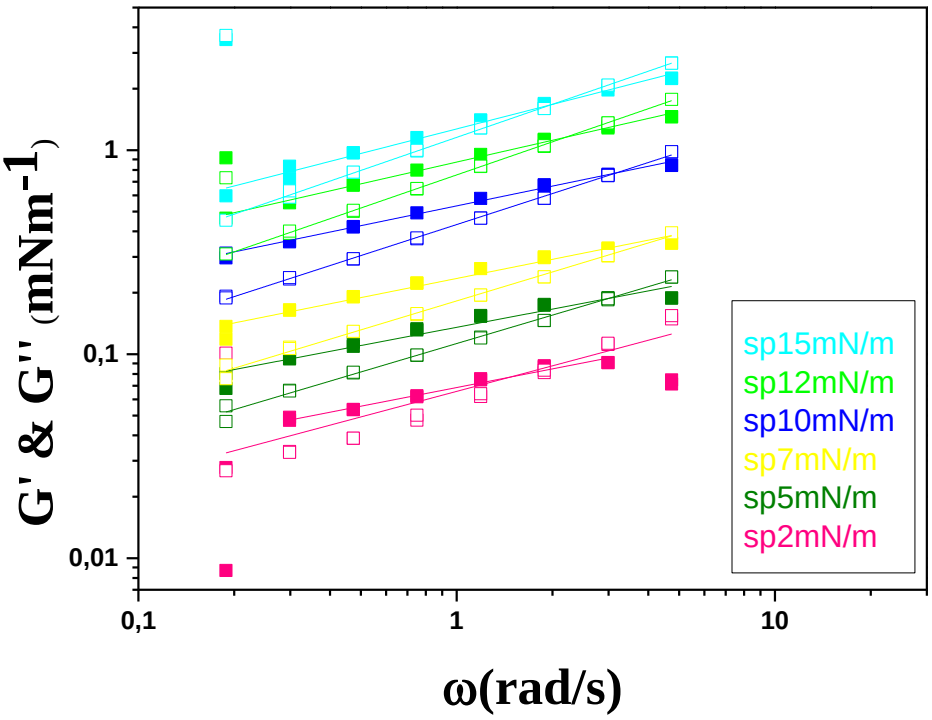

Figure 34: Rheology for linear sydiotactic PMMA 4. G' is symbol full, G" is symbol empty, c=1mg/ml, V=25µl, T=25ºC. Spreading close to channel, mixing of the layer. Lines are drawn to guide the eye.

We then proceeded with the analysis of the data. Equations (7) and (8) were used to calculate the data for the Figure 35. Remarks about viscosity and surface pressure were similar to those for linear atactic PMMA (see relevant chapter).

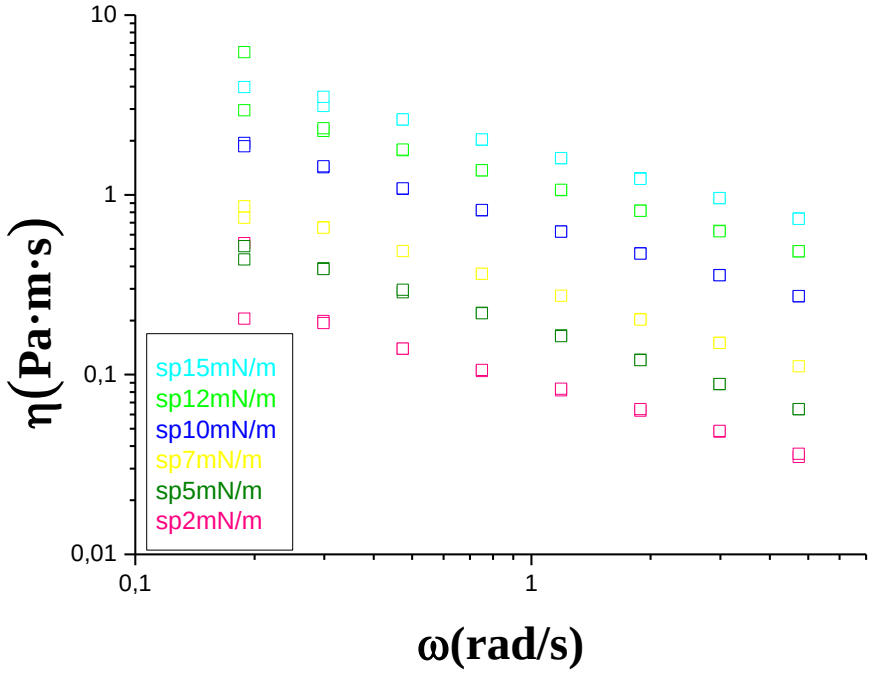

Figure 35 : Zero- shear viscosity vs frequency for PMMA 4.

We analyze the experimental results and we find that G' and G'' increase with increasing surface pressure. There is a characteristic time where G' and G'' crossed over each other, which is independent from the molecular weight. The viscosity data are of course consistent with the viscoelastic moduli. Zero-shear viscosity cannot be extracted.

3.3. DENDRITIC PMMA: EFFECT OF MOLECULAR WEIGHT ON STRUCTURE AND RHEOLOGY

3.3.1. Surface Pressure Area Isotherms

Figures 36 and 37 show the compression- expansion experiment of dendritic PMMAs (G1 and G4). The experiment was performed at temperature 25ºC, volume of the solution PMMA 25μl and with the Wilhelmy plate vertical to the trough.

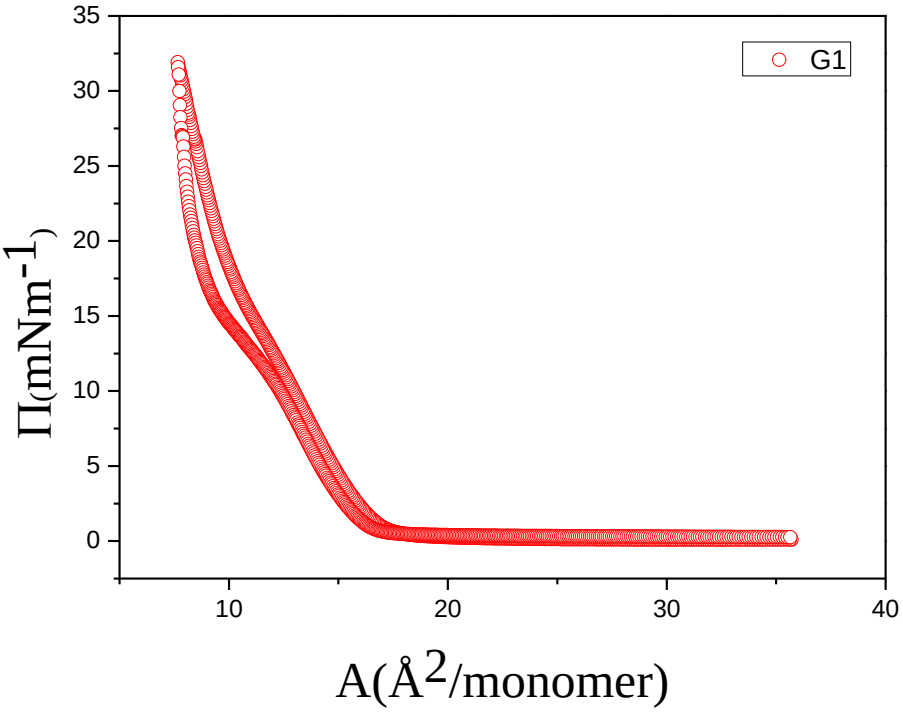

Figure 36: Compression - expansion data (pressure isotherm) for dendritic PMMA G1 (c=1mg/ml, V=25μl, T=25ºC, barrier speed 10mm/min).

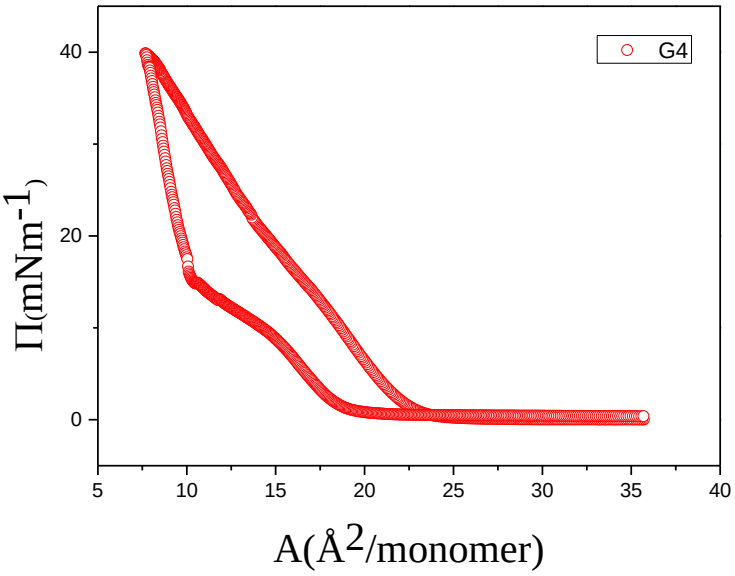

Figure 37: Compression - expansion data (pressure isotherm) for dendritic PMMA G4 (c=1mg/ml, V=25μl, T=25°C, barrier speed 10mm/min).

Initially, experiments of reproducibility (Figures 38, 39) were performed to verify the stability of the results.

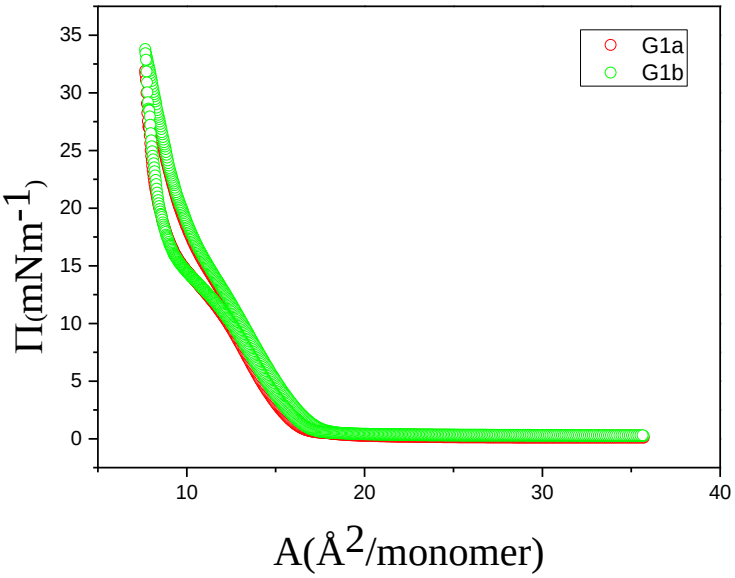

Figure 38: Reproducibility test for PMMA G1 (c=1mg/ml, V=25μl, T=25°C, barrier speed 10mm/min).

We observe reversibility of the PMMA dendritic layers before a specific pressure (about 15mNm^{-1}) as seen in Figure 38.

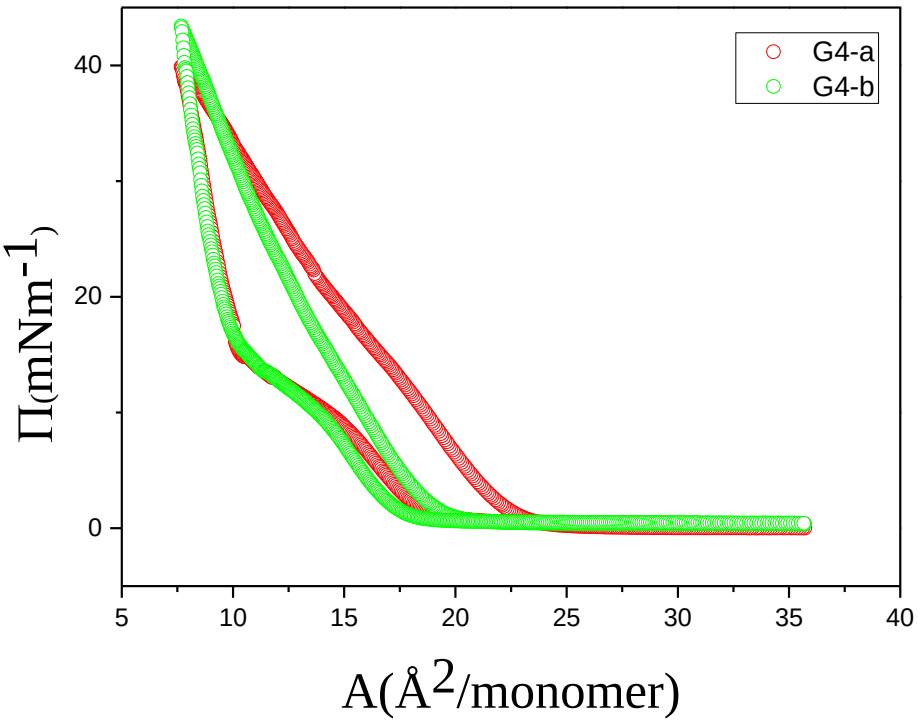

Figure 39: Reproducibility test for PMMA G4 (c=1mg/ml, V=25μl, T=25°C, barrier speed 10mm/min).

Figure 40 shows the differences from the 1st to 4th circle with different final target pressure. The Flory radius analysis (Figures 41 and 42) suggests behavior akin to ideal conditions but unfortunately the fact that we have only two data points prohibits strong statements concerning lack of architecture effects (generation) on the static properties.

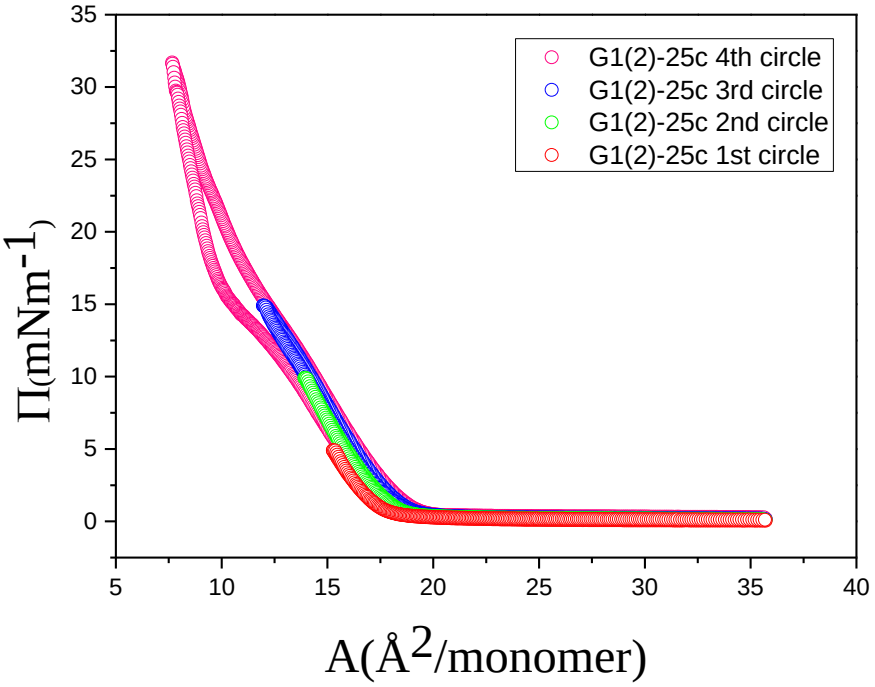

Figure 40: Compression - expansion data (pressure isotherm) for G1, 1st circle (red) has target pressure 5mNm-1, 2nd circle (green) has target pressure 10mNm-1, 3rd circle (blue) has target pressure 15mNm-1 and 4th circle (pink) is the full compression and expansion (c=1mg/ml, V=25µl, T=25°C, barrier speed 10mm/min).

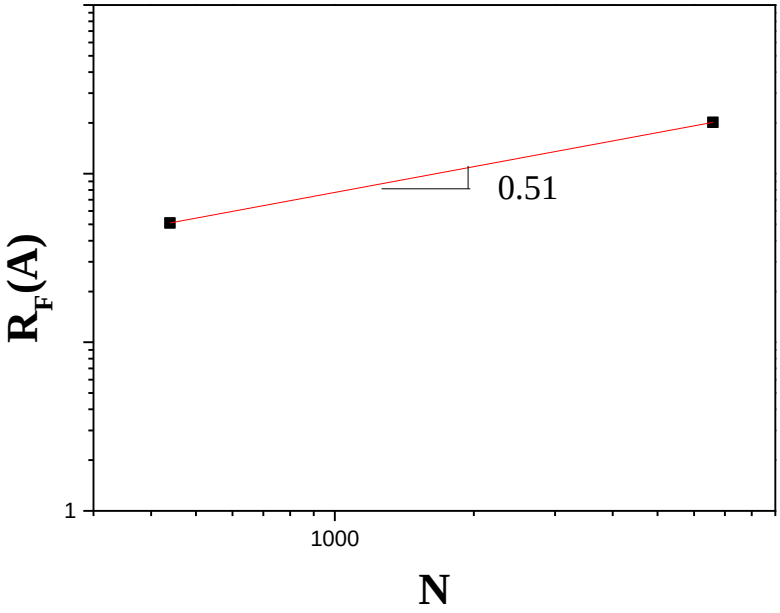

Figure 41: Flory radius analysis. The error bar is much smaller than the point size.

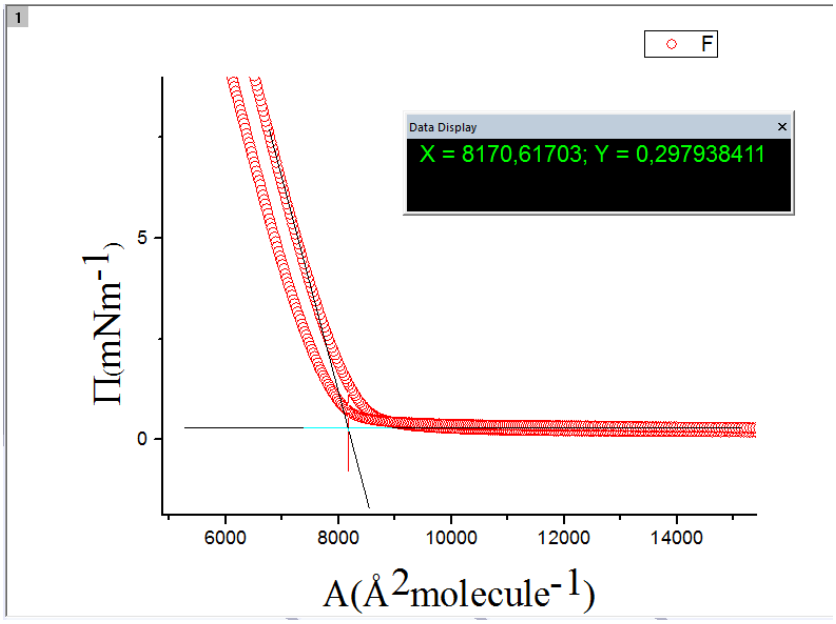

Figure 42: Graphic determination of the Flory radius. The area at the intersection is used to find RF.

3.3.2. Interfacial Rheology

Dendritic PMMAs were subjected to rheological experiments. The temperature (T) was 25ºC, the volume (V) of the solution PMMA was 25µl, the plate was vertical to the trough, the spreading was symmetric and close to the channel and we mixed the layer. The following Figures 43 and 44 show the dynamic frequency sweeps and the analysis of dendritic PMMAs with different surface pressures. We observe that a terminal regime with G'~ω2 and G"~ω and G">G' is not reached. Moreover the moduli appear to increase with surface pressure and follow essentially the same scaling with frequency.

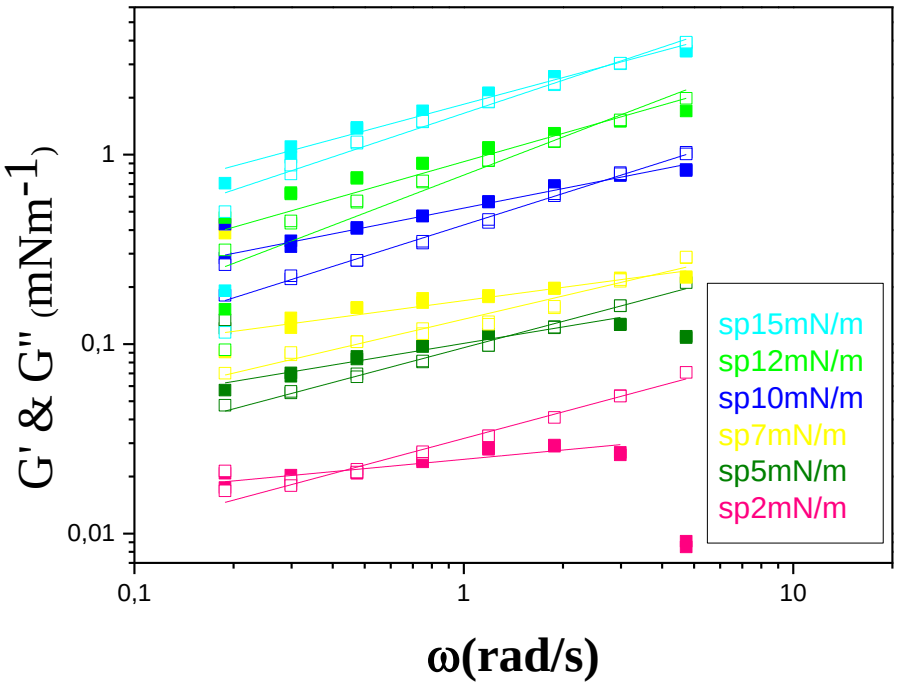

Figure 43: Rheology for dendritic PMMA G1, G' is symbol full, G" is symbol empty, c=1mg/ml, V=25µl, T=25ºC. Lines are drawn to guide the eye.

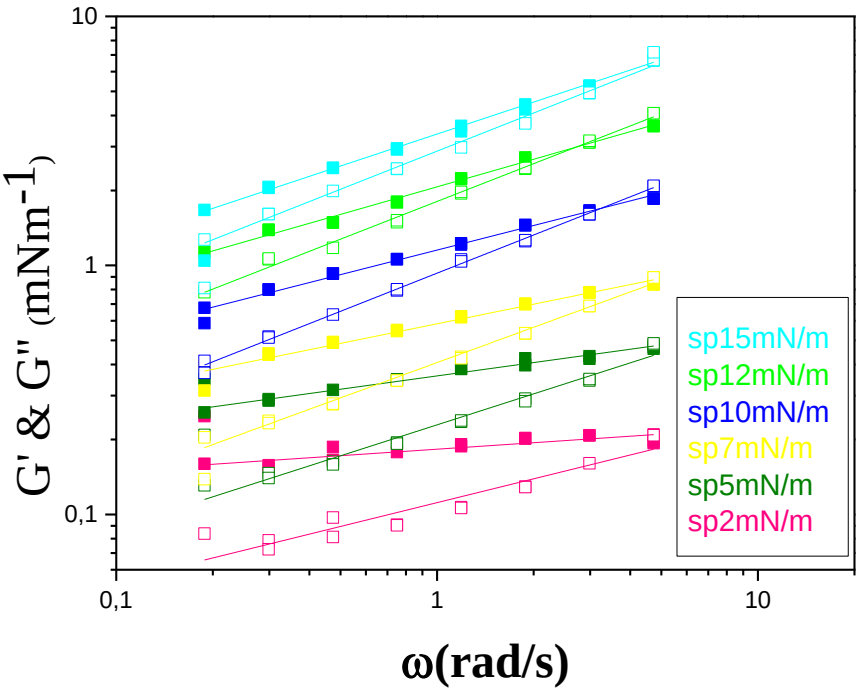

Figure 44: Rheology for dendritic PMMA G4, G' is symbol full, G'' is symbol empty, c=1mg/ml, V=25μl, T=25°C. Lines are drawn to guide the eye.

Finally the equations (7) and (8) were used to demonstrate the data of the following figures (Figure 45, 46). As in linear syndiotactic polymers, the observations about viscosity and surface pressure were the same as linear atactic PMMA (see relevant chapter).

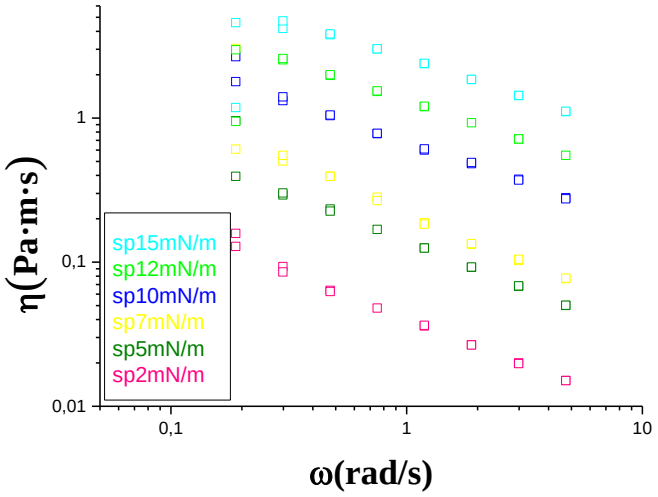

Figure 45: Zero- shear viscosity vs frequency for PMMA G1.

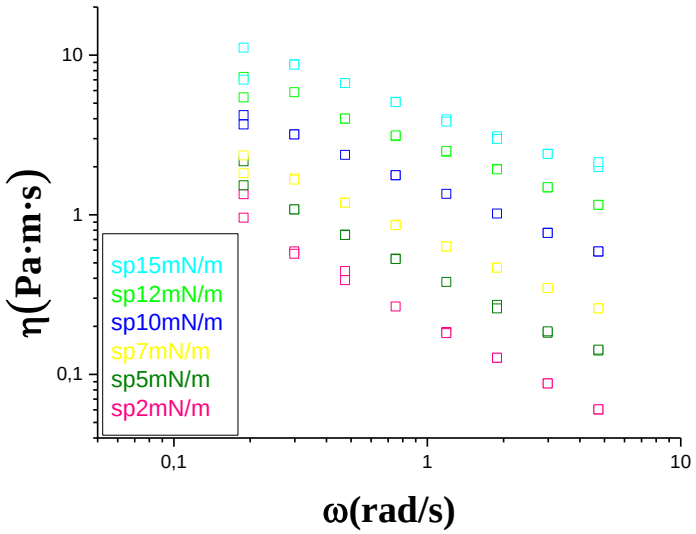

Figure 46: Zero- shear viscosity vs frequency for PMMA G4.

We verify that G' and G'' became higher with the increase of the surface pressure. There is a characteristic time where there is a crossover between G' and G'' (Figures 43 and 44). This time is independent from the molecular weight. Finally graphs viscosity versus frequency show absence of terminal regime.

3.4. LINEAR PBA AT AIR-WATER INTERFACE: STRUCTURAL AND RHEOLOGICAL EXPERIMENTS

3.4.1. Surface Pressure Area Isotherms

Figures 47 shows the compression –expansion measurement of the linear PBA. The temperature (T) was 25ºC, the volume (V) of the solution PBA was 20μl, the plate was vertical to the trough and the spreading was symmetric.

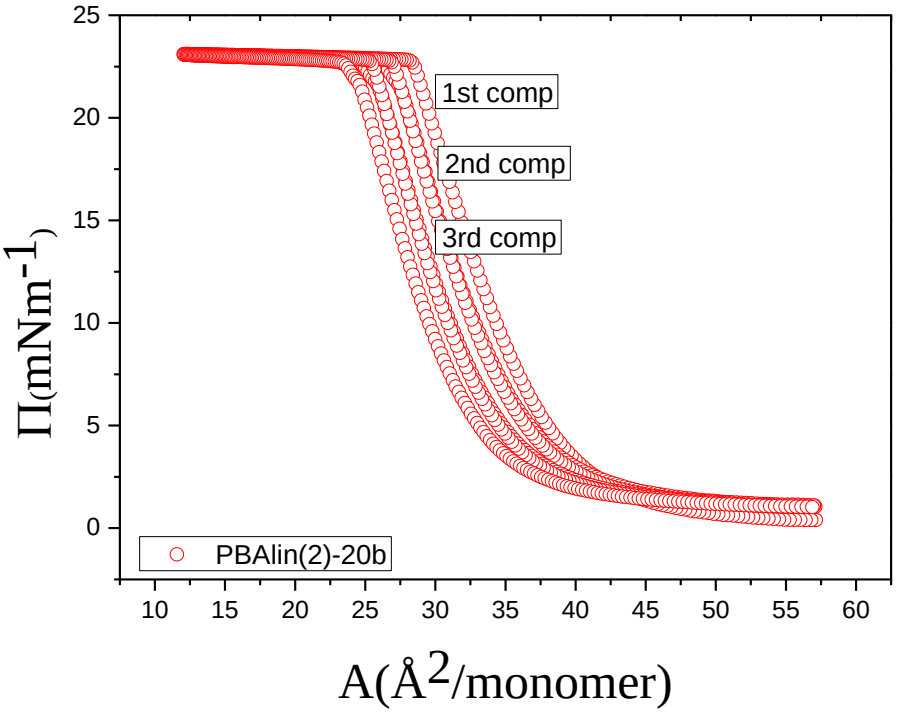

Figure 47: Compression - expansion data (pressure isotherm) for linear PBA (c=1mg/ml, V=20μl, T=25ºC, barrier speed 10mm/min).

The area in the figures indicate the energy (E~Π*A) which is dissipated in each circle. Furthermore, Figure 48 shows the differences from the 1st to 2nd or 3rd circle (comp) with different final target pressure. We note that after the plateau the layer is not reversible. For this reason, we did many circles of compression and expansion and the results are shown in figure 49 where we can observe that after nine full circles the difference between compression and expansion became less. On the other hand, two observations are suggestive: (i) final surface pressure is identical, hence there is no evidence of loss of material. (ii) the onset area for pressure increase becomes progressively smaller, hence the layer is being reorganized with possible more of material close to the barriers and/or some buckling.

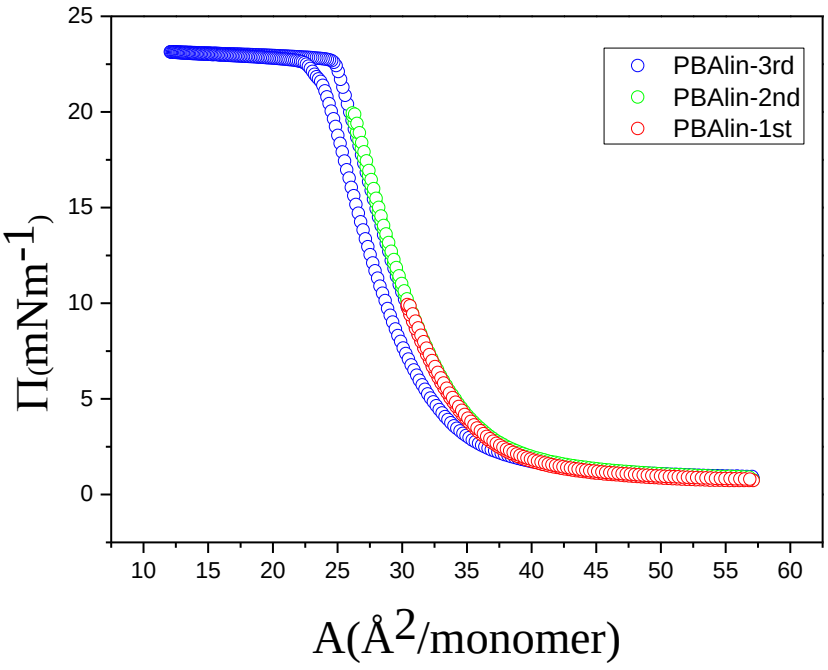

Figure 48: Compression - expansion data (pressure isotherm) for linear PBA, 1st circle (red) has target pressure 10 mNm-1, 2nd circle (green) has target pressure 20mNm-1 and 3rd circle (blue) is the full compression and expansion (c=1mg/ml, V=20μl, T=25°C, barrier speed 10mm/min).

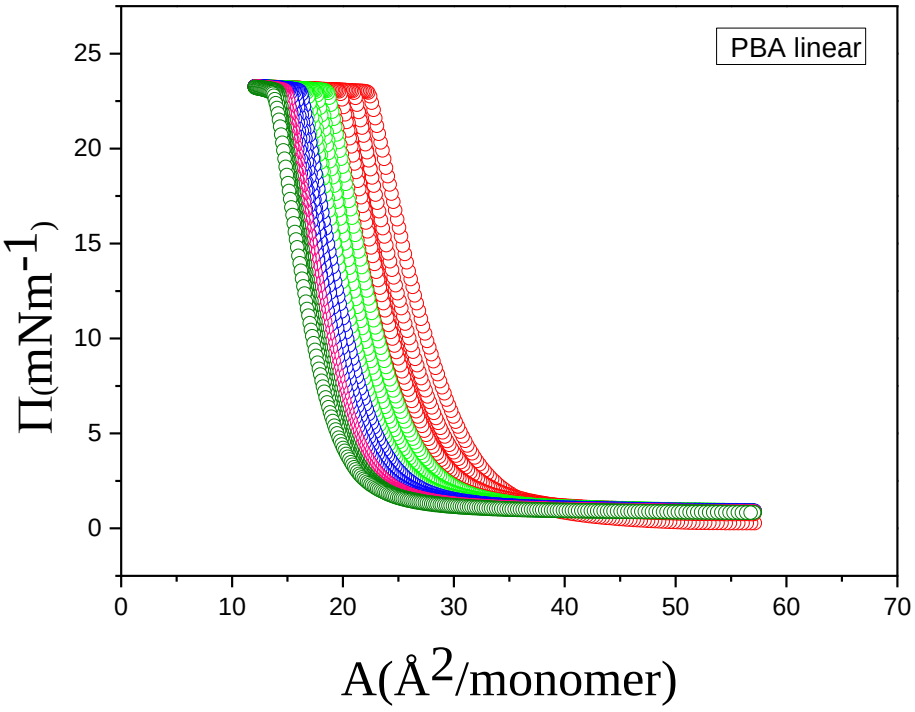

Figure 49: Compression - expansion data (pressure isotherm) for linear PBA Each color consist from three circles (c=1mg/ml, V=20µl, T=25°C, barrier speed 10mm/min).

3.4.2. Interfacial Rheology

Rheological measurements were performed at temperature (T) 25ºC with the volume (V) of the solution PBA 20μl, the Wilhelmy plate was vertical to the trough and the spreading symmetric around and close to channel. We did not mix the layer and the following Figure 50 shows the rheology of that sample. Also we measured a new layer after fifteen full circles and figure 51 depicts the results. At the first experiment we show a difference when we increase the pressure but at the second one not. We have to note that in both cases the results are close to the results of measuring water without a layer at the top.

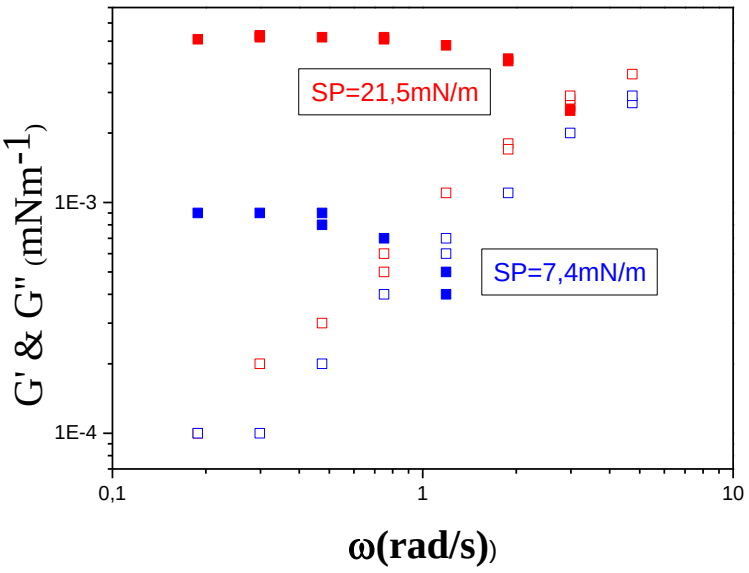

Figure 50: Rheology for linear PBA, G' is symbol full, G" is symbol empty, c=1mg/ml, $V_{(blue)}$=30μl, $V_{(red)}$=40μl, T=25ºC Spreading close to channel, without mixing of the layer.

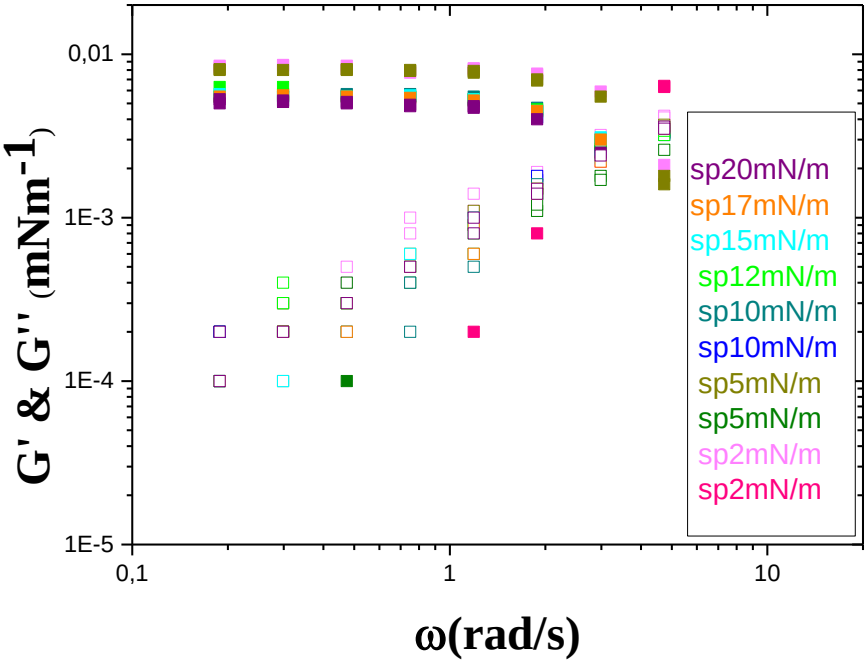

Figure 51: Rheology linear PBA, G' is symbol full, G" is symbol empty, c=1mg/ml, V=20µl, T=25°C Spreading close to channel, Mixing of the layer.

Compared to PMMA the rheological signal is very weak, at the limit of the resolution. We conclude that at present conditions the rheology of PBA layer could not be resolved.

3.5. STAR PBA: EFFECT OF MOLECULAR WEIGHT ON STRUCTURE AND RHEOLOGY

3.5.1. Surface Pressure Area Isotherms

Another set of samples which we study at this thesis is PBA star polymers. Unlike atactic PMMA, the glass transition of PBA is very law, here about -55ºC. Figure 52 shows a characteristic example of the behavior of PBA star samples. The temperature (T) was 25ºC, the volume (V) of the solution PBA was 25μl, the plate was vertical to the trough and the spreading was symmetric. This sample exibits the same behavior with the linear PBA. There is a high-pressure plateau and figure 53 depicts the change after repeated compression- expansion cycles. As noted before, there is no evidence of material but of layer rearrangemet instead (maybe same material accumulated closer to the barriers) At the same time, a weak layer irreversibility is observed. Appendix III reports the results for all the samples.

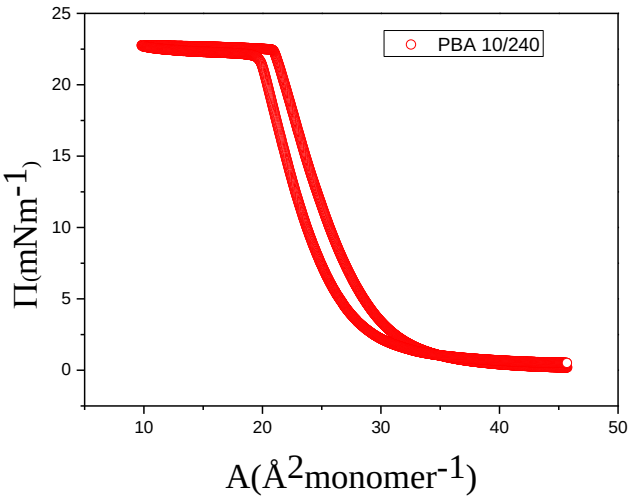

Figure 52: Compression - expansion data (pressure isotherm) for PBA 10/240 (308k), (c=1mg/ml, V=25µl, T=25°C, barrier speed 10mm/min).

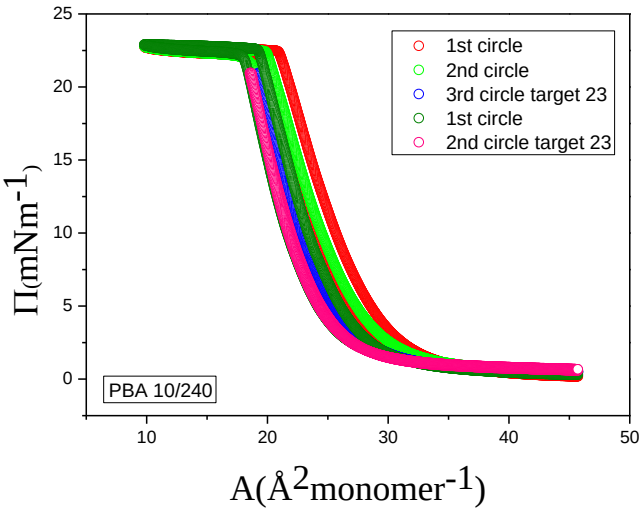

Figure 53: Reproducibility test for PBA 10/240, 1st circle (red) and 2nd circle (light green) show all the compression and expansion, 3rd circle (blue) has target pressure 23mNm-1, 1st circle (olive) show all the compression and expansion and 2nd circle (pink) has target pressure 23mNm-1 (c=1mg/ml, V=25µl, T=25°C, barrier speed 10mm/min).

In figure 54 we compare the PBA samples with respect to pressure isotherms. We observe a faster onset of pressure increase (at large area) as we increase the molecular weight. This point to different layer at highter molecular weight.

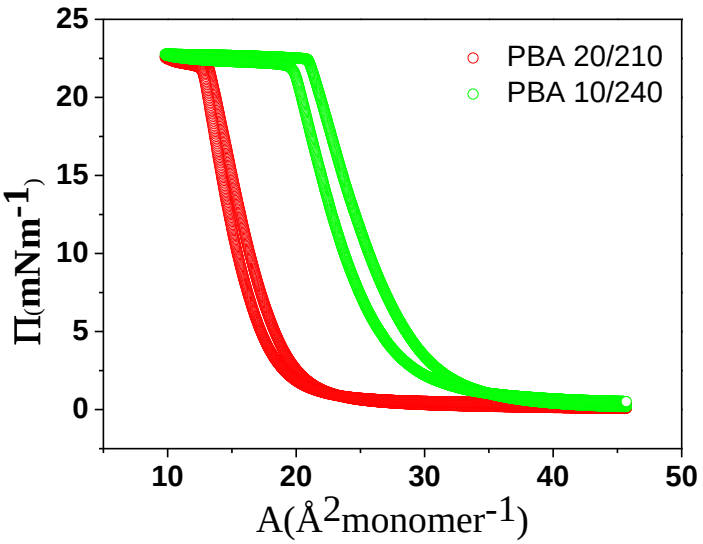

Figure 54: Compression - expansion data (pressure isotherm) for star PBA(c=1mg/ml, V=25µl, T=25°C, barrier speed 10mm/min) 10/240 and 20/210.

The Flory radius analysis of PBA is shown at figures 55 and 56. The procedure used to extract R_F was the same as for PMMA. Results suggest that film behaves like 2D materials in theta or bad solvent conditions (Figure 55).

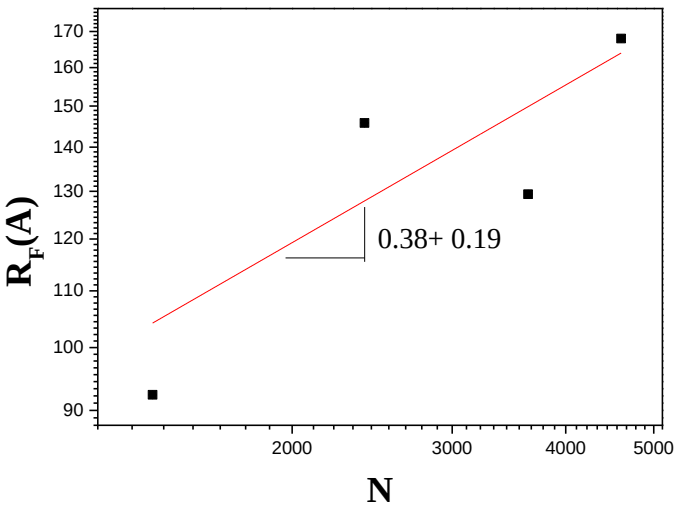

Figure 55: Flory radius analysis. The error bar is much smaller than the point size.

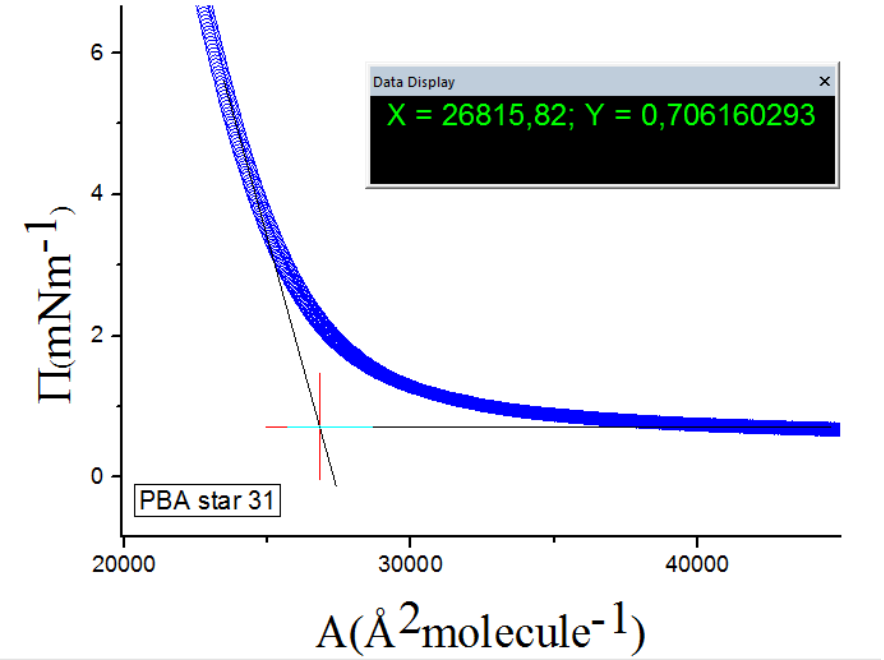

Figure 56: Graphic determination of the Flory radius. The area at the intersection is used to find RF.

3.5.2. Interfacial Rheology

Rheological measurements were also conducted with these samples (Figure 57). Unfortunately we have the same behavior as with linear PBA. The results are the same with water subphase although there is a layer of PBA at the surface. Therefore, we understand that we cannot measure this material because the signal is very weak. Hence, we did not pursue the rheological investigation further.

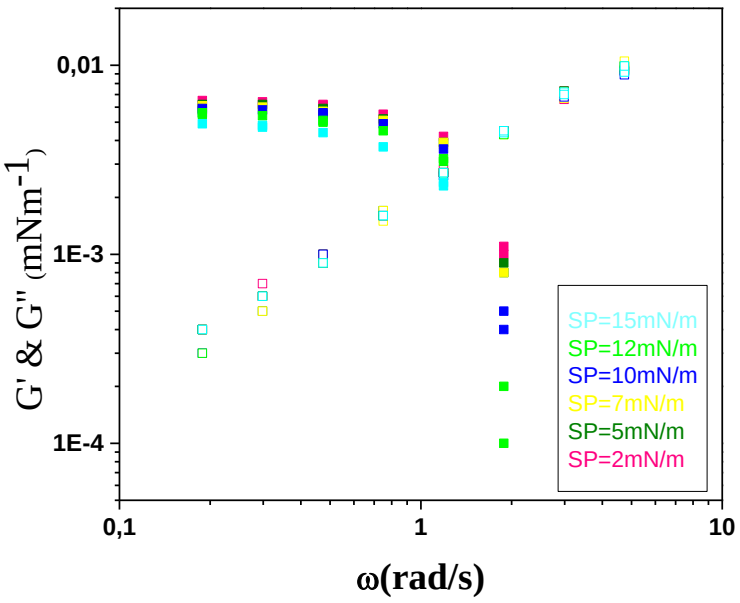

Figure 57: Rheology for star PBA 10/240, G' is symbol full, G" is symbol empty, c=1mg/ml, V=25µl, T=25°C Spreading close to channel, Mixing of the layer.

3.6. ATACTIC - SYNDIOTACTIC LINEAR PMMA: COMPARISON

3.6.1. Surface Pressure Area Isotherms

Figure 58 shows the compression- expansion experimet of atactic and syndiotactic PMMAs (PMMA65k, PMMA 5 and PMMA 120k, PMMA 11).

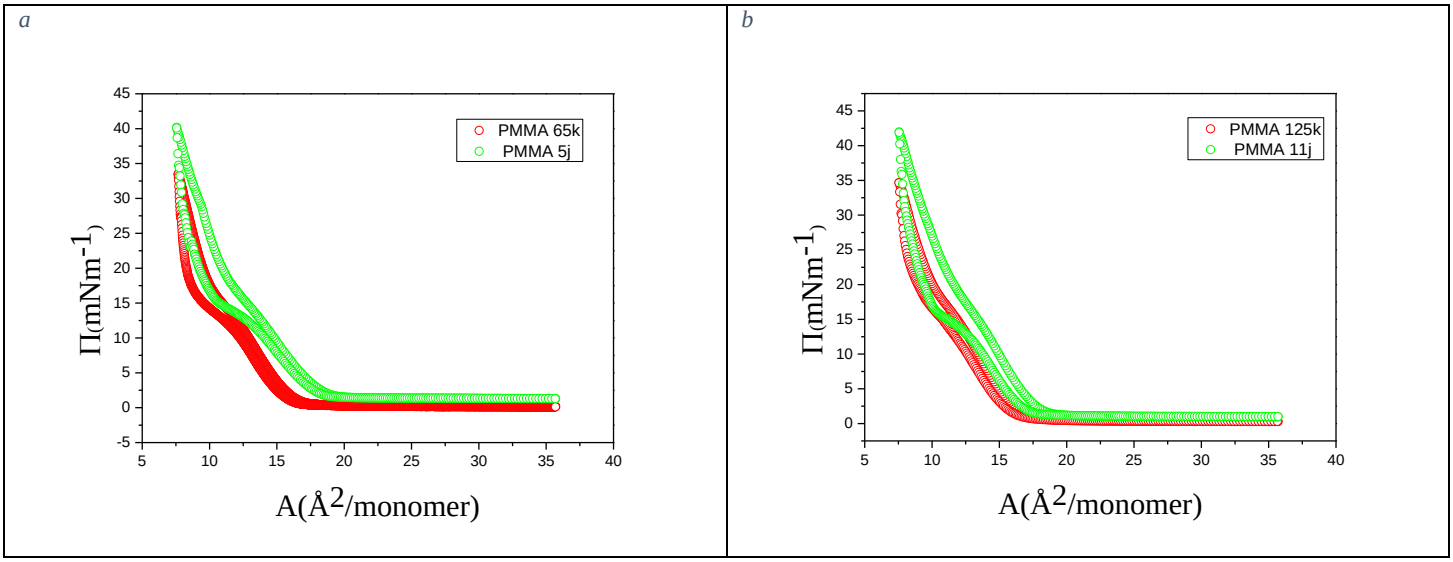

Figure 58: Compression - expansion data (pressure isotherm) for atactic and syndiotactic PMMAs (c=1mg/ml, V=25μl, T=25°C, barrier speed 10mm/min).

It is observed that in both graphs the green curve (syndiotactic) increases at higher area even though the samples have the same Mw and spreading volume. This behavior implies that molecules interact earlier for the case of syndiotactic PMMA. A possible explanation is that due the tacticity they take up more space at the interface. Another point we wish to make is that for the same compression, syndiotactic PMMA molecules reach larger pressure. Finally, hysteresis during expansion is more enhanced for syndiotactic PMMA.

Flory radii are compared in figure 59. Flory radius analysis shows that the film behaves like materials in theta solvent conditions for atactic PMMA and like materials in good solvent conditions for syndiotactic samples. However, due to limited data available we reframe from drawing definite canclusions.

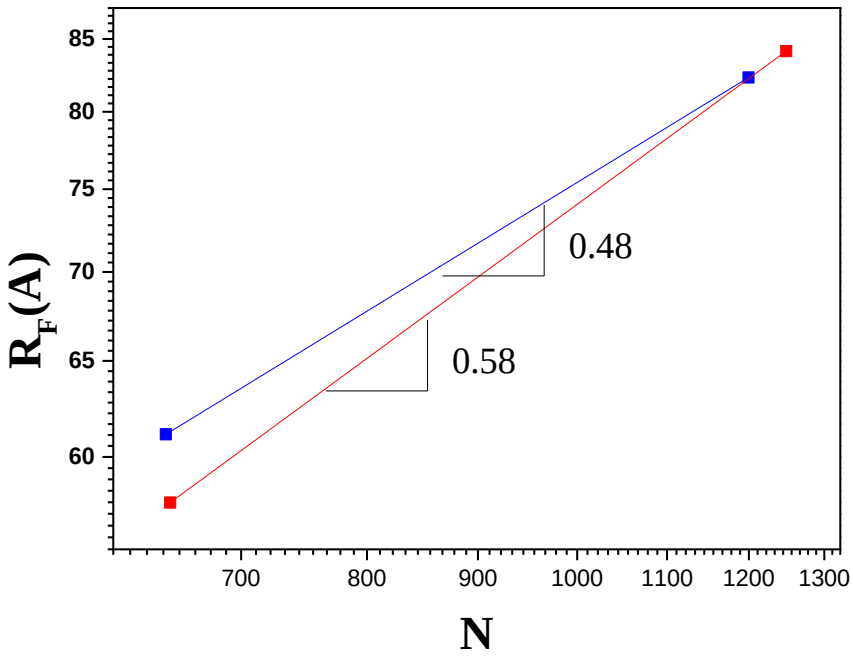

Figure 59 : Flory radius analysis. Red line is for the linear atactic PMMAs and blue line is for the linear syndiotactic PMMAs. The error bar is much smaller than the point size.

3.6.2. Interfacial Rheology

Rheological experiments are compared in figure 60 for different molecular weights. Note that the molecular weight of PMMA 5 is close to PMMA 65k and PMMA 11 is close to PMMA 125k.

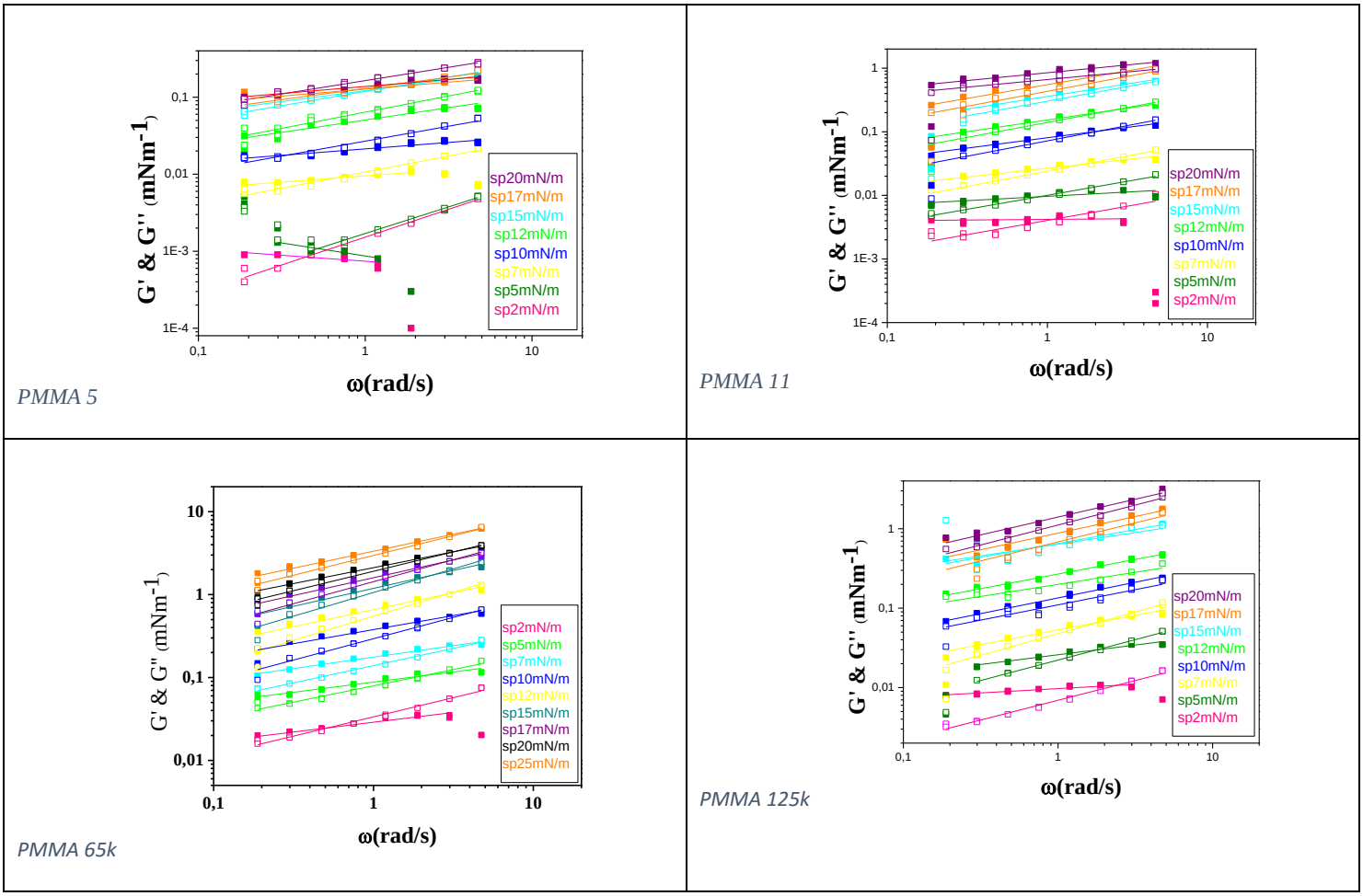

Figure 60: Rheology for dendritic and linear PMMAs, G' is symbol full, G" is symbol empty, c=1mg/ml, V=25µl, T=25°C Spreading close to channel, Mixing of the layer. Lines are drawn to guide the eye.

We did not observe any major qualitative difference in the plots. However, there are quantitative differences: PMMA 65 has higher moduli (typically by one decade), whereas the respective difference for higher molecular weight (125k) are less than factor of 2. Though we do not have a clear explanation at present, we tentatively attribute the differences to the

different layer organization. Hence, the compression and expansion of atactic and syndiotactic PMMA depend both on molecular weight and configuration. G’ and G’’ increased with increasing surface pressure. There is a characteristic time where G’ and G’’ crossed. This time is independent of the molecular weight. Finally, graphs zero- shear viscosity versus frequency show absence of terminal regime.

3.7. ATACTIC LINEAR - DENDRITIC PMMA: COMPARISON

3.7.1. Surface Pressure Area Isotherms

Figure 61 depics the comparison of compression- expansion measurements of dendritic and linear PMMAs (G1, PMMA and G4, PMMA).

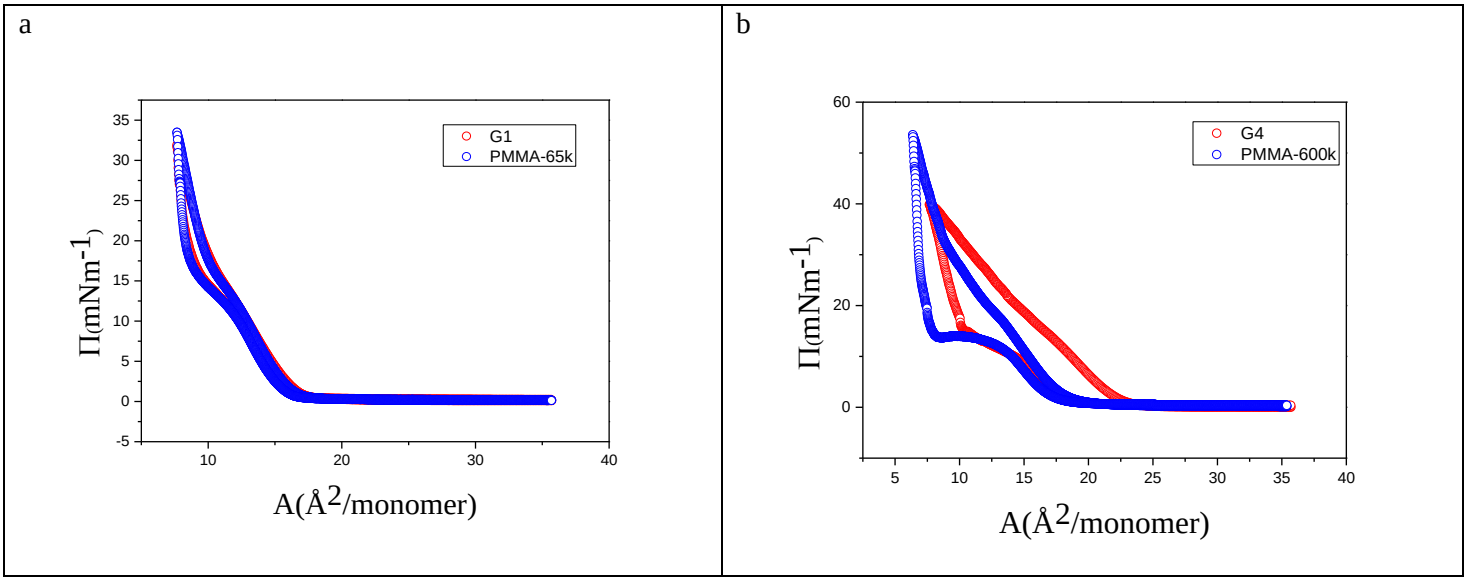

Figure 61: Compression - expansion data (pressure isotherm) for dendritic and linear PMMAs (c=1mg/ml, V=25μl, T=25°C, barrier speed 10mm/min).

As we can see on the left graph, where we compare a linear atactic PMMA with Mw of 65k, and the first generation dendritic PMMA with molecular weight of 44k, the curves coincide. That may imply that dendritics take up more surface and we need less quantity to achieve the same results. This is consistent with the right graph, where there is small difference in molecular weight and the pressure of the dendritic (red curve) rises earlier (at lower area). We conclude that the compression and expansion of linear and dendritic PMMA depends more on total the molecular weight than configuration.

Flory radii are identical, as shown at figure 62.

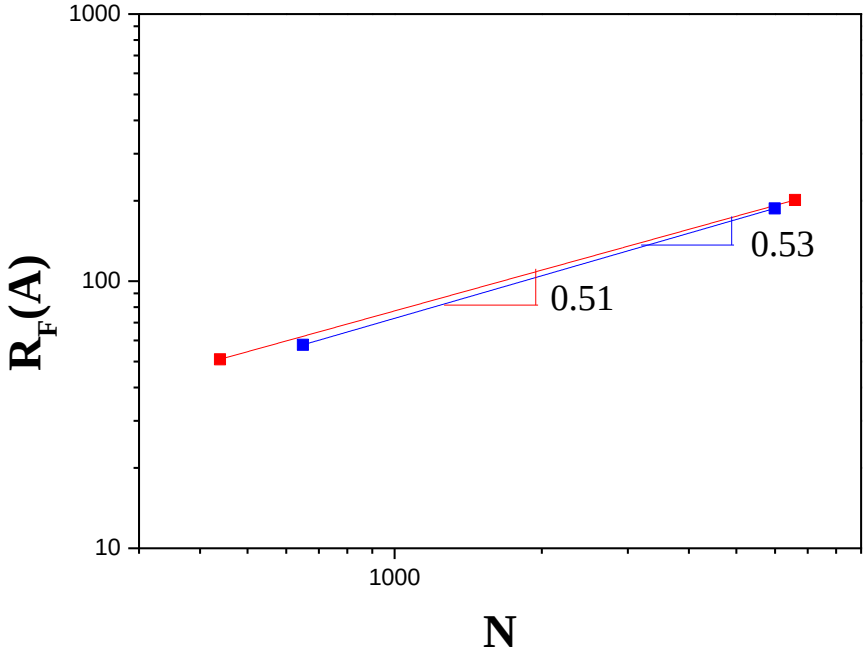

Figure 62: Flory radius analysis. Red line is for the dendritic PMMAs and blue line is for the linear PMMAs. The error bar is much smaller than the point size.

3.7.2. Interfacial Rheology

Rheological measurements are performed in figure 63 at different molecular weights and the same conditions. The molecular weight of G1 is close to PMMA 65k and about G4 is close to PMMA 600k.

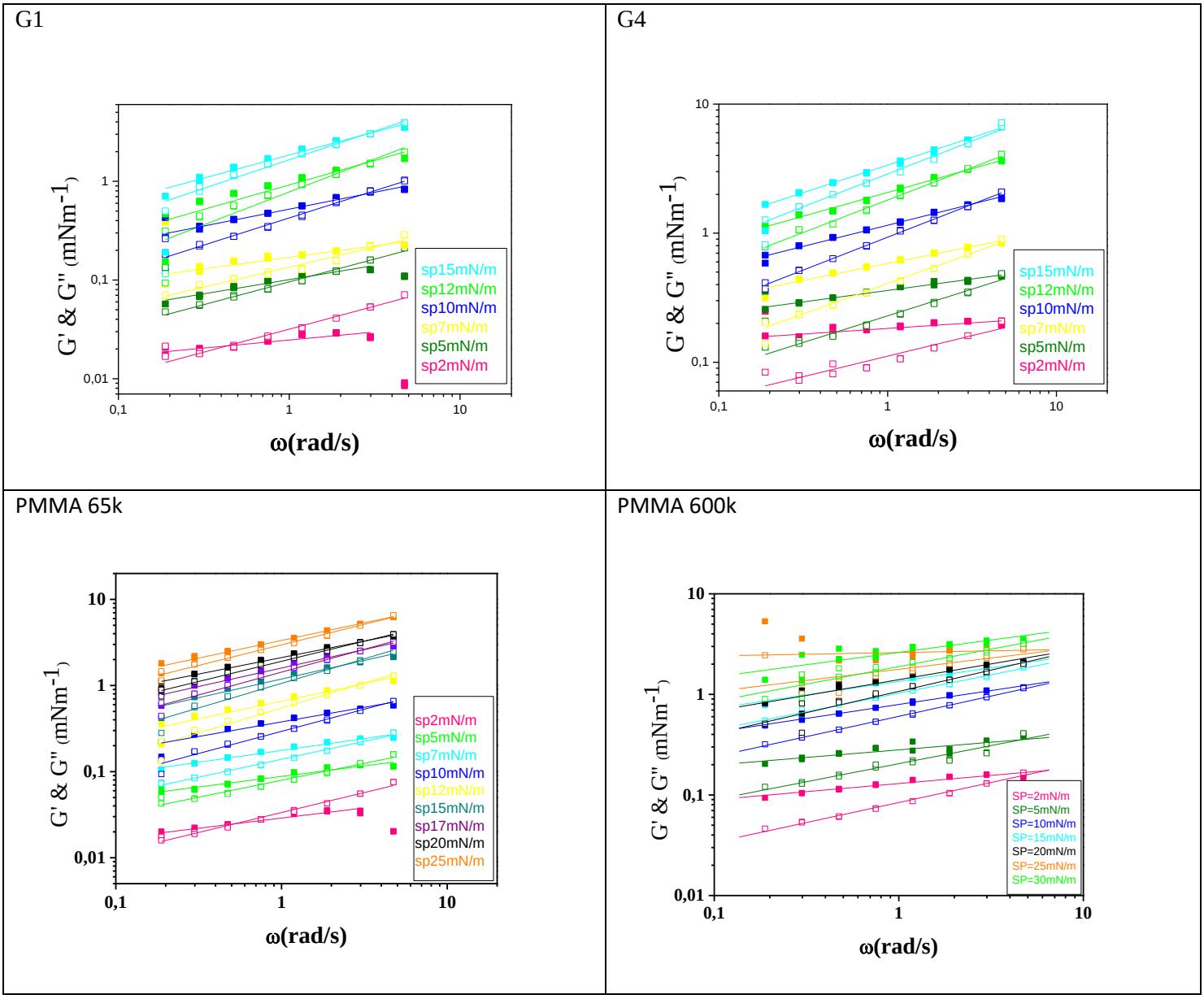

Figure 63: Rheology for dendritic and linear PMMAs, G' is symbol full, G" is symbol empty, c=1mg/ml, V=25µl, T=25°C Spreading close to channel, Mixing of the layer. Lines are drawn to guide the eye.

The emerging pictures is that of neither qualitative nor quantitative difference between the two differente types. One can only note slight smaller slopes for linear PMMA, especially at larger molar masses. There is a characteristic time where G’ and G’’ crossed. This time is independent of molecular weight and finally graphs zero-shear viscosity versus frequency show absence of terminal regime.

3.8. ATACTIC LINEAR PMMA: EFFECT OF CONCENTRATION ON STRUCTURE AND RHEOLOGY

As already mentioned, another control parameter for polymeric layers is the concentration of the polymer solution spread at the interface. We have explored this for glassy atactic linear PMMA. The motivation for studying its effect have comes from the fact that upon dropwise deposition at the interface, chloroform evaporates fast and PMMA vitrifies. Hence, glassy discs are formed, which will not form a coherent network on compression. To investigate the properties of network at the interface, we deposit drops from high concentration well above the overlap concentration c*, hence (vitrified) networks of PMMA can be formed. The experiments were performed with the atactic linear PMMA of molecular weight 600k. The temperature was 25ºC and the volume of the solution PMMA was 10μl. Concentrations 1.5mg/ml, 15mg/ml, 30mg/ml, 45mg/ml and 60mg/ml were used as we can see in figure 64.

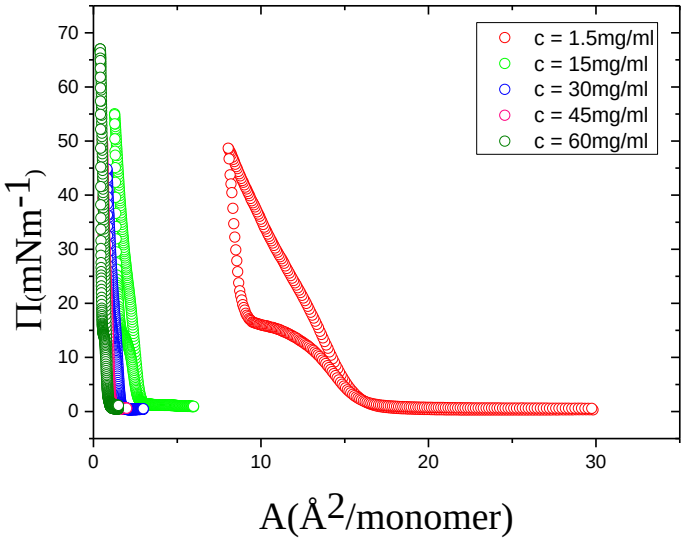

Figure 64: Compression - expansion data (pressure isotherm) for PMMA 600k (c=1.5mg/ml, 15mg/ml, 30mg/ml, 45mg/ml, 60mg/ml, V=10µl, T=25ºC, barrier speed 10mm/min).

We observed that the pressure isotherms do not overlap, suggesting a strong heterogeneity of the layers. To further explore this possibility so rheological experiments were conducted. However, these experiments could not be performed due to exactly this reason, i.e., the layer heterogeneity. Figure 67 attempts at showing this situation (visible to naked eye).

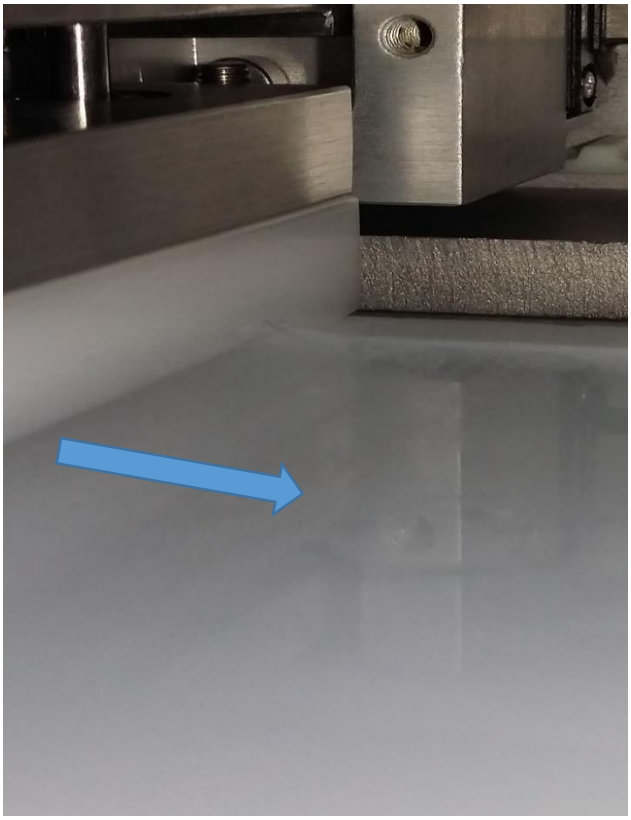

Figure 65: Heterogeneous layer of glassy PMMA 600k at concentration 15mg/ml.

We conclude that increasing concentration, a polymer network is created on deposition. The whole network is glassy at temperatures below Tg, as can be seen on Figure 65. This leads to large surface heterogeneities, which are responsible for the great difference of compression and expansion curves at higher concentrations when compared with 1.5 mg/ml sample (Figure 66).

3.9. PMMA NETWORK IN STEP COMPRESSION: RELAXATION TIME OF THE LAYER

To obtain an indication of relaxation time, step compression experiments were conducted with the same sample (PMMA 600k) at different concentrations and pressures. The procedure was the following: Initially the trough was cleaned and then the spreading became symmetric. We waited 15 min for the solvent to evaporate and then mixed the layer twice. Subsequently, the layer was compressed to a target pressure and the drop of the pressure was recorded. Figure 66 is an example from these experiments. In Appendix IV there all results and comparisons between relaxation time versus concentration and pressure are reported.

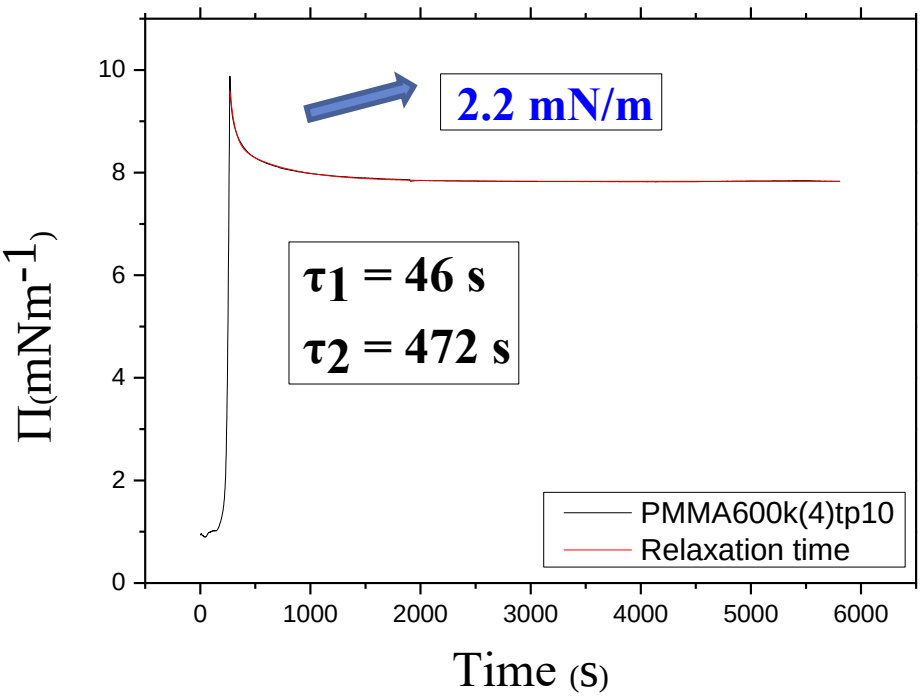

Figure 66: Relaxation time of PMMA600k c=15mg/ml, target pressure=10mN/m, V=10μl, T=25ºC.

It is evident that there is a decay in pressure which eventually reaches a non- zero plateau. The following equation with double exponential decay was used in order to extract relaxation time.

$$\Pi = A_1 e^{\frac{-t}{\tau_1}} + A_2 e^{\frac{-t}{\tau_2}} + \Pi_o \quad (9)$$

where, Π is the pressure, τ_1 and τ_2 are the fast and slow relaxation time respectively and Π_o is the final pressure.

Overall the layer relaxation on compression suggests stiff, viscoelastic solid-like response of a highly heterogeneous sample. This finding, together with the high Tg of PMMA, leads again to the conclusion that there are glassy areas in the layer.

4. DISCUSSION

We have investigated the structural and rheological properties of molecular systems at the air-water interface, as well as the stability of the formed films. We used a series of two different acrylic polymers, PMMA and PBA with different architectures, linear atactic and syndiotactic, dendritic and star systems. All systems investigated revealed the important role of the microstructural details of the film components in driving the rheological response of the layers and the interplay between structure and mechanical response.

PMMA seems to be reversible up to the phase transition point, where the slope of the pressure curve changes, or there is a plateau at 15mN/m. It is evident that there is hysteresis (Figure 67). That phenomenon happens because glassy PMMA molecules are slow to reexpand to a previous equilibrium state.

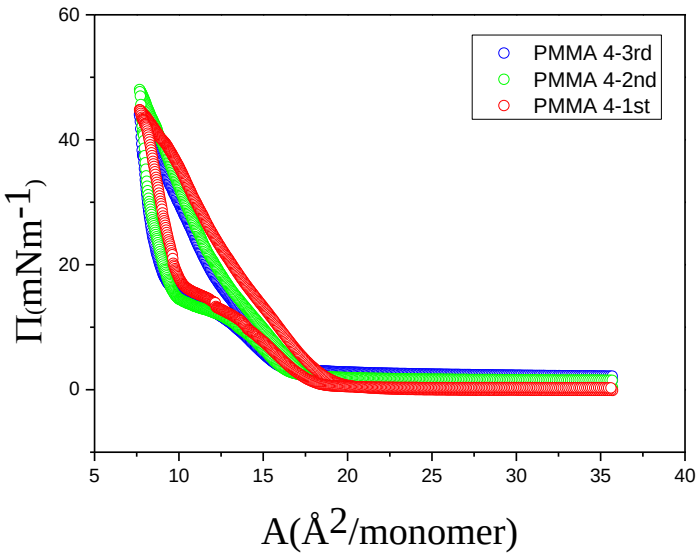

Figure 67: Compression – expansion data (pressure isotherms) for PMMA linear (3 circles, c=1mg/ml, V=25μl, T=25°C).

Concerning PBA, there seems to be a plateau at 23 mN/m. Before that plateau, which marks the phase transition, the layer is reversible. Also, hysteresis seems to take place above the plateau and it is different with the PMMA. Thus, with each subsequent cycle, the compression expansion curve moves to the left (Figure 68). This kind of behavior was observed for the PBA stars as well. One possible solution of that behavior is the difference of Tg. Here we remind that Tg for PMMA is close to 110ºC but for PBA it is -55ºC and the experiments took place at room temperature. So for PMMA measurements were obtained below Tg, but for PBA the measurements were obtained above Tg, thus possibly explaining the liquid like behavior of the polymer layer. Irrespectively of this fundamental difference, the isotherms indicate no loss of material but layer reorganization and possible material accumulation near the barriers.

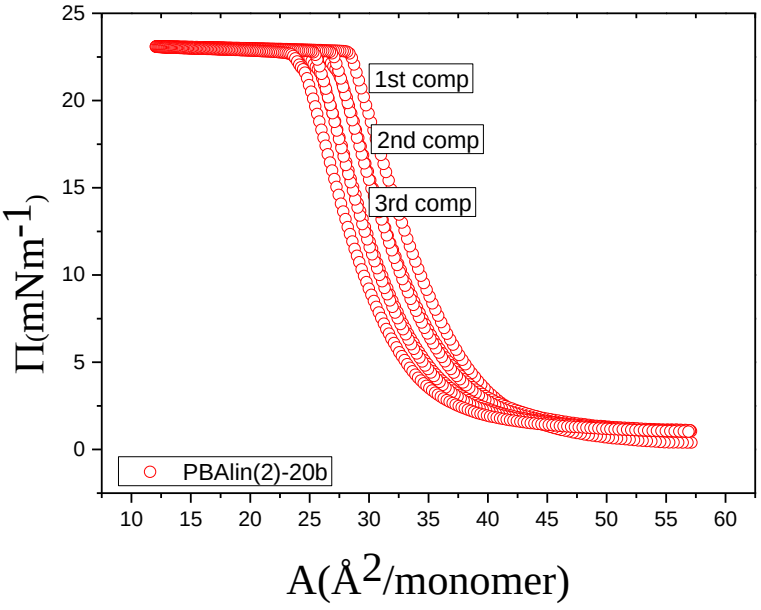

Figure 68: Compression – expansion data (pressure isotherms) for PBA linear (3 circles, c=1mg/ml, V=20μl, T=25ºC).

Flory radius analysis can explain the behavior of the materials. In the bulk, it is well known that the behavior of the polymer chain depends from the solvent. For example $CHCl_3$ can be good solvent for some polymers and theta or bad for others. The size will be affected by solvent quality (RUBINSTEIN AND COLBY (2003)). In the bulk, for good solvent the radius scales with the number of polymerization to the power of three fifth ($R \sim N^{3/5}$), for theta solvent $R \sim N^{1/2}$ and for bad solvent $R \sim N^{1/3}$. At interfaces there is a difference for good solvent with $R \sim N^{3/4}$ and poor solvent $R \sim N^{1/2}$ (RUBINSTEIN AND COLBY (2003)).

Applying Flory radius analysis to our samples, we find that PMMA systems behave akin to theta solvent conditions. The slopes were 0.5, 0.57, 0.51 for atactic, syndiotactic and dendritic, respectively. On the other hand, PBA systems behave as they were in bad solvent conditions with slope equal to 0.38.

In all the series of samples, where the role of molecular weight was investigated, we observed that as the molecular weight increased, the pressure increased more rapidly (higher area). For PMMA, the maximum pressure achieved increased with increase of molecular weight (Figure 69), whereas in PBA, maximum pressure was independent of molecular weight.

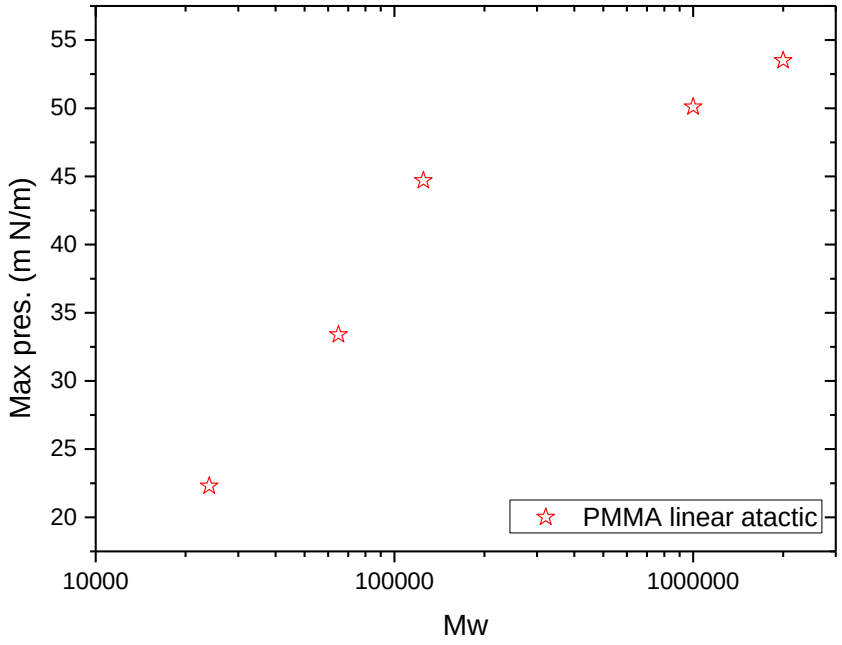

Figure 69: Maximum pressure from the compression- expansion experiment versus molecular weight for the linear atactic PMMAs.

Concerning tacticity, for the same molecular weight samples, compared to atactic (figure 58) syndiotactic samples increased their pressure faster. The difference at tacticity implies that the material is stiffer in local scale. Also we note that syndiotactic samples were more polydisperse. Moreover, we can observe at figure 58 that syndiotactic samples applied a maximum pressure higher than atactic. Therefore, they create different structures on the interface and likely they take up more space. Furthermore, the plateau is sharper so the phase transition is more discernible.

Concerning the role of the architecture in PMMA layer, in order to achieve the same characteristics of the layers, a lower molecular weight of dendritic systems is needed. This is implied from the isotherms of figure 62 where the curves overlapped and the molecular weight of the dendritic lower.

We attribute this to the fact that due to their architecture, dendritics take up more area at the interface. Therefore, the right selection between molecular weight, tacticity and architecture can be made, so as to have the targeted results.

The relaxation experiments with different glassy PMMA layers (different concentrations) revealed two different times (fast and slow) on step compression. The overall behavior is suggestive of stiff viscoelastic, solid like response, suggesting highly heterogeneous samples. As already discussed, in the bulk the characteristic time scales with $M^{3.4}$ for entangled polymers. Also MAESTRO EL AL. (2010) presented a similar behavior for the PtBA. From our analysis, as shown in figures 70 and 71, it is evident that the characteristic time exhibit different response, $\tau \sim c^0$ and $\tau \sim M^0$.

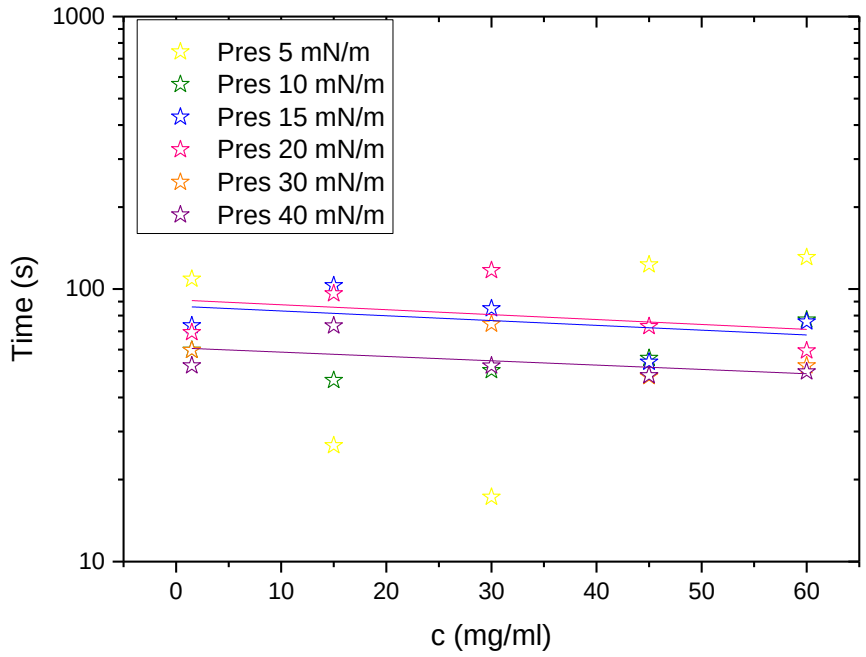

Figure 70: Characteristic time (fast relaxation time) versus concentration for different pressures. Lines are drawn to guide the eye.

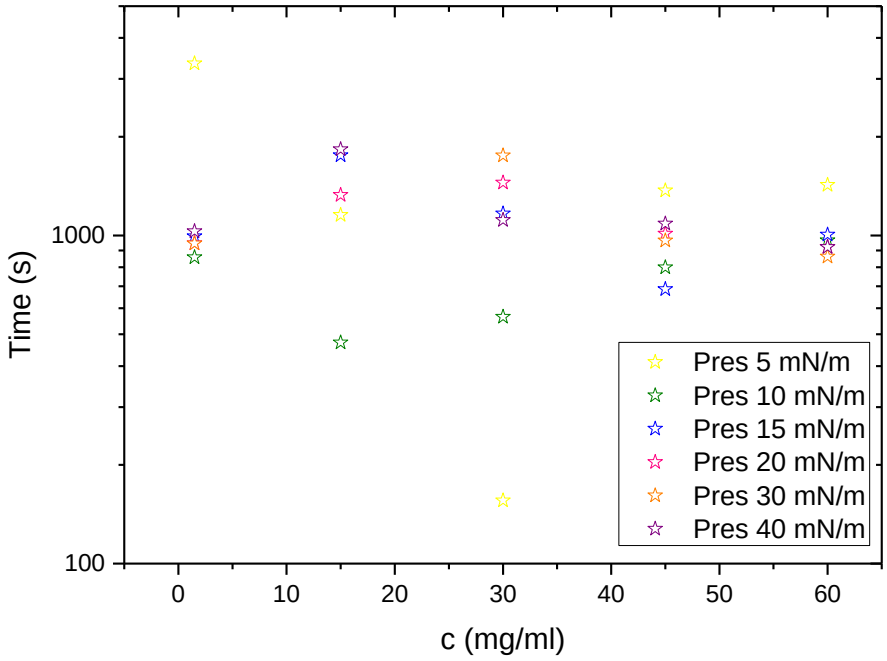

Figure 71: Characteristic time (slow relaxation time) versus concentration for different pressures.

Finally, concerning rheology experiments the ISR could not resolve due viscoelastic response of PBA layers. For PMMA layers we observed that moduli increased with surface pressure. There is a characteristic time where there is a crossover between G' and G", independent from the molecular weight (figure 72).

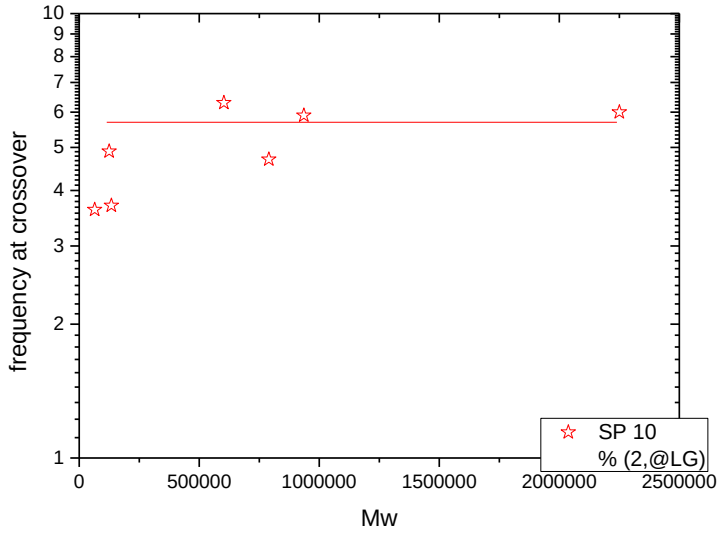

Figure 72: Frequency at the crossed of G' and G'' versus molecular weight for surface pressure 10mN/m. Lines are drawn to guide the eye.

For the figure 72 we can extract the characteristic time ($\tau=1/\omega$) as shows figure 73.

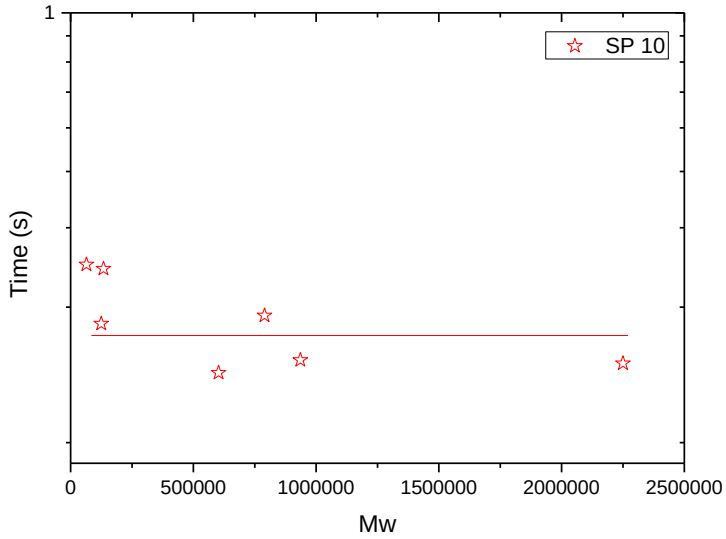

Figure 73: Characteristic time versus molecular weight for surface pressure 10mN/m. Lines are drawn to guide the eye.

The time does not depend on molecular weight.

In summary, PMMA and PBA samples at interface have a completely different behavior than the bulk but also are different from the PtBA at the interface. A reason is probably the difference Tg and at the conformation of the layer. Our key findings, are listed in Table 6.

Table 6 : Parameters which checked for the samples.

	Reversibility before plateau	Reproducibility	R_F	State	Characteristic Time
PMMA linear atactic	✓	✓	0.5	Glassy	~Mw^0
PMMA linear syndiotactic	✓	✓	0.57	Glassy	~Mw^0
PMMA dendritic	✓	✓	0.51	Glassy	~Mw^0
PBA linear	✓	✓	-	Liquid like	-
PBA star	✓	✓	0.38	Liquid like	-

5. CONCLUSIONS AND PERSPECTIVES

We have investigated the structural and rheological properties of acrylic polymers and specifically PMMA and PBA at air- water interfaces, with the aim to understand the role of molecular weight, tacticity, architecture and concentration on the properties. As far as molecular weight is concerned we found that as it increased, the characteristic relaxation time remained constant. Also, the tacticity does not seem to change the interfacial structure significantly, although we note the higher pressure at the same compressed surface area. Furthermore, comparison of linear and dendritic PMMA does not reveal any major difference. When we increase the concentration and deposit a network to the interface, we observe constant characteristic times, in disagreement with the bulk results. Therefore, acrylic polymers behave very differently at the interface compared to the bulk.

There are still many open questions, which will need being addressed in order to obtain a better and more complete picture of the interfacial structure and rheological behavior of these materials. They include rheological experiments in bulk solution to compare against interfacial rheology, as well as DLS experiments at different configurations, in order to better understand the role of tacticity and creep tests which can be done with the use of double wall ring in order to measure the interfacial rheology of PBA samples. In addition, step compression experiments with PBA will complement the emerging picture of relaxation times. Finally, attempting to investigate the response of different polymers such as PDMS will be an important complement to this work. PDMS is flexible, has very low Tg and

can sit at the air-water interface. However, extracting relaxation time us a challenge worth pursuing.

6. REFERENCES

Berry G.C., Fox T.G. (1968) Adv. Polym. Sci.

Blodgett, K. (1939). Use of interface to extinguish reflection of light from glass. Physical Review, 55, 391.

Brooks, C. F., G. G. Fuller, C.W. Frank, and C. R. Robertson (1999). An interfacial stress rheometer to study rheological transitions in monolayers at the air-water interface. Langmuir, 15(7), 2450–2459.

Capana I., R. Capana, T. Tanriseverb, S. Can (2005) Poly(methyl methacrylate) monolayers at the air–water interface. Materials Letters 59, 2468–2471

Clements, J. A. and Avery M.E. (1998). Lung surfactant and neonatal respiratory distress syndrome. American Journal of Respiratory and Critical Care Medicine, 157(4), S59–S66

Dickinson E., J. A. Hunt, and D. G. Dalgleish (1991). Competitive adsorption of phosvitin with milk proteins in oil-in-water emulsions. Food Hydrocolloids, 4(5), 403–414.

Espinosaa G., Iván López-Monterob Francisco Monroya and Dominique Langevina (2010) Shear rheology of lipid monolayers and insights on membrane fluidity, PNAS, 108(15), 6008-6013

Fuller G.G., (2003) RHEOLOGY OF MOBILE INTERFACES Rheology Reviews, 77–123.

Gaines, G. L. (1966). Insoluble monolayers at liquid-gas interfaces. John Wiley and Sons, Inc.

Gavranovic G. T., Joshua M. Deutsch and Gerald G. Fuller, (2005), Two-Dimensional Melts: Polymer Chains at the Air-Water Interface. Macromolecules, 38, 6672-6679

de Gennes, P. G. d. J. Chem. Phys. 1971, 55, 572.

Georgieva D., A. Cagna, and D. Langevin (2009). Link between surface elasticity and foam stability. Soft Matter, 5(10), 2063–2071.

Gerard J. F. (2001), Macromolecular Symposia, Fillers and Filled Polymers Wiley-VCH ed

Grimard R., P. Tancrede, and C. Gicquaud (1993). Interaction of actin with positively charged phospholipids - a monolayer study. Biochemical and Biophysical Research Communications, 190(3), 1017–1022.

Hsu Wen-Ping, Yuh-Lang Lee, Shu-Hua Liou (2005) Monolayer characteristics of stereoregular PMMA at the air/water interface. Applied Surface Science 252, 4312–4320

Langmuir I. (1917). THE CONSTITUTION AND FUNDAMENTAL PROPERTIES OF SOLIDS AND LIQUIDS. II. LIQUIDS. 1. Journal of the American Chemical Society, 39(9), 1848-1906

Langmuir I. (1920). The mechanism of the surface phenomena of flotation. Transactions of the Faraday Society, 15(June), 62-74

Maestro A., F. Ortega, F. Monroy, J. Kragel and R. Miller (2009) Molecular Weight Dependence of the Shear Rheology of Poly(methyl methacrylate) Langmuir Films: A Comparison between Two Different Rheometry Techniques, Langmuir, 25(13), 7393–7400

Maestro A. et al., (2010) Reptation in langmuir polymer monolayers Soft Matter, 6, 4407–4412

Maestro A., F. Ortega, R. G. Rubio, M. A. Rubio, J. Krägel, and R. Miller (2011) Rheology of poly(methyl methacrylate) Langmuir monolayers: Percolation transition to a soft glasslike system. J. Chem. Phys., 134, 104704

Pockels, A. (1891). Surface Tension. Nature, 43, 437.

Pockels, A. (1892). Nature, 46, 418.

Pockels, A. (1894). Nature, 50, 223.

Riess J. G. (2009). Highly fluorinated amphiphilic molecules and self-assemblies with biomedical potential. Current Opinion in Colloid and Interface Science, 14(5), 294–304.

Roth C.B. and Dutcher J.R. (2003) Glass transition temperature of freely-standing films of atactic poly(methyl methacrylate). The European Physical Journal E

Rubinstein M. and Colby R.H. (2003) Polymer physics Oxford University Press

Samaniuk J. R. and Vermant J. (2014) Micro and macrorheology at fluid–fluid interfaces. Soft Matter, 10, 7023–7033

Snijkers F., Cho H. Y., Nese A., Matyjaszewski K., Pyckhout-Hintzen W. and Vlassopoulos D. (2014) Effects of Core Microstructure on Structure and Dynamics of Star Polymer Melts: From Polymeric to Colloidal Response. Macromolecules, 47, 5347−5356

Srivastava S., D. Leiske, J. K. Basu and G. G. Fuller (2011) Interfacial shear rheology of highly confined glassy polymers. Soft Matter, 7, 1994

Swalen J. D., D. L. Allara, J. D. Andrade, E. A. Chandross, S. Garoff, J. Israelachvili, T. J. McCarthy, R. Murray, R. F. Pease, and et al. (1987). Molecular monolayers and films. a panel report for the materials sciences division of the department of energy. Langmuir, 3(6), 932–950.

Van Ruymbeke E., E. B. Muliawan, T. Watanabe, S. G. Hatzikiriakos, A. Hirao, D. Vlassopoulos, (2010), Viscoelasticity and extensional rheology of model Cayley-tree polymers of different generations, Journal of Rheology, 54, 642-662.

Van Ruymbeke E., Krzysztof Matyjaszewski , Ed B. Muliawan, Dimitris Vlassopoulos, Haifeng Gao e (2011) European Polymer Journal 47, 746–751

Verwijlen T., P. Moldenaers, H. Stone, and J. Vermant (2011). Study of the flow field in the magnetic rod interfacial stress rheometer. Langmuir, 27, 945.

Zasadzinski J. A., J. Ding, H. E. Warriner, F. Bringezu, and A. J. Waring (2001) The physics and physiology of lung surfactants. Current Opinion in Colloid and Interface Science, 6(5-6), 506–513.

APPENDIX I - Experimental data for linear atactic PMMA (pressure isotherms and rheology)

This part presents the compression- expansion data of linear atactic PMMAs for different molecular weights. Also the rheological experiments and the zero shear viscosity versus frequency graphs are presented.

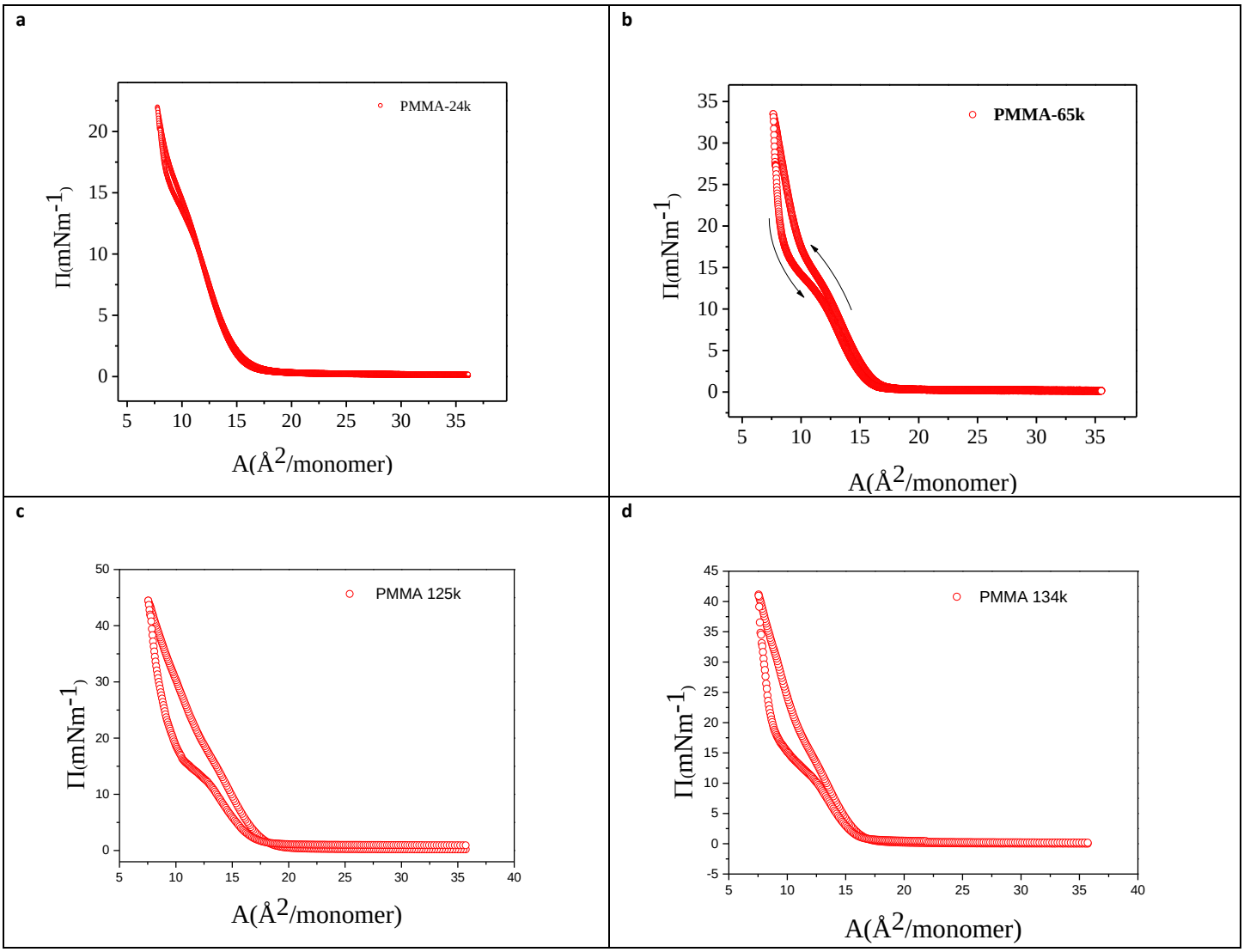

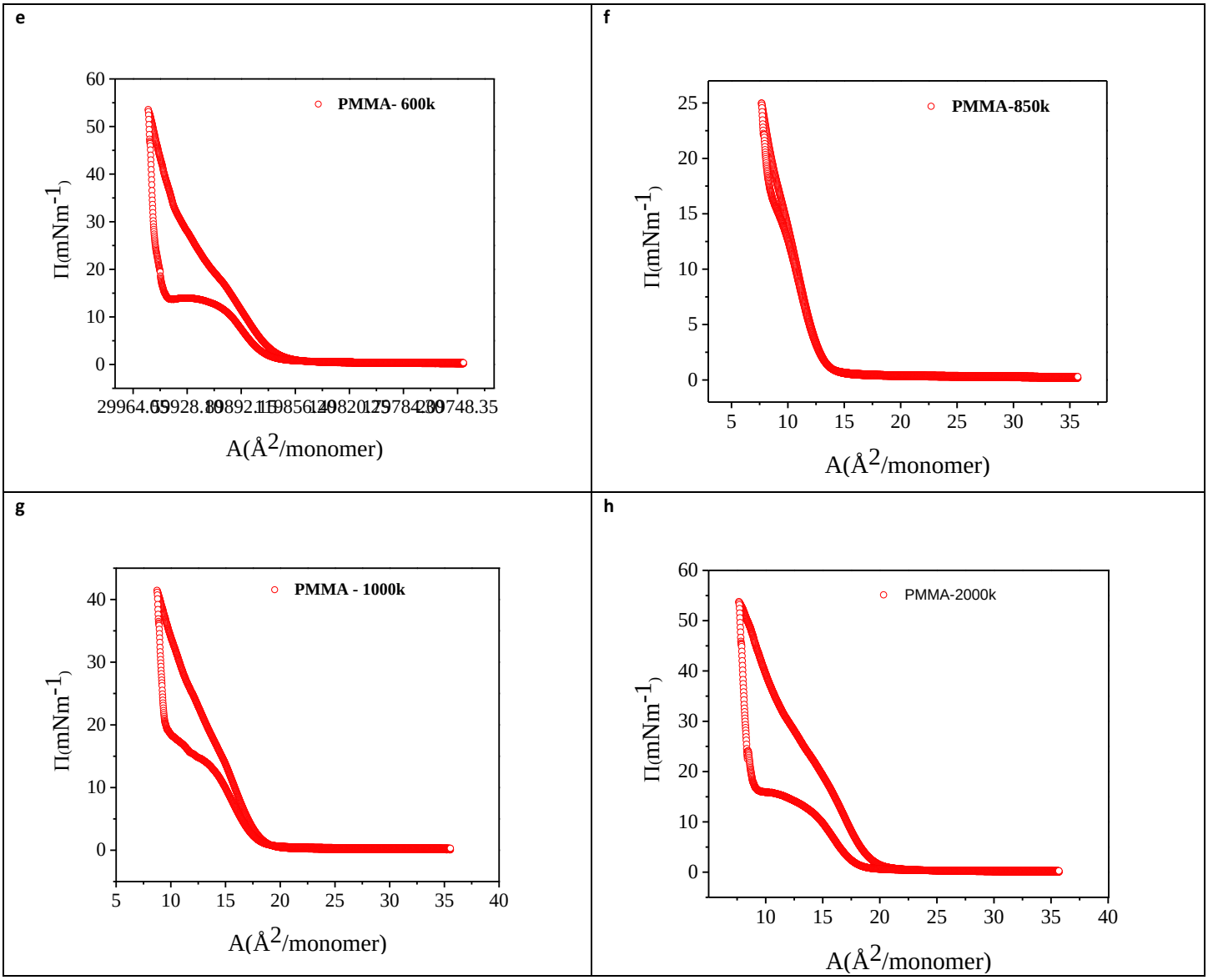

Figure 74: Compression - expansion data (pressure isotherm) for linear PMMAs Pressure vs Area (c=1mg/ml, V=25µl, T=25°C, barrier speed 10mm/min) a=24k, b=65k, c=125k, d=134k, e=600k, f=850k, g=1000k, h=2000k.

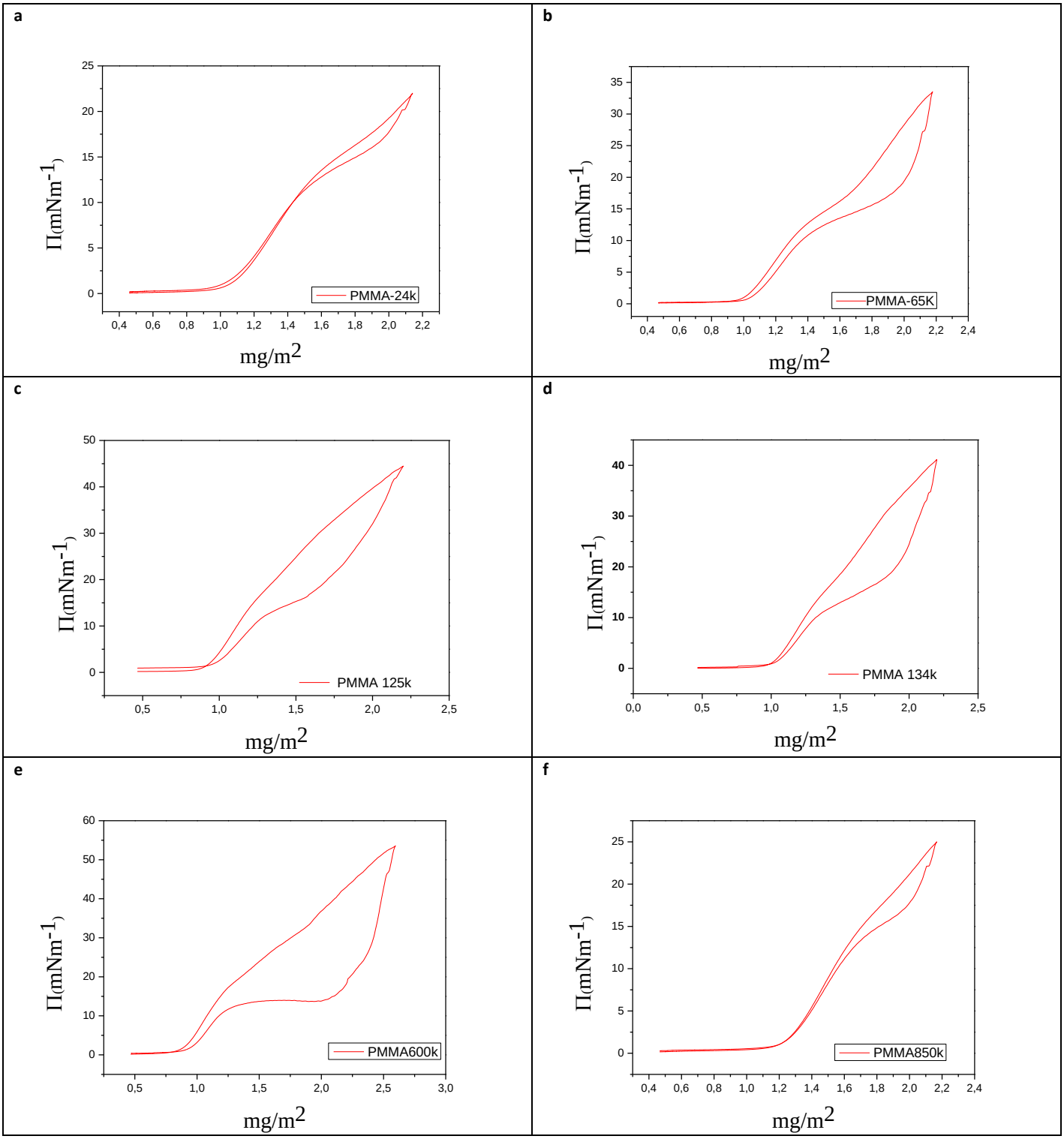
a
Π(mNm-1)
mg/m2
PMMA-24k
b
Π(mNm-1)
mg/m2
PMMA-65K
c
Π(mNm-1)
mg/m2
PMMA 125k
d
Π(mNm-1)
mg/m2
PMMA 134k
e
Π(mNm-1)
mg/m2
PMMA600k
f
Π(mNm-1)
mg/m2
PMMA850k

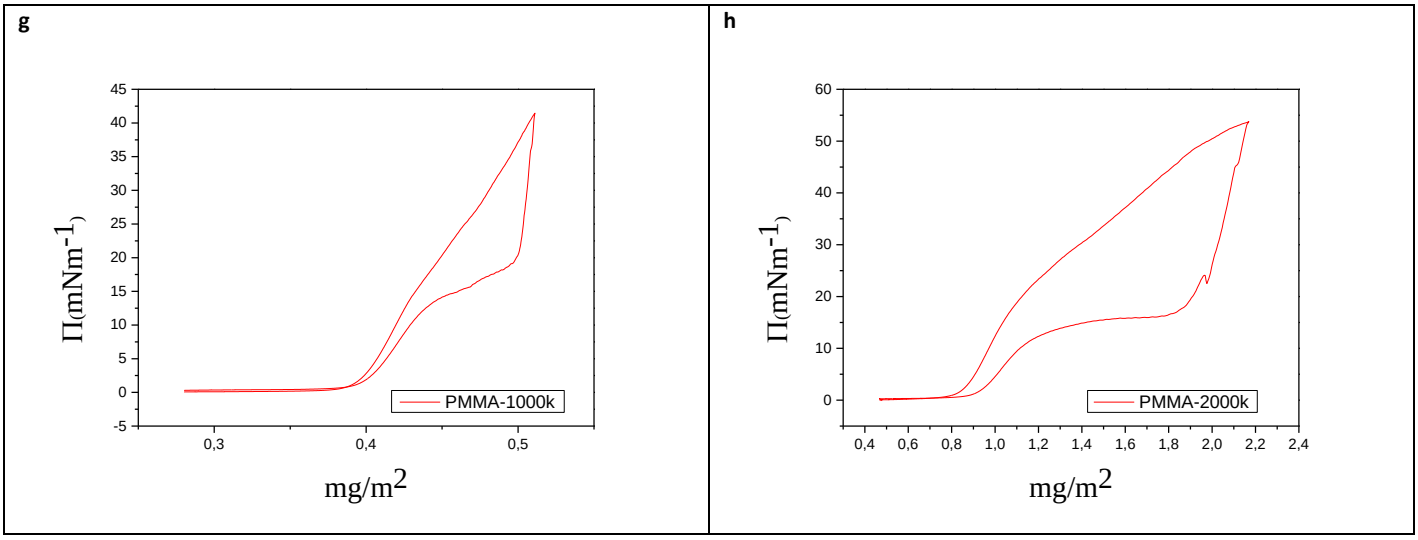

Figure 75 : Compression - expansion data (pressure isotherm) for linear PMMAs Pressure vs Concentration (c=1mg/ml, V=25µl, T=25°C, barrier speed 10mm/min) a=24k, b=65k, c=125k, d=134k, e=600k, f=850k, g=1000k, h=2000k..

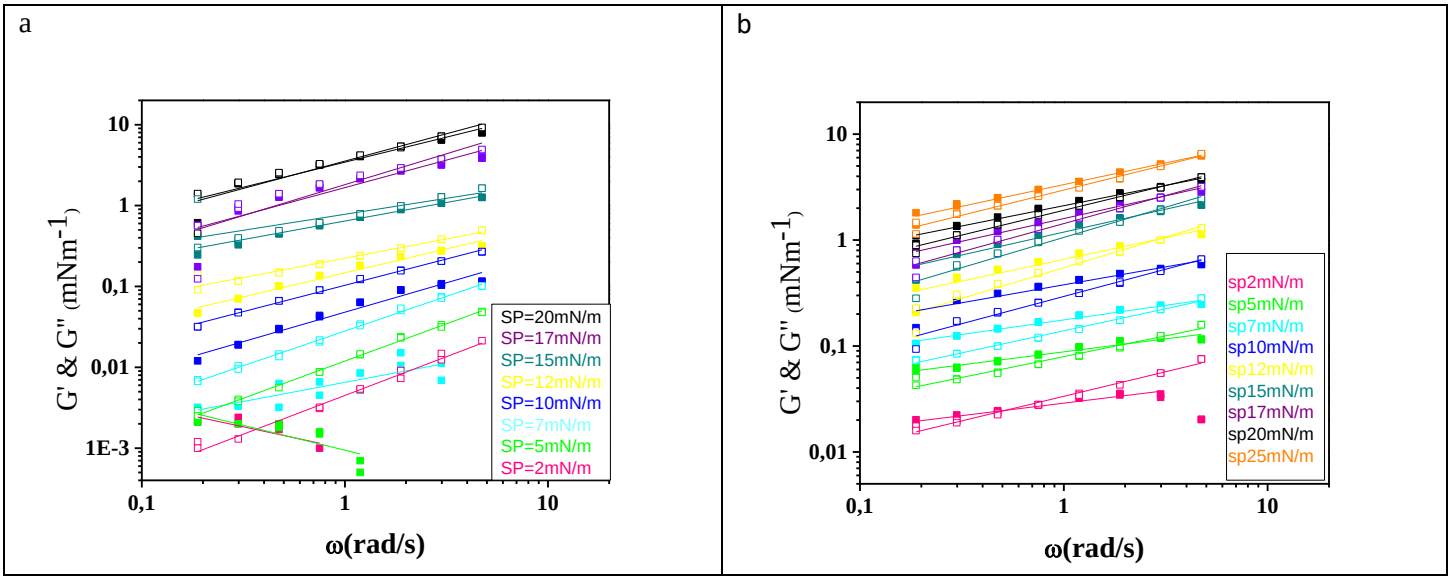

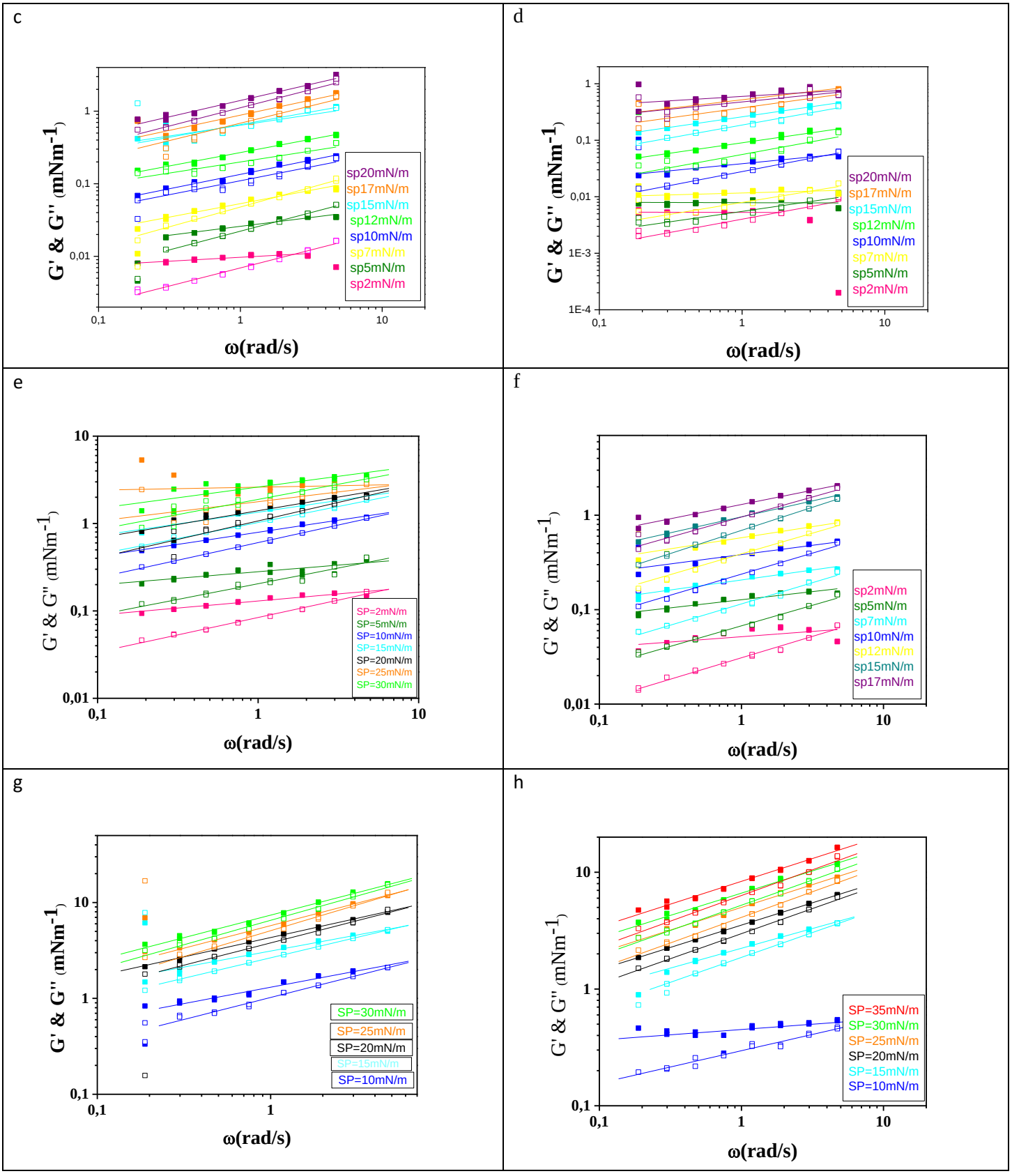

Figure 76: Rheology for linear PMMAs, G' is symbol full, G" is symbol empty, c=1mg/ml, V=25µl, T=25°C, a=24k, b=65k, c=125k, d=134k, e=600k, f=850k, g=1000k, h=2000k. Lines are drawn to guide the eye.

APPENDIX II - Experimental data for linear syndiotactic PMMA (pressure isotherms and rheology)

We present the compression- expansion data of linear syndiotactic PMMAs for different molecular weights. Also the rheological experiments and the zero shear viscosity versus frequency graphs are reported.

a

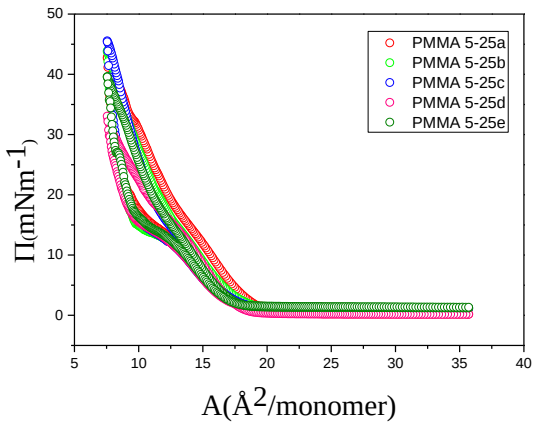

b

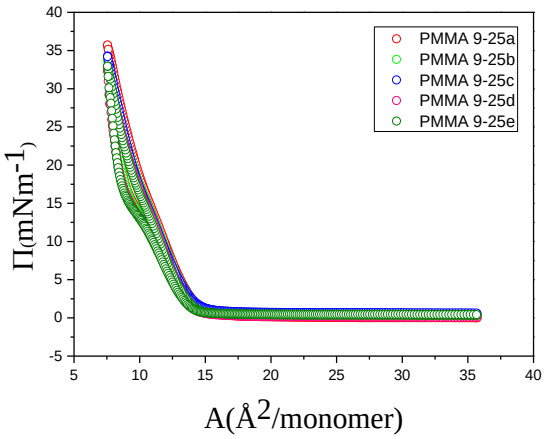

c

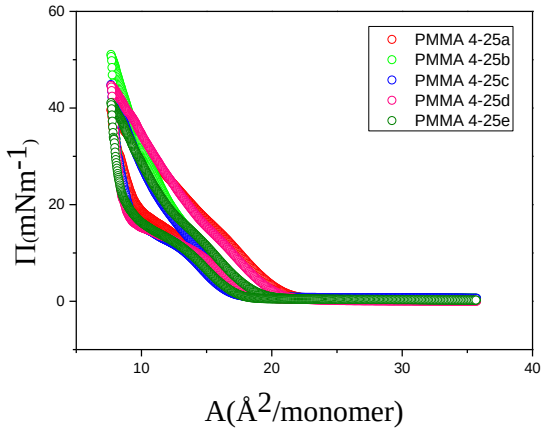

d

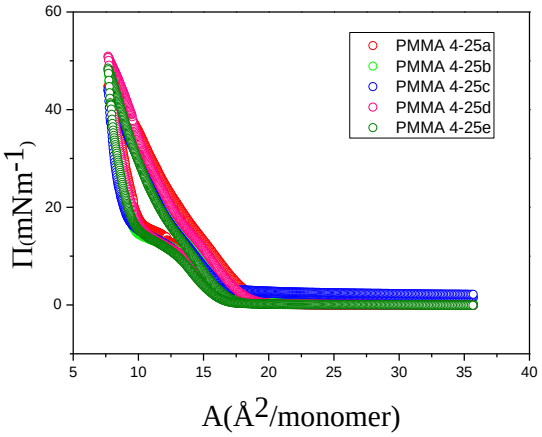

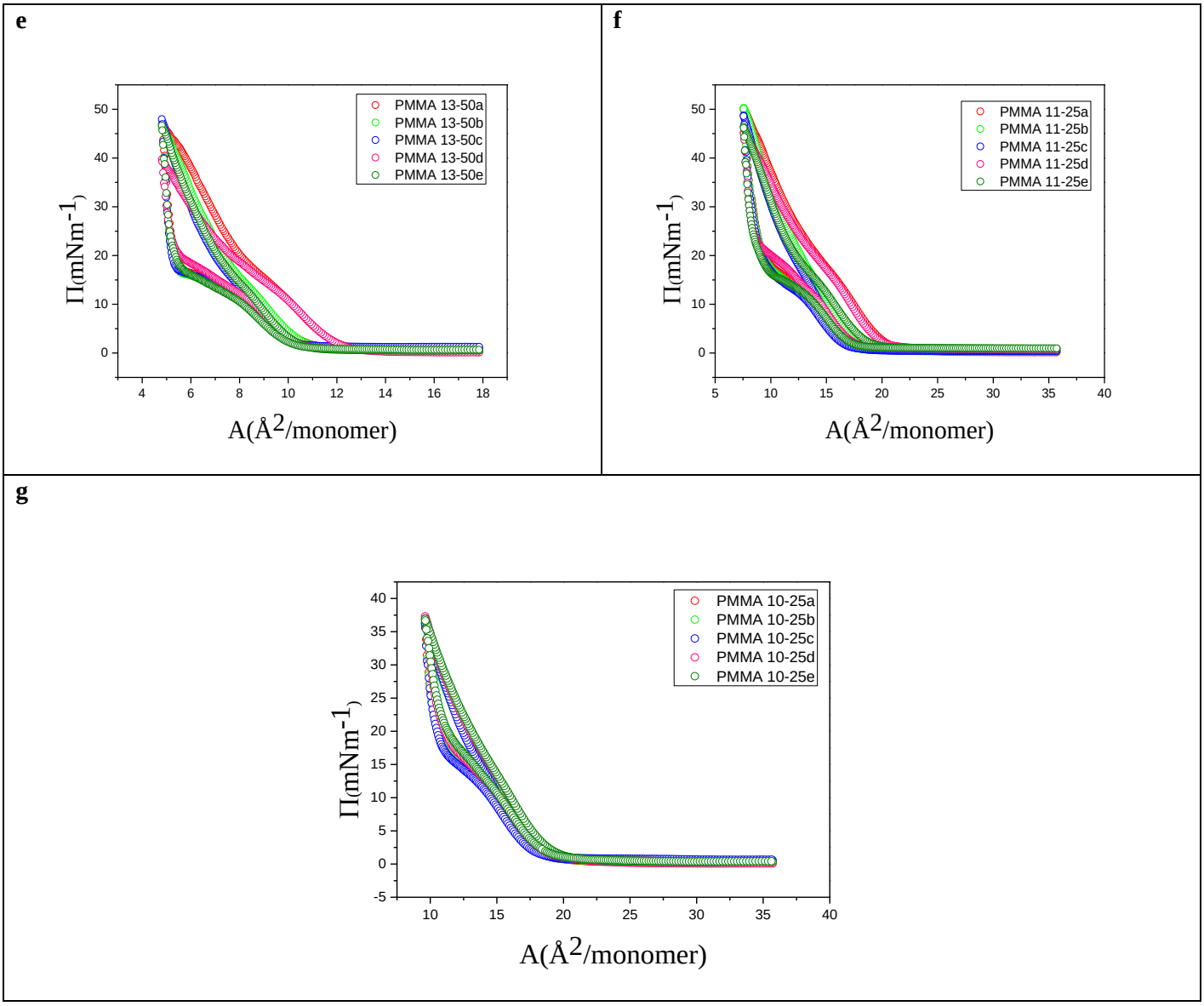

Figure 77: Reproducibility compression- expansion experiments of linear syndiotactic PMMAs (c=1mg/ml, V=25µl, T=25°C, barrier speed 10mm/min) a=PMMA 5, b=PMMA 9, c=PMMA 3, d=PMMA 4, e=PMMA 13, f=PMMA 11, g=PMMA 10.

a

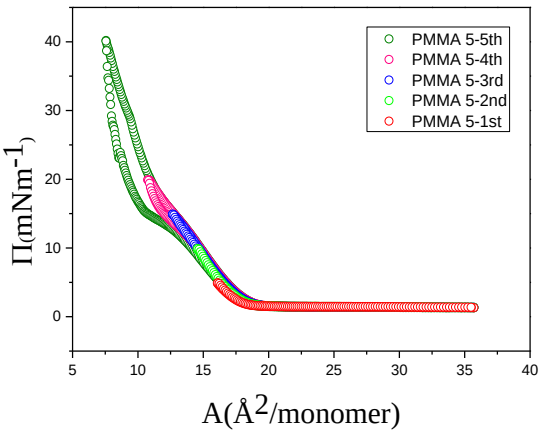
PMMA 5-5th
PMMA 5-4th
PMMA 5-3rd
PMMA 5-2nd
PMMA 5-1st
Π(mNm-1)
A(Å2/monomer)

b

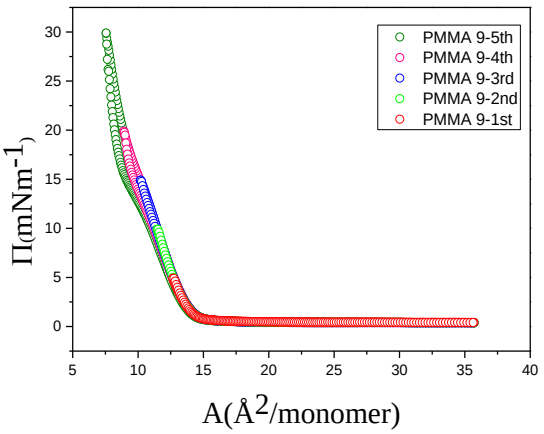
PMMA 9-5th
PMMA 9-4th
PMMA 9-3rd
PMMA 9-2nd
PMMA 9-1st
Π(mNm-1)
A(Å2/monomer)

c

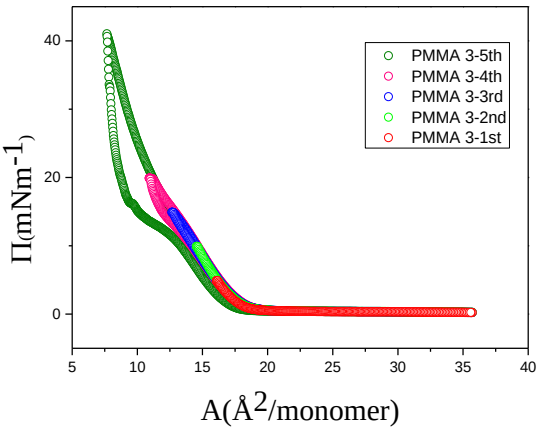
PMMA 3-5th
PMMA 3-4th
PMMA 3-3rd
PMMA 3-2nd
PMMA 3-1st
Π(mNm-1)
A(Å2/monomer)

d

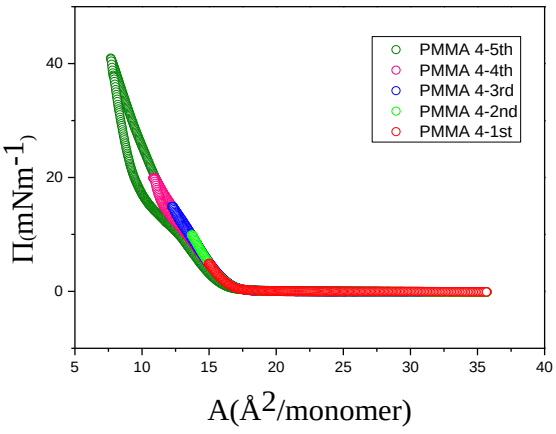
PMMA 4-5th
PMMA 4-4th
PMMA 4-3rd
PMMA 4-2nd
PMMA 4-1st
Π(mNm-1)
A(Å2/monomer)

e

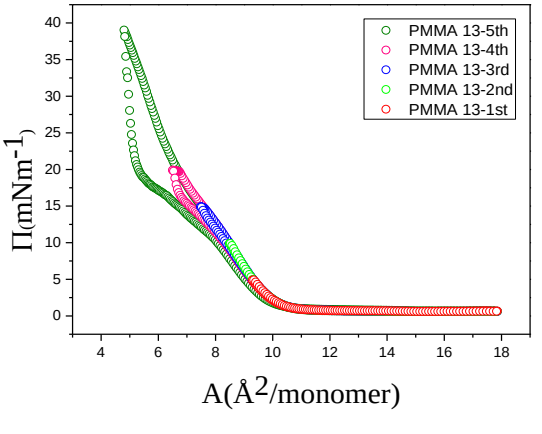
PMMA 13-5th
PMMA 13-4th
PMMA 13-3rd
PMMA 13-2nd
PMMA 13-1st
Π(mNm-1)
A(Å2/monomer)

f

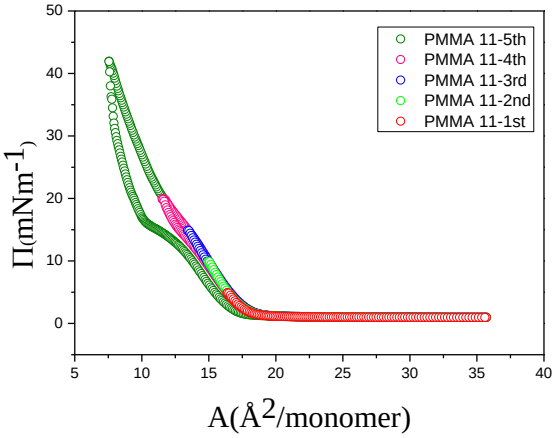
PMMA 11-5th
PMMA 11-4th
PMMA 11-3rd
PMMA 11-2nd
PMMA 11-1st
Π(mNm-1)
A(Å2/monomer)

g

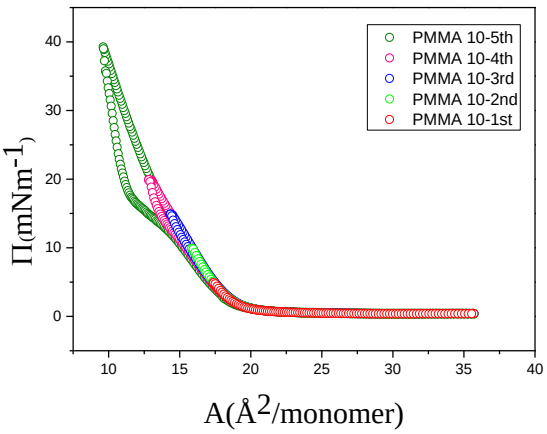

Figure 78: Compression - expansion data (pressure isotherm) for linear syndiotactic PMMAs (c=1mg/ml, V=25µl, T=25°C, barrier speed 10mm/min, 1st circle (red) has target pressure 5mNm-1, 2nd circle (green) has target pressure 10mNm-1, 3rd circle (blue) has target pressure 15mNm-1, 4th circle (pink) has target pressure 20mNm-1, 5th circle (olive) has maximum target pressure) a=PMMA 5, b=PMMA 9, c=PMMA 3, d=PMMA 4, e=PMMA 10, f=PMMA 11, g=PMMA 13.

a

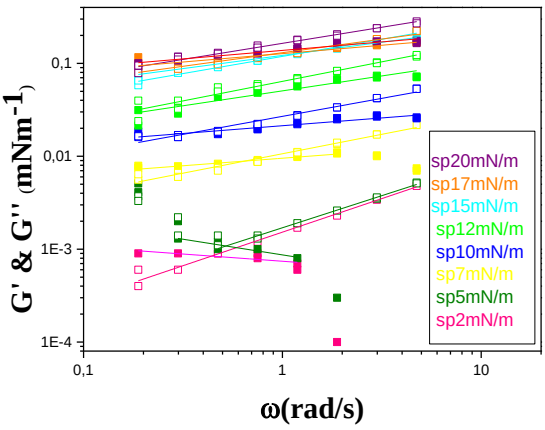
G' & G'' (mNm-1)
0,1
0,01
1E-3
1E-4
0,1
1
10
ω(rad/s)
sp20mN/m
sp17mN/m
sp15mN/m
sp12mN/m
sp10mN/m
sp7mN/m
sp5mN/m
sp2mN/m

b

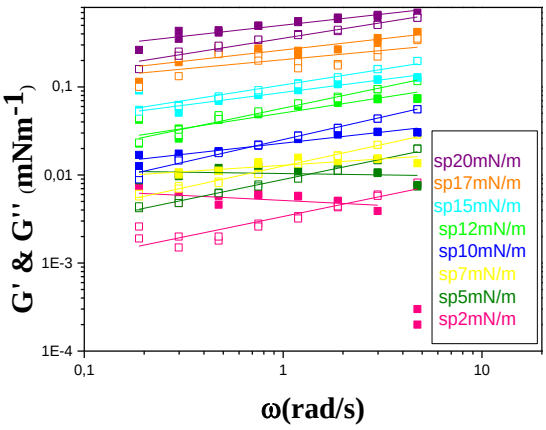
G' & G'' (mNm-1)
0,1
0,01
1E-3
1E-4
0,1
1
10
ω(rad/s)
sp20mN/m
sp17mN/m
sp15mN/m
sp12mN/m
sp10mN/m
sp7mN/m
sp5mN/m
sp2mN/m

c

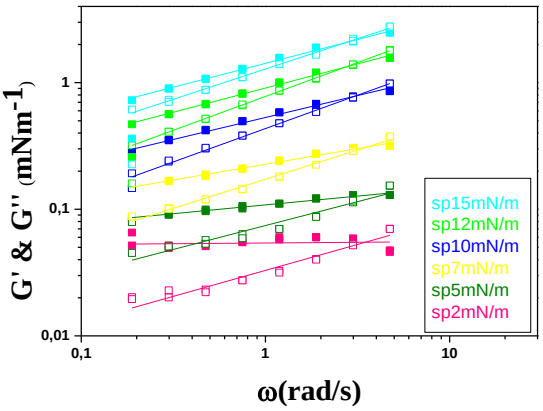
G' & G'' (mNm-1)
1
0,1
0,01
0,1
1
10
ω(rad/s)
sp15mN/m
sp12mN/m
sp10mN/m
sp7mN/m
sp5mN/m
sp2mN/m

d

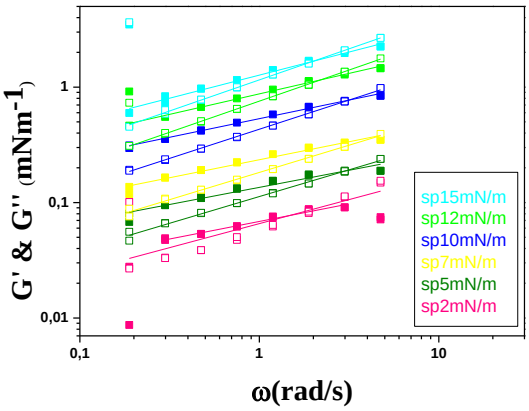
G' & G'' (mNm-1)
1
0,1
0,01
0,1
1
10
ω(rad/s)
sp15mN/m
sp12mN/m
sp10mN/m
sp7mN/m
sp5mN/m
sp2mN/m

e

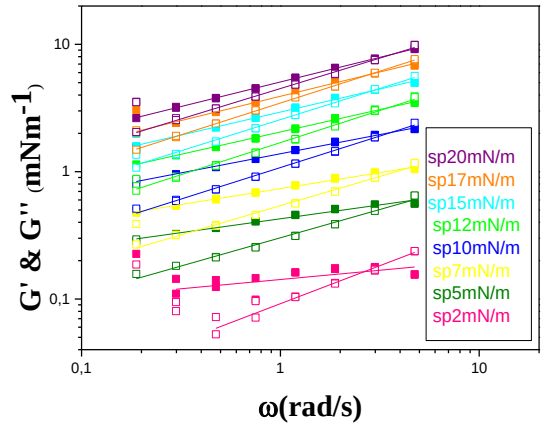
G' & G'' (mNm-1)
10
1
0,1
0,1
1
10
ω(rad/s)
sp20mN/m
sp17mN/m
sp15mN/m
sp12mN/m
sp10mN/m
sp7mN/m
sp5mN/m
sp2mN/m

f

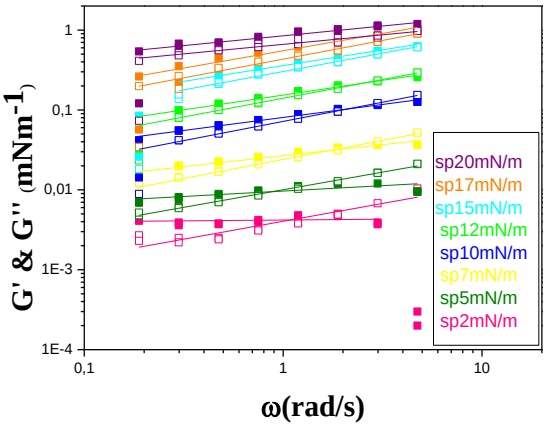
G' & G'' (mNm-1)
1
0,1
0,01
1E-3
1E-4
0,1
1
10
ω(rad/s)
sp20mN/m
sp17mN/m
sp15mN/m
sp12mN/m
sp10mN/m
sp7mN/m
sp5mN/m
sp2mN/m

g

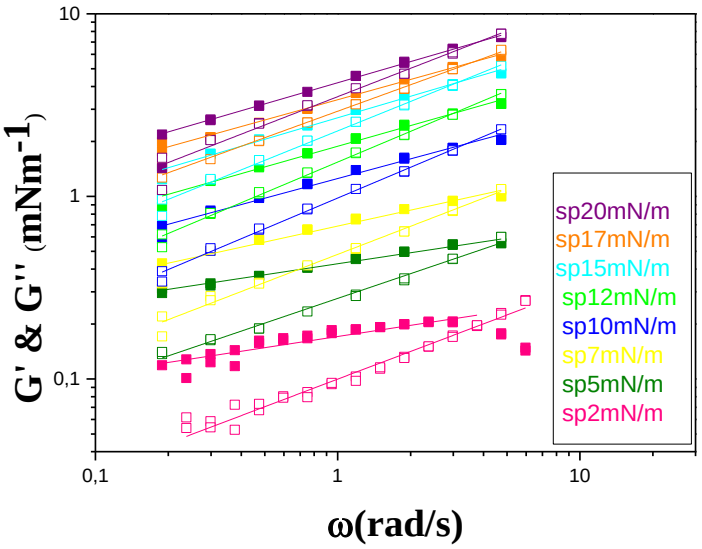

Figure 79: Rheology for linear sydiotactic PMMAs G' is symbol full, G" is symbol empty, c=1mg/ml, V=25µl, T=25°C. Spreading close to channel, Mixing of the layer, a=PMMA 5, b=PMMA 9, c=PMMA 3, d=PMMA 4, e=PMMA 13, f=PMMA 11, g=PMMA 10. Lines are drawn to guide the eye.

APPENDIX III - Experimental data for star PBA (pressure isotherms)

This part reports the compression- expansion data of star PBAs for different molecular weights.

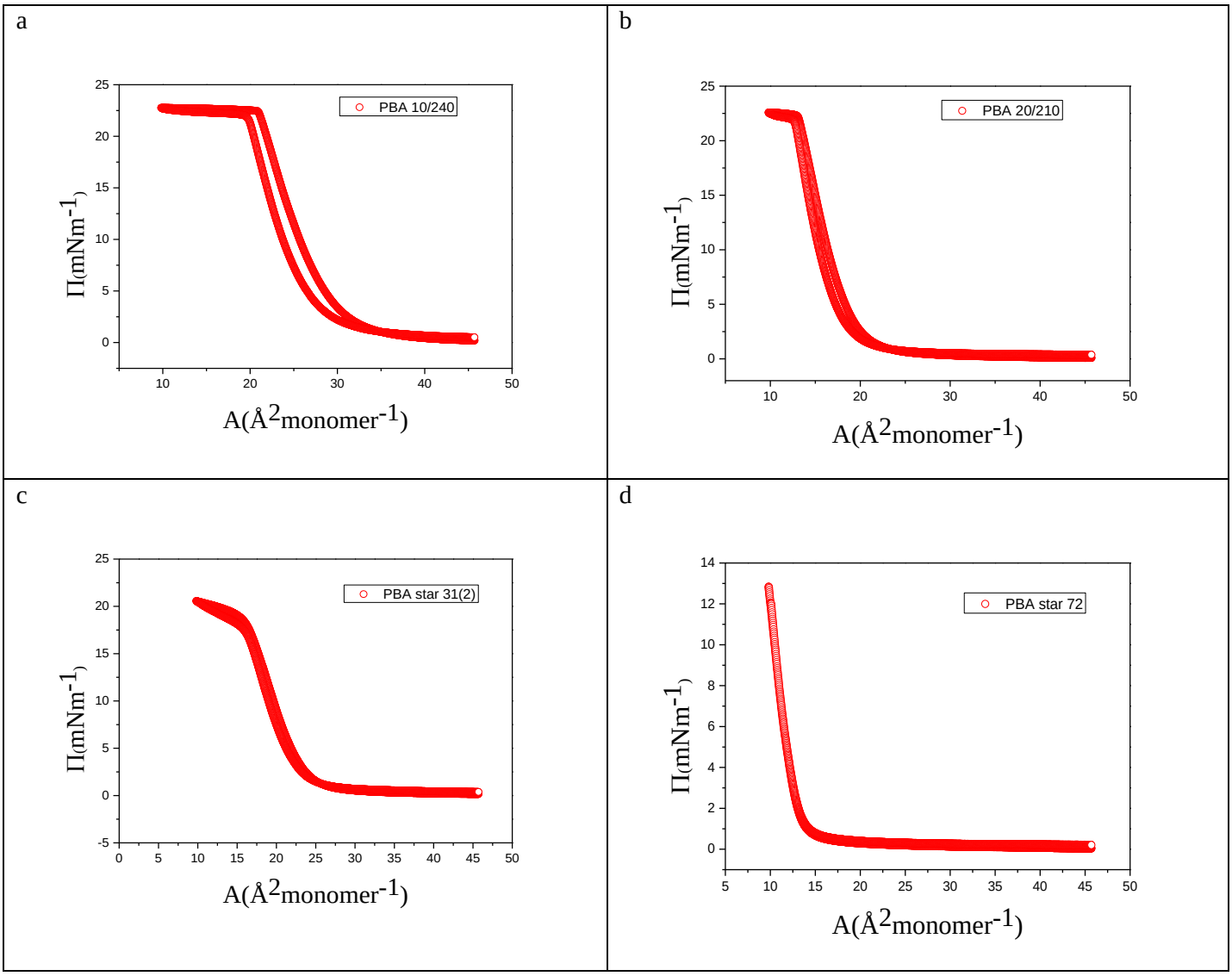

Figure 80 : Compression - expansion data (pressure isotherm) for star PBA Pressure vs Area (c=1mg/ml, V=25µl, T=25°C, barrier speed 10mm/min) a=308k, b=590k, c=180k, d=466.1k.

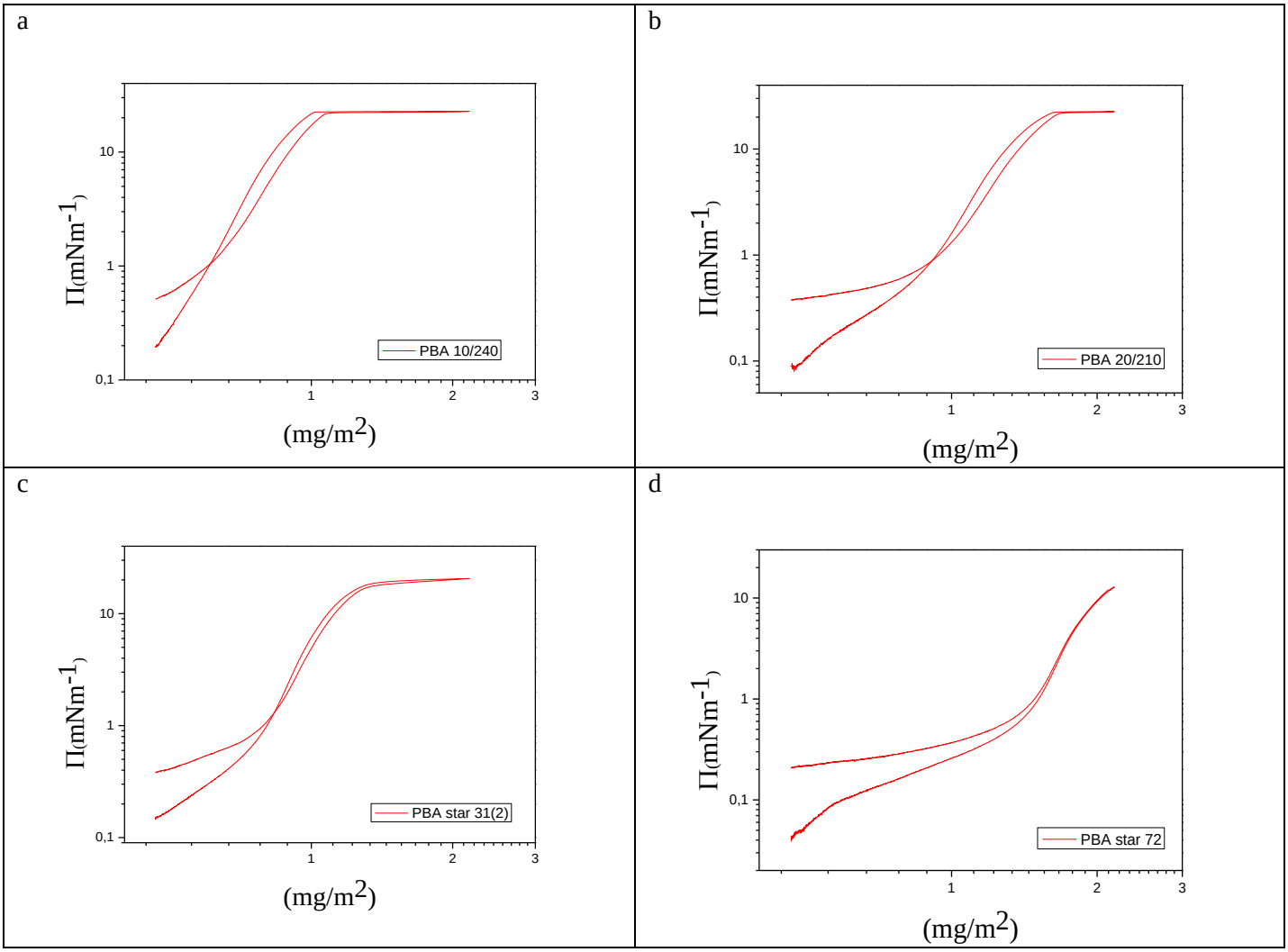

Figure 81: Compression - expansion data (pressure isotherm) for star PBA Pressure vs Concentration(c=1mg/ml, V=25µl, T=25°C, barrier speed 10mm/min) a=308k, b=590k, c=180k, d=466.1k.

APPENDIX IV - Experimental data for linear PMMA 600k (relaxation time and comparisons)

We present the step compression and relaxation data of linear atactic PMMAs 600k for different concentrations and different maximum pressure. Also comparison of fast and slow relaxation time with maximum pressure and concentration are presented.

a

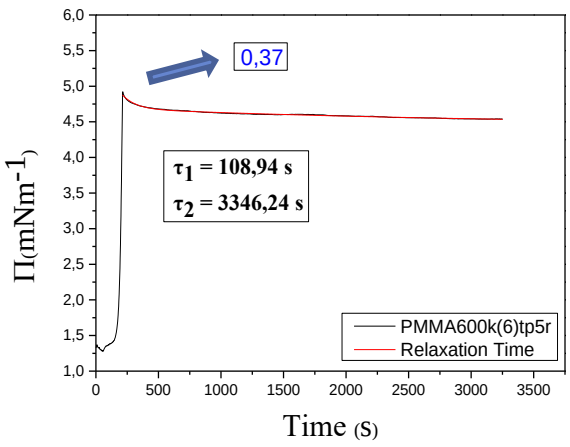

b

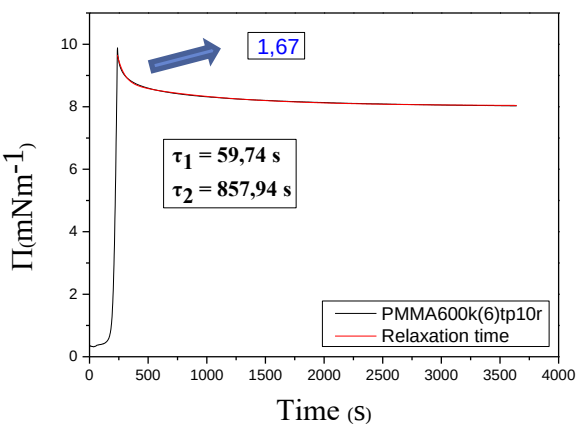

c

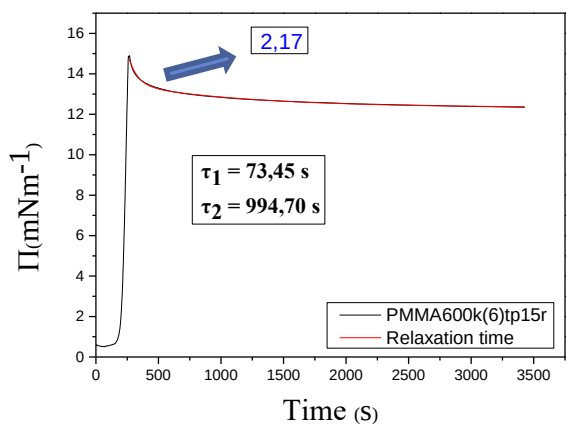

d

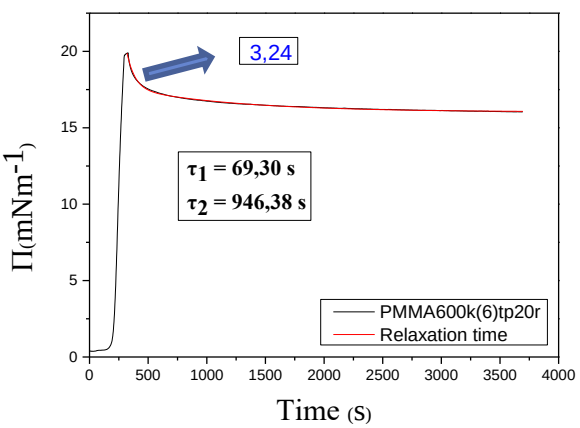

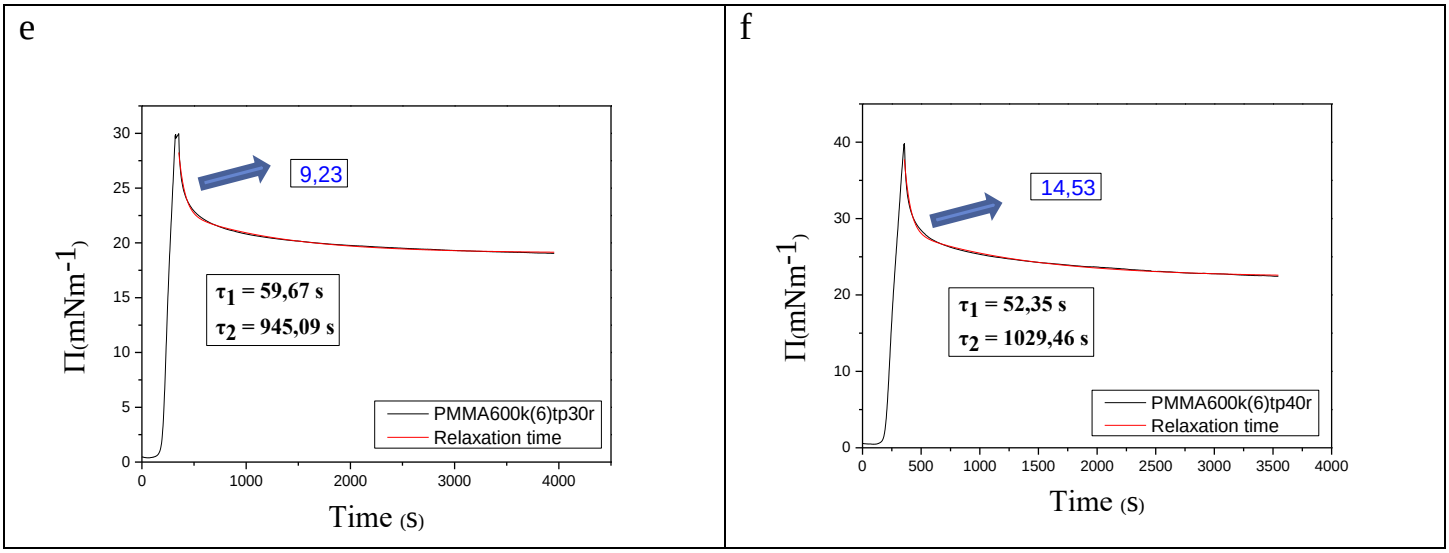

Figure 82: Relaxation Time of PMMA600k (c=1.5mg/ml, V=20µl, T=25°C, a:Pmax=5mN/m, b:Pmax=10mN/m, c:Pmax=15mN/m, d:Pmax=20mN/m, e:Pmax=30mN/m, f:Pmax=40mN/m).

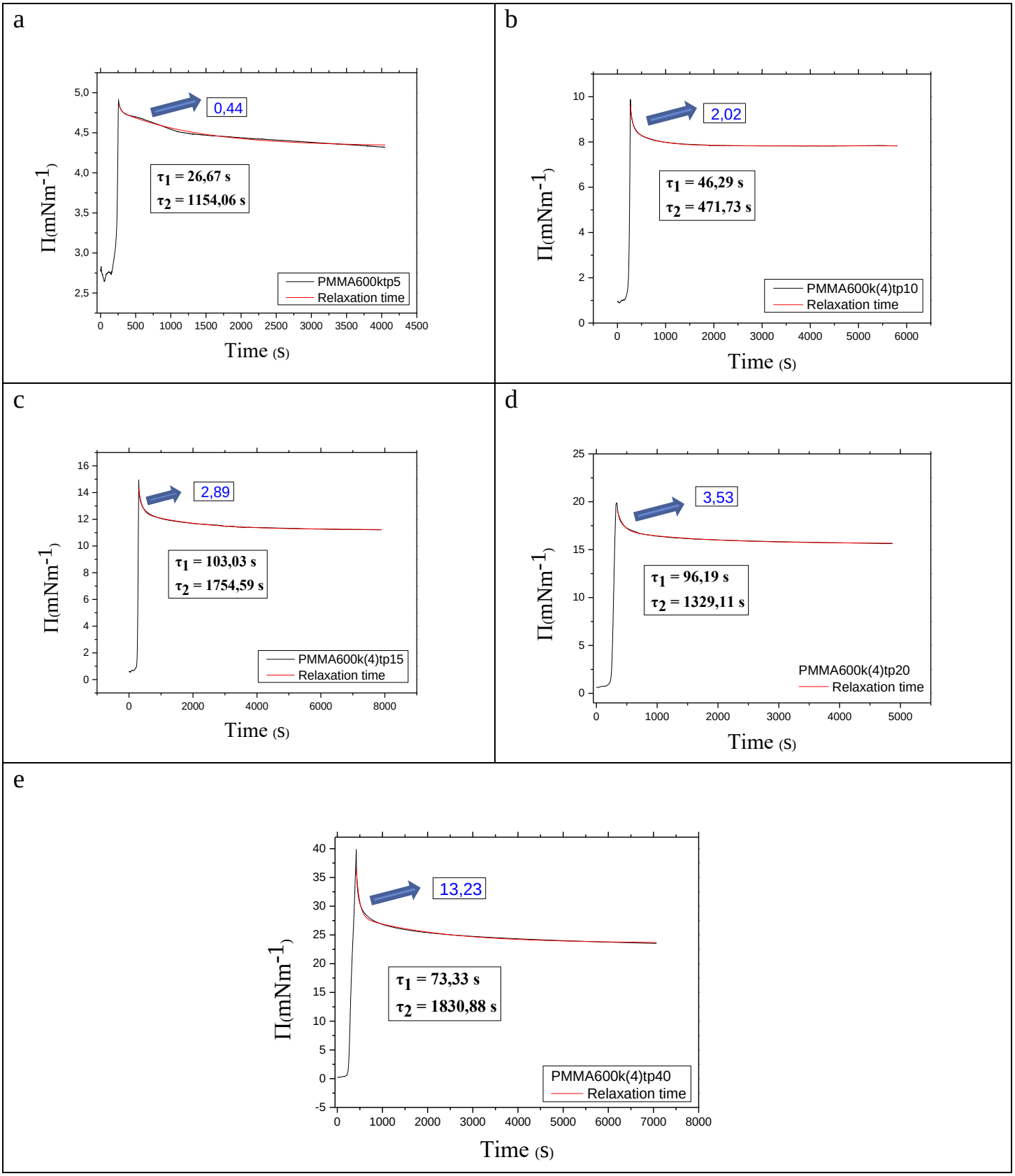

Figure 83: Relaxation Time of PMMA600k (c=15mg/ml, V=10µl, T=25°C, a:Pmax=5mN/m, b:Pmax=10mN/m, c:Pmax=15mN/m, d:Pmax=20mN/m, e:Pmax=40mN/m).

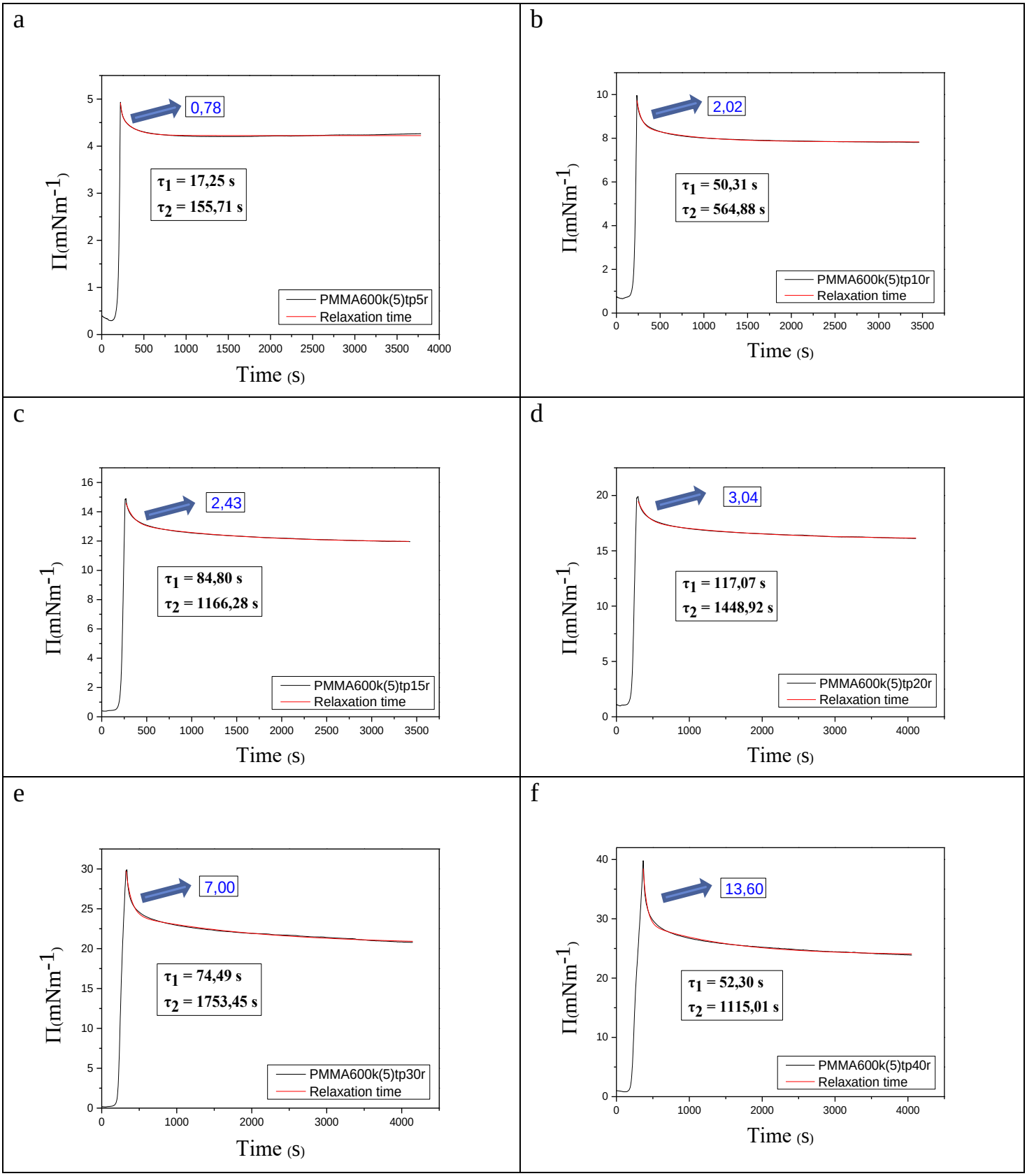

Figure 84 : Relaxation Time of PMMA600k (c=30mg/ml, V=10µl, T=25°C, a:Pmax=5mN/m, b:Pmax=10mN/m, c:Pmax=15mN/m, d:Pmax=20mN/m, e:Pmax=30mN/m, f:Pmax=40mN/m).

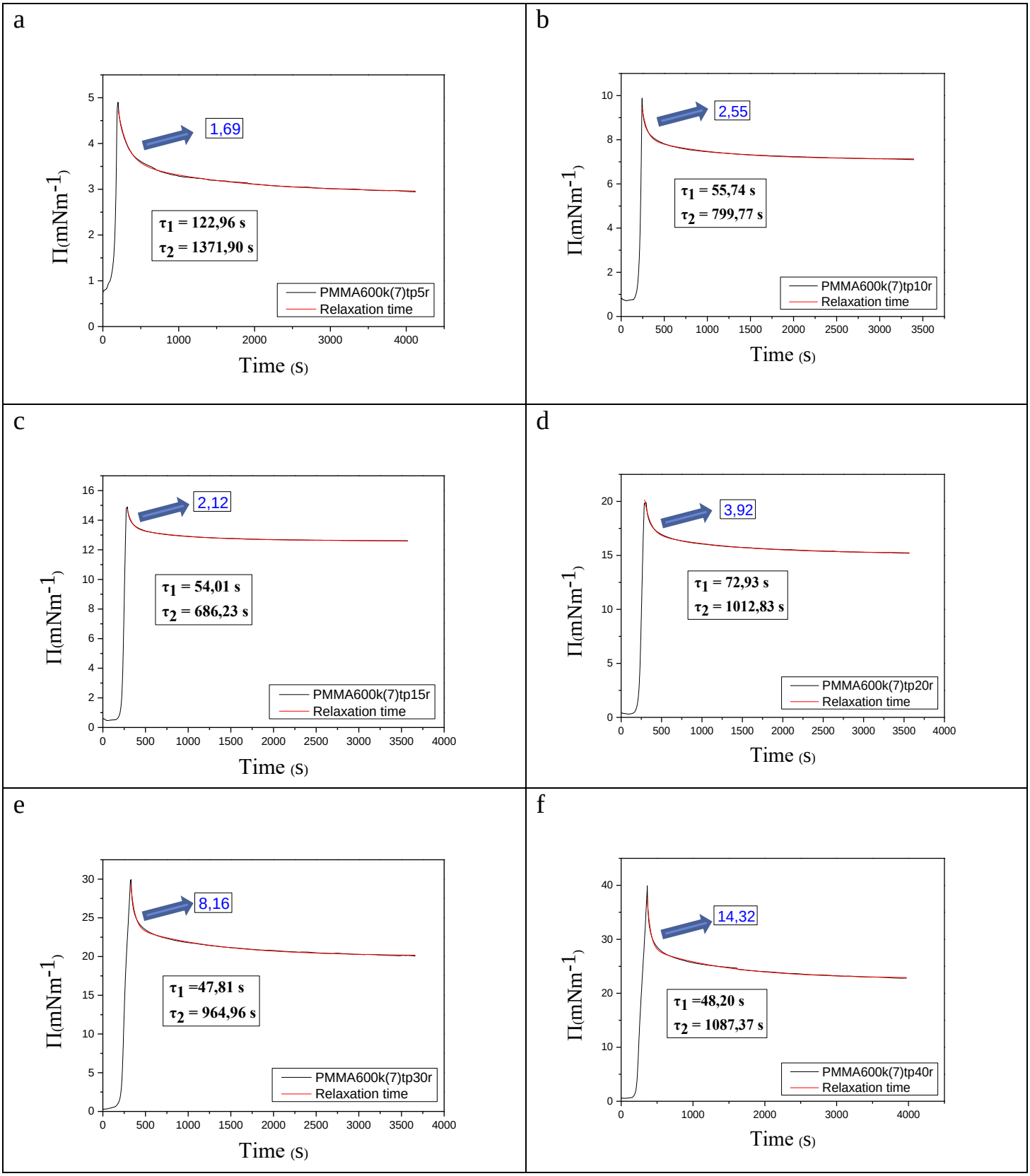

Figure 85: Relaxation Time of PMMA600k (c=45mg/ml, V=10µl, T=25°C, a:Pmax=5mN/m, b:Pmax=10mN/m, c:Pmax=15mN/m, d:Pmax=20mN/m, e:Pmax=30mN/m, f:Pmax=40mN/m).

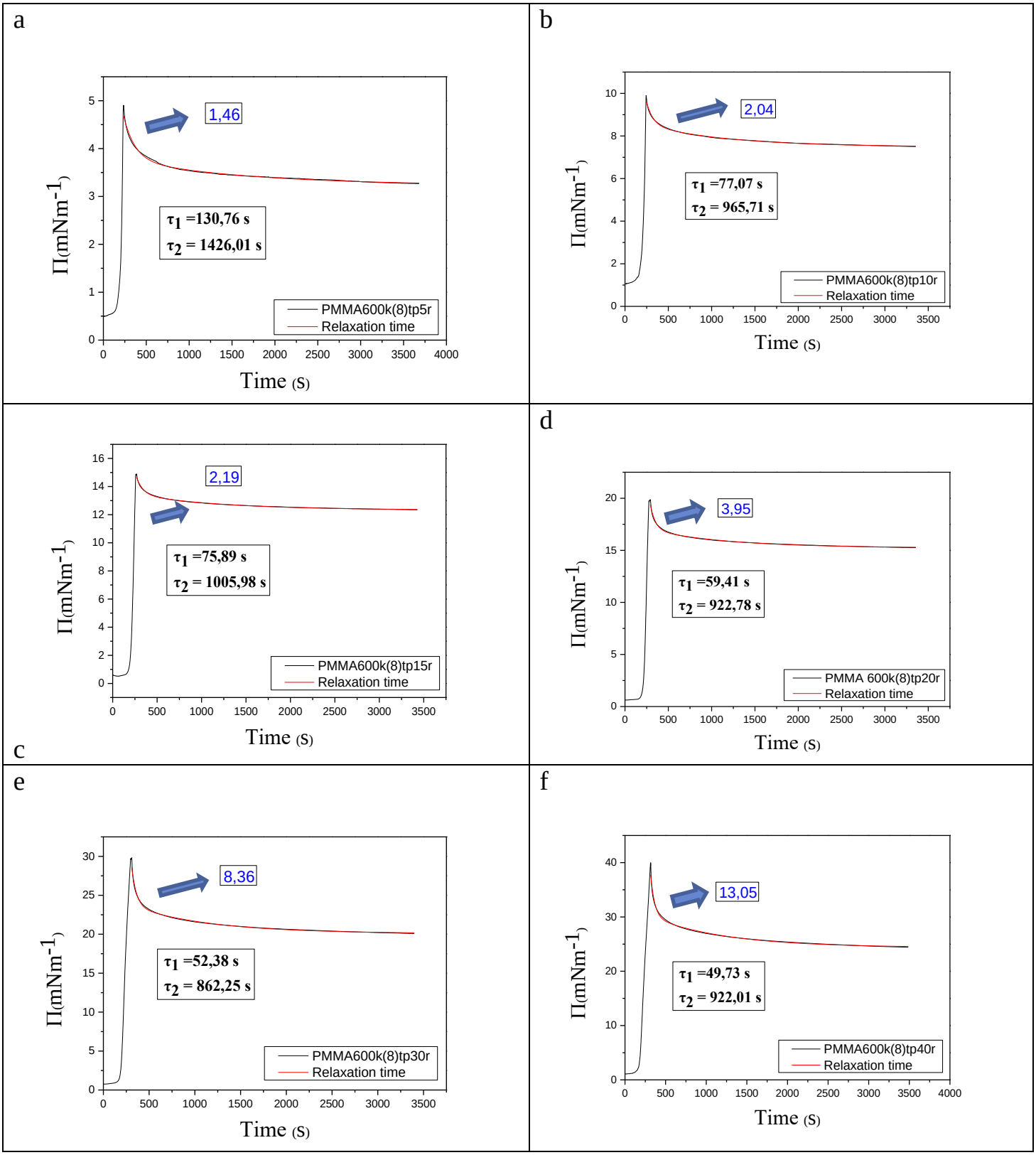

Figure 86: Relaxation Time of PMMA600k (c=60mg/ml, V=10µl, T=25°C, a:Pmax=5mN/m, b:Pmax=10mN/m, c:Pmax=15mN/m, d:Pmax=20mN/m, e:Pmax=30mN/m, f:Pmax=40mN/m).

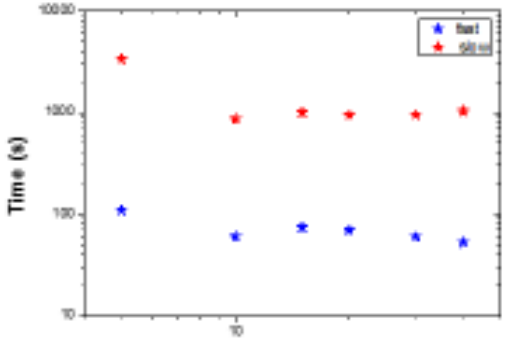

c=1.5mg/ml
V=20µl

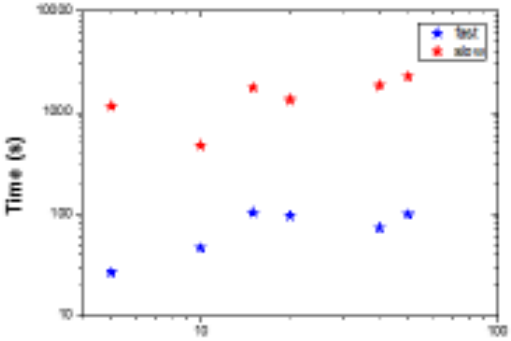

c=15mg/ml
V=10µl

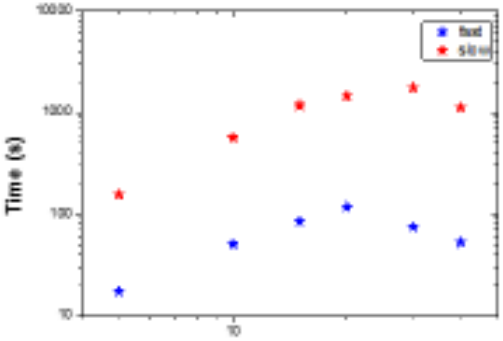

c=30mg/ml
V=10µl

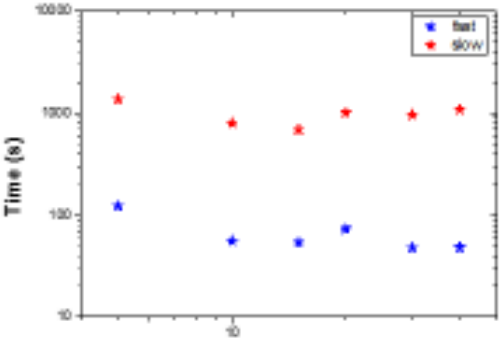

c=45mg/ml
V=10µl

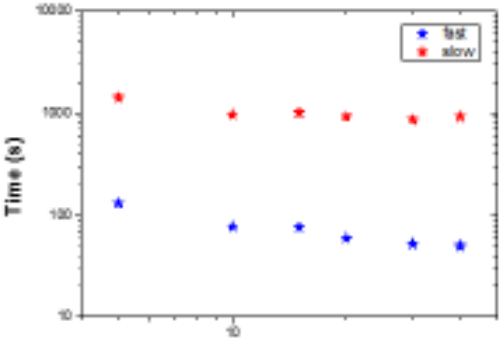

c=60mg/ml
V=10µl

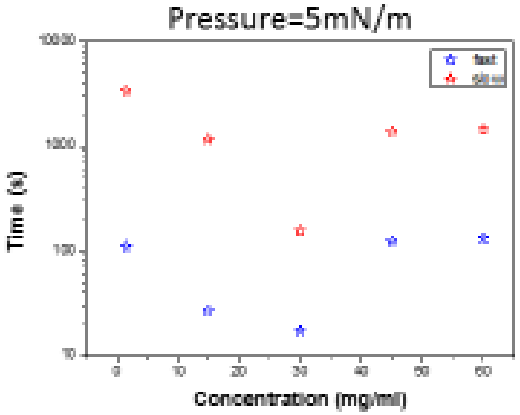
Pressure=5mN/m
Time (s)
Concentration (mg/ml)

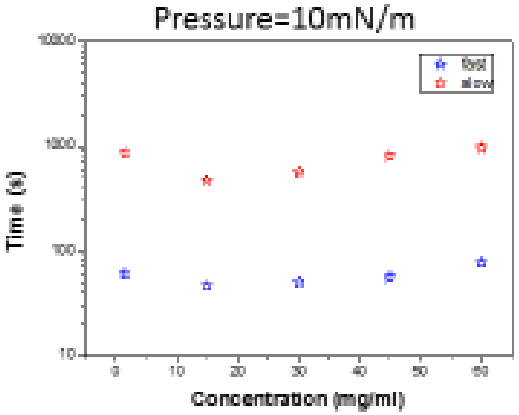
Pressure=10mN/m
Time (s)
Concentration (mg/ml)

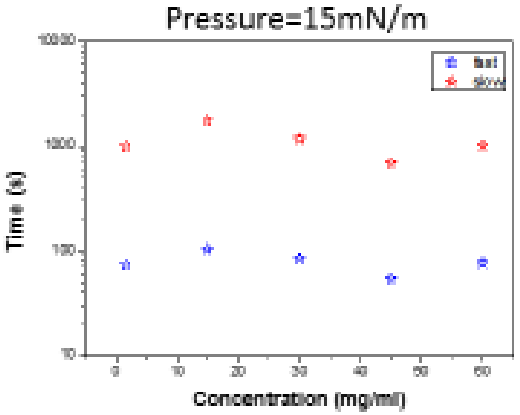
Pressure=15mN/m
Time (s)
Concentration (mg/ml)

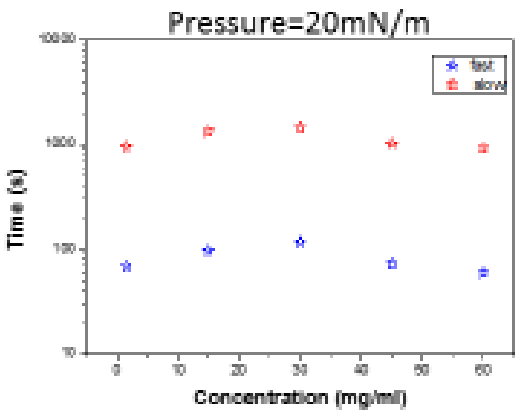
Pressure=20mN/m
Time (s)
Concentration (mg/ml)

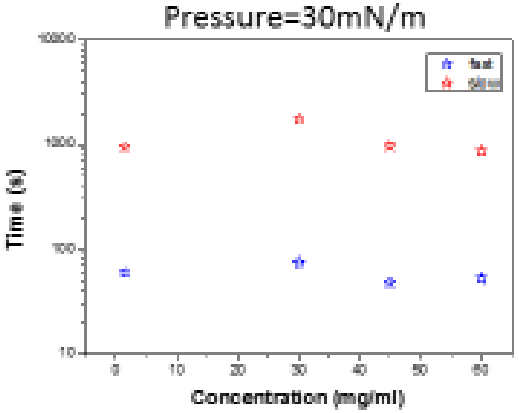
Pressure=30mN/m
Time (s)
Concentration (mg/ml)

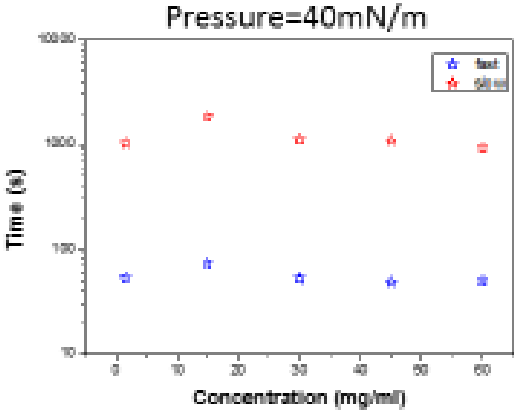
Pressure=40mN/m
Time (s)
Concentration (mg/ml)